

28262

**MARINE IMPACT ASSESSMENT OF THERMAL POWER PLANTS:  
A CASE STUDY**

**A Master's Thesis  
Presented by  
Cem ÇAKIROĞLU**

**to  
the Graduate School of Natural and Applied Sciences  
of Middle East Technical University  
in Partial Fulfillment for the Degree of**

**MASTER OF SCIENCE**

**in**

**ENVIRONMENTAL ENGINEERING**

**T.C. YÜKSEKÖĞRETİM KURULU  
DOKÜMANTASYON MERKEZİ**

**MIDDLE EAST TECHNICAL UNIVERSITY  
ANKARA**

**March, 1993**

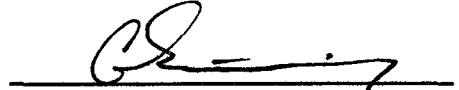
Approval of the Graduate School of Natural and Applied Sciences.



Prof. Dr. Alpay Ankara

Director

I certify that this thesis satisfies all the requirements as a thesis for the degree of Master of Science.



Prof. Dr. Gülerman Sürücü

Chairman of the Department

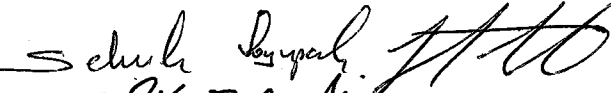
We certify that we have read this thesis and that in our opinion it is fully adequate, in scope and quality, as a thesis for the degree of Master of Science in Environmental Engineering.



Assoc. Prof. Dr. Coşkun Yurteri


Supervisor

Examining Committee in Charge:

Prof. Dr. Selçuk Soyupak 

Assoc. Prof. Dr. Coşkun Yurteri 

Prof. Dr. Celal F. Gökçay 

Assoc. Prof. Dr. Mustafa Oğuz 

Prof. Dr. Erdal Özhan 

## **ABSTRACT**

### **MARINE IMPACT ASSESSMENT OF THERMAL POWER PLANTS: A CASE STUDY**

**ÇAKIROĞLU, Cem**

**M.S. Thesis in Environmental Engineering**

**Supervisor: Assoc. Prof. Dr. Coşkun Yurteri**

**March 1993, 216 pages**

In this study, an efficient procedure was developed in order to assess the impacts of thermal power plants on marine environment. The developed algorithm was applied to the case of the proposed Aliağa Thermal Power Plant (ATPP). The proposed marine impact assessment procedure consists of the following steps:

- (i) dilution prediction studies for the liquid waste discharge of the proposed power plant
- (ii) hydrothermal modeling studies for the cooling water discharge of the proposed power plant
- (iii) prediction and assessment of the biological effects

Extensive field and literature data was collected as a preliminary step within the context of the study. Several mathematical (analytical and numerical) models were applied to the case of the proposed ATPP in order to achieve the above purposes.

**The results of the case study revealed that:**

- the liquid wastes of the ATPP will be sufficiently diluted and dispersed by a minimum factor of 3500 on the coastline;
- the cooling water discharge will result in a maximum temperature of 1 °C at the surface and 0.15 °C at the open boundary of the Gencelli Harbor (proposed site for the ATPP);
- the short-term impacts of the cooling water operations on the flora and fauna of the harbor will be insignificant;
- the long-term impacts of the cooling water operations on the commercially important fish species of the harbor will be notable in the sense that the number of individuals will decrease by a certain fraction until the shut-down of the plant.

**Keywords:** Thermal Power Plant, Environmental Impact Assessment, Marine Pollution, Mathematical Modeling, Life-cycle Models, Discharge.

**Science Code:** 615.02.01



## ÖZ

### TERMİK SANTRALLARIN DENİZ ETKİ DEĞERLENDİRMESİ KONUSUNDA BİR ÇALIŞMA

ÇAKIROĞLU, Cem

Yüksek Lisans Tezi, Çevre Mühendisliği Ana Bilim Dalı

Tez Yöneticisi: Doç. Dr. Coşkun Yurteri

Mart 1993, 216 sayfa

Bu çalışmada, termik santrallerin deniz ortamında neden olabilecekleri etkilerin tahmin edilebilmesi ve değerlendirebilmesi için etkin bir prosedür geliştirilerek, kurulması önerilen Aliağa Termik Santrali (ATS) örneğine uygulanmıştır. Önerilen prosedür, aşağıdaki aşamaları içermektedir:

- (i) önerilen santralin sıvı atık deşarjları için seyrelme tahmin çalışmaları
- (ii) önerilen santralin soğutma suyu deşarjları için hidrotermal modelleme çalışmaları
- (iii) biyolojik etkilerin kestirilmesi ve değerlendirilmesi

Çalışma kapsamında, ilk aşamada pek çok saha ve literatür verisi elde edilmiştir. Yukarıdaki amaçları gerçekleştirmek amacıyla, belirli sayıda matematiksel model (analitik ve sayısal) ATS örneğine uygulanmıştır.

Uygulama çalışmasında elde edilen bulgular ışığında, aşağıdaki sonuçlara varılmıştır:

- ATS'nın sıvı atıklarının kıyı çizgisinde en az 1:3500 mertebesinde seyreceği
- soğutma suyu deşarjının deniz suyu sıcaklığında, yüzeyde 1°C'lik, Gencelli Limanı'nın açık deniz sınırında ise 0.15°C'lik bir değişime neden olacağı
- soğutma suyu faaliyetlerinin, Gencelli Limanı'nın flora ve fauna türleri üzerinde kısa dönemde belirgin bir etki yapmayacağı
- soğutma sularının uzun dönemli etkilerinin, santral devre dışı kalana kadar canlı nüfusunda belirli bir azalma yaratması bakımından kayda değer olacağı

**Anahtar Kelimeler:** Termik Santral, Çevresel Etki Değerlendirmesi, Deniz Kirlenmesi, Matematiksel Modelleme, Yaşam Döngüsü Modelleri, Deşarj.

**Bilim Dalı Sayısal Kodu:** 615.02.01

## **ACKNOWLEDGEMENTS**

Sincere gratitude is due to the supervisor of this study, Assoc. Prof. Dr. Coşkun Yurteri, for his perfect supervision, support, encouragement, discussions and fun-times. Special thanks are due to Serpil Yurteri, for her endurance her husband's absence from home for supervising this study.

The author wishes to express his appreciation to Prof. Dr. Ahmet Kocataş, Prof. Dr. Savaş Mater and Dr. Melahat Toğulga of the Ege University Biology Department, for their friendly help in providing hydrobiological data.

Special thanks are due to Prof. Dr. Metin Ger, Yaşar F. Öztürk, Prof. Dr. Erdal Özhan for their helpful courses and discussions.

Special thanks are also due to the librarian staffs of Ege University, Biology Department and Faculty of Science; Dokuz Eylül University, Institute of Aquatic Products and Marine Sciences and Technology; İstanbul University, Biology Department, for their friendly help during the literature survey visits.

The author wishes to express his appreciation to Ege Egemen and Bora Arpacioğlu for their friendly and academical contributions.

Apologies are due to the author's mother for leaving her alone at days and nights of the long period of project and academical studies. He also wishes to express his deep appreciations to his mother for her perfect support and encouragement during the whole educational life.

## TABLE OF CONTENTS

	Page
ABSTRACT .....	iii
ÖZ .....	v
ACKNOWLEDGEMENT .....	vii
LIST OF TABLES .....	xv
LIST OF FIGURES .....	xviii
 CHAPTER I: INTRODUCTION .....	 1
1.1 General .....	1
1.2 Scope and Objectives of the Present Study .....	2
1.2.1 Dilution Prediction Studies for the Liquid Waste Discharge .....	4
1.2.2 Hydrothermal Modeling Studies for the Cooling Water Discharge .....	4
1.2.3 Prediction and Assessment of the Biological Effects .....	5
 CHAPTER II: SYSTEM DESCRIPTION AND PROBLEM DEFINITION .....	 6
2.1 General .....	6
2.2 Aliğa Thermal Power Plant .....	6
2.2.1 General .....	6
2.2.2 Cooling Water System .....	9
2.2.3 Liquid Waste Treatment and Discharge System .....	14
2.3 Plant Site Physical Environment .....	17
2.3.1 General .....	17
2.3.2 Bathymetry .....	17

2.3.3 Flow Characteristics .....	19
2.3.4 Meteorology .....	19
2.3.5 Sea Water Quality .....	20
2.3.6 Bottom Sediment Quality .....	23
2.4 Plant Site Biological Environment .....	24
2.4.1 General .....	24
2.4.2 Fish Species of the Gencelli Harbor .....	25
2.4.3 Ichtioplankton Species of the Gencelli Harbor .....	28
2.4.4 Benthic Algal Species of the Gencelli Harbor .....	29
2.4.5 Phytoplankton and Protozooplankton of the Gencelli Harbor	30
2.4.6 Zooplanktons of the Gencelli Harbor .....	30
2.4.7 Zoobenthic Fauna of the Gencelli Harbor .....	31
2.4.8 Heavy Metals in Marine Organisms of the Gencelli Harbor	32
2.5 Potential Risks and Their Sources .....	34
2.5.1 General .....	34
2.5.2 Effects Due to Cooling Water Operations .....	34
2.5.3 Liquid Waste Discharge .....	37
2.5.4 Marine Transportation .....	37
<b>CHAPTER III: LIQUID WASTE DILUTION AND DISPERSION</b>	
<b>MODELING STUDIES .....</b>	<b>38</b>
3.1 General .....	38
3.2 Theoretical Background .....	40
3.2.1 General .....	40
3.2.2 Initial Dilution ( $S_1$ ) .....	41
3.2.3 Dilution Due to Dispersion ( $S_2$ ) .....	44
3.2.4 Dilution Due to Bacterial Decay ( $S_3$ ) .....	46
3.3 Results .....	46
3.4 Summary .....	49

<b>CHAPTER IV:</b>	<b>HYDROTHERMAL MODELING STUDIES:</b>	
	<b>NEAR-FIELD</b>	<b>51</b>
4.1	General	51
4.2	Prediction of Dilution in Stagnant Environment (the model of CRIEPI)	53
4.2.1	General	53
4.2.2	Dilution Ratio Along the Jet Axis	54
4.2.3	The Jet Trajectory	55
4.2.4	Spread Width of the Jet	56
4.2.5	Thickness of the Thermal Field	56
4.2.6	Maximum Horizontal Velocity at the Surface	58
4.3	Prediction of Dilution in Flowing Water (Adams Model)	58
4.3.1	General	58
4.3.2	Theoretical Background	58
4.4	Results and Discussion	62
4.4.1	Design Features of the Cooling Water Discharge Structure	62
4.4.2	Dilution in Stagnant Environment	63
4.4.3	Cross-Flowing Environment	64
<b>CHAPTER V:</b>	<b>HYDROTHERMAL MODELING STUDIES:</b>	
	<b>INTERMEDIATE AND FAR-FIELD</b>	<b>66</b>
5.1	General	66
5.2	Study Approach	66
5.3	Description of GLLVHT	67
5.3.1	Background of GLLVHT	67
5.3.2	Assumptions, Equations and Solution Techniques	68
5.3.3	Boundary Conditions	70
5.3.4	Input Data for Model Parameters	72
5.4	Model Setup	73
5.4.1	Grid System	73
5.4.2	Meteorological Conditions	77

5.4.3 Ambient Temperatures and Salinities .....	79
5.4.4 Boundary Conditions .....	79
5.4.5 Current Velocities .....	79
5.4.6 Outfall Conditions .....	80
5.5 Setup validation .....	80
5.6 Model Simulations .....	83
5.6.1 General .....	83
5.6.2 Simulation 1 .....	84
5.6.3 Simulation 2 .....	84
5.6.4 Simulation 3 .....	84
5.6.5 Simulation 4 .....	88
5.6.6 Simulation 5 .....	88
5.7 Model Simulations for Water Circulation .....	88
5.8 Summary and Conclusions .....	93
 CHAPTER VI:       MARINE BIOLOGICAL IMPACTS OF THE ATPP:	
SHORT-TERM .....	98
6.1 General .....	98
6.2 Effects on Fish .....	99
6.2.1 Thermal Effects on Fish .....	99
6.2.2 Chemical Effects on Fish .....	102
6.2.3 Mechanical Effects on Fish .....	102
6.3 Effects on Ichtioplankton .....	104
6.3.1 Effects on Ichtioplankton Due to Entrainment .....	104
6.3.2 Effects on Ichtioplankton Due to Warming of the Receiving Waterbody .....	109
6.3.3 Effects on Ichtioplankton Due to Decrease in Dissolved Oxygen Level .....	110
6.3.4 Effects on Ichtioplankton Due to Antifouling Chemicals .	110
6.4 Effects on Algae .....	110

6.5 Effects on Phytoplankton and Protozooplankton .....	112
6.6 Effects on Zooplankton .....	112
6.7 Effects on Zoobenthose .....	113
6.8 Effect on Heavy Metal Toxicity .....	114
6.9 Effects of Liquid Waste Discharge .....	115
6.10 Effects of Construction Facilities on Marine Life .....	115
6.11 Effects of Fuel Delivery, Conveyance and Storage .....	116

CHAPTER VII: MARINE BIOLOGICAL IMPACTS OF THE ATPP:	
LONG-TERM .....	116
7.1 General .....	116
7.2 Study Approach .....	116
7.3 Theoretical Basis and Structure of the LCM .....	117
7.3.1 Life Stages .....	117
7.3.2 Assumptions of the LCM .....	119
7.3.3 Formulation and Computational Steps .....	121
7.3.4 Data Requirement of the LCM .....	135
7.3.5 Estimation of Mortality Coefficients .....	135
7.4 Application of the LCM on <i>Mullus Barbatus</i> .....	137
7.4.1 Application Approach .....	137
7.4.2 Model Inputs and Setup .....	138
7.4.3 Sensitivity Tests .....	138
7.4.4 LCM Simulations for <i>Mullus Barbatus</i> .....	142
7.5 Application of the LCM on <i>Sparus aurata</i> .....	144
7.5.1 Model Inputs and Setup .....	144
7.5.2 Sensitivity Tests .....	148
7.5.3 LCM Simulations for <i>Sparus aurata</i> .....	150
7.6 Summary and Recommendations .....	152

CHAPTER VIII: CONCLUSION AND RECOMMENDATIONS .....	153
--	-----



8.1 General .....	153
8.2 Conclusions .....	154
8.2.1 Dilution Prediction Studies for the Liquid Waste Discharge	154
8.2.2 Hydrothermal Modeling Studies for the Cooling	
Water Discharge .....	154
8.2.3 Prediction and Assessment Studies of the Biological Effects	155
8.3 Recommendations .....	156
8.3.1 Recommendations for Monitoring Studies .....	156
8.3.2 Recommendations for Project Modifications .....	157
8.3.3 Recommendations for Legislative Modifications .....	158
REFERENCES .....	159
APPENDICES	
APPENDIX A. LIST OF MARINE SPECIES OBSERVED	
IN THE GENCELLI HARBOR .....	172
APPENDIX B. SENSITIVITY TESTS FOR LIQUID	
WASTE DISCHARGE .....	184
B.1 General .....	184
B.2 Tests for the Discharge Depth .....	185
B.3 Tests for the Discharge Velocity .....	186
B.4 Tests for the Degree of Stratification .....	187
B.5 Tests for the $T_{90}$ Value .....	188
B.6 Tests for the Discharge Length .....	188
B.7 Tests for the Watewater Density .....	189
B.8 Tests for the Ambient Current Velocity .....	190

APPENDIX C. THEORETICAL BASIS OF GLLVHT .....	191
APPENDIX D. SENSITIVITY TESTS FOR COOLING WATER	
DISCHARGE .....	200
D.1 General .....	200
D.2 Tests for the Bathymetric Data .....	202
D.3 Tests for the Chezy Coefficient .....	205
D.4 Tests for the Horizontal Momentum .....	206
D.5 Tidal Height .....	208
D.6 Cloud Cover and Shortwave Solar Radiation .....	209
D.7 Tests for the Rate of Return Ratio .....	210
D.8 Wind Speed .....	212
APPENDIX E. BATHYMETRY ALTERNATIVES FOR	
THE GENCELLI HARBOR .....	214

## LIST OF TABLES

	Page
Table 2.1. Cooling Water Intake System Characteristics . . . . .	11
Table 2.2. Cooling Water Discharge System Characteristics . . . . .	13
Table 2.3. Liquid Waste Characteristics . . . . .	15
Table 2.4. Liquid Waste Discharge Features . . . . .	15
Table 2.5. Annual Percentage Frequency of Wind Speed Classes and Directions . . . . .	21
Table 2.6. Sea Water Quality Parameters of the Gencelli Harbor . . .	22
Table 2.7. Sediment Quality of the Gencelli Harbor . . . . .	24
Table 2.8. Heavy Metal Concentrations in Certain Species of the Gencelli Harbor . . . . .	33
Table 3.1. Prediction Parameters of Liquid Waste Discharge . . . . .	47
Table 3.2. Predicted Values for the Dilution Ratios . . . . .	48
Table 4.1. Features of the Discharge Structure and Area . . . . .	62
Table 4.2. Dilution and Surface Velocity in Stagnant Conditions . . .	63
Table 4.3. The results of the Near-Field Hydrothermal Studies for Cross-Flow Conditions . . . . .	64
Table 5.1. Hypsometric Data for the Modeled Portion of Gencelli Harbor	76
Table 5.2. Meteorology Data Used in the Runs and Simulations . . .	77
Table 5.3. The Setup Simulations of the GLLVHT . . . . .	82
Table 5.4. Simulations for the Proposed ATPP . . . . .	83
Table 6.1. Critical Sea Water Temperatures for the Commercially Important Fish Species of the Gencelli Harbor (°C) . . . . .	100

Table 6.2.	Tolerance Limits of Some Species Observed in the Gencelli Harbor .....	101
Table 6.3.	Lethal Temperatures for Algal Species .....	111
Table 6.4.	Tolerance Limits for Algae .....	111
Table 7.1.	Year-class Structures of Different Sites on Turkish Coasts	139
Table 7.2.	Reported Values of Mortality Rates for <i>Mullus Barbatus</i> .	140
Table 7.3.	Base Case Parameters and Values .....	141
Table 7.4.	The Results of the Sensitivity Tests .....	142
Table 7.5.	Effects of Entrainment on <i>Mullus Barbatus</i> Fish Population of the Gencelli Harbor .....	144
Table 7.6.	Reported Values of Mortality Rates for <i>Sparus aurata</i> ...	145
Table 7.7.	Length Data for <i>Sparus aurata</i> .....	146
Table 7.8.	Weight Data for <i>Sparus aurata</i> .....	147
Table 7.9.	Mortality Data on the Pre-recruit Stage of <i>Sparus aurata</i>	147
Table 7.10.	Base Case Parameters and Values for <i>Sparus aurata</i> ...	149
Table 7.11.	The Results of the Sensitivity Tests .....	150
Table 7.12.	Effects of Entrainment on <i>Sparus aurata</i> Fish Population of the Gencelli Harbor .....	152
Table A.1.	List of Fish Species Captured in Gencelli Harbor .....	173
Table A.2.	Fish Larvae of Gencelli Harbor .....	175
Table A.3.	Fish Eggs of Gencelli Harbor .....	175
Table A.4.	List of Algal Species in Gencelli Harbor .....	176
Table A.5.	Phytoplanktons and Protozooplanktons of Gencelli Harbor	177
Table A.6.	Zooplankton Species of the Gencelli Harbor .....	178
Table A.7.	Zoobenthose Species in the Gencelli Harbor .....	180
Table B.1.	Base-case Parameters and Abbreviations of Tests .....	185
Table C.1.	Heat Exchange Components and Relevant Measurable Parameters Necessary to Compute the Components .....	198

Table D.1.	Base Case Parameters And Their Abbreviations Used in Sensitivity Tests . . . . .	202
Table D.2.	Bathymetric Data Test Results for the Calm Case . . . . .	203
Table D.3.	Chezy Coefficient Test Results for the Calm Case . . . . .	205
Table D.4.	Dispersion Coefficient Test Results for the Calm Case . . . . .	207
Table D.5.	Tidal Amplitude Test Results for the Calm Case . . . . .	208
Table D.6.	Rate of Return Ratio Test Results for the Calm Case . . . . .	211
Table E.1.	Mean Depth of Each Cell of Bathymetry-1 . . . . .	215
Table E.2.	Mean Depth of Each Cell of Bathymetry-2 . . . . .	215
Table E.3.	Mean Depth of Each Cell of Bathymetry-3 . . . . .	216
Table E.4.	Mean Depth of Each Cell of Bathymetry-4 . . . . .	216



## LIST OF FIGURES

	Page
Figure 1.1. Outline of the Study . . . . .	3
Figure 2.1. Location of the Proposed ATPP in Türkiye . . . . .	7
Figure 2.2. Location of the the Proposed ATPP in the Gencelli Harbor . . . . .	8
Figure 2.3. Cooling Water System of the Proposed ATPP . . . . .	10
Figure 2.4. Typical Thermal Power Plant Scheme . . . . .	12
Figure 2.5. Liquid Waste Discharge System . . . . .	16
Figure 2.6. Observed Bathymetry of the Gencelli Harbor . . . . .	18
Figure 2.7. Sea Current Characteristics of the Gencelli Harbor . . . . .	20
Figure 2.8. Locations of Marine Biology Sampling Stations of 1990 Spring Studies . . . . .	25
Figure 2.9. Locations of Marine Biology Sampling Stations of 1991 Autumn Studies . . . . .	25
Figure 2.10. Trawl Routes (1991) . . . . .	26
Figure 2.11. Location of Zoobenthose Sampling Stations (1991) . . . . .	26
Figure 2.12. Effects of Thermal Power Plants on Marine Environment	35
Figure 4.1. Diffuser types . . . . .	52
Figure 4.2. Spread Width ( $b'$ ) of Horizontally-Issued Warm Jet . . . . .	57
Figure 4.3. Details for Adams Model . . . . .	61
Figure 5.1. A Comparison of Observed Sea-Water Temperatures with the Values Predicted by GLLVHT . . . . .	69
Figure 5.2. National Bathymetric Map . . . . .	74
Figure 5.3. Finite Difference Discretization of the Study Area . . . . .	75
Figure 5.4. Surface Excess Temperature Distribution for Simulation 1	85

Figure 5.5.	Surface Excess Temperature Distribution for Simulation 2	86
Figure 5.6.	Surface Excess Temperature Distribution for Simulation 3	87
Figure 5.7.	Surface Excess Temperature Distribution for Simulation 4	89
Figure 5.8.	Surface Excess Temperature Distribution for Simulation 5	90
Figure 5.9.	Surface Circulation With Plant (Wind) . . . . .	91
Figure 5.10.	Surface Circulation Without Plant (Wind) . . . . .	91
Figure 5.11.	Surface Circulation With Plant (Calm) . . . . .	92
Figure 5.12.	Surface Circulation Without Plant (Calm) . . . . .	92
Figure 6.1.	Entrainment Ratios for Various Flow Rates . . . . .	108
Figure 7.1.	Life-cycle Scenario of Fish . . . . .	119
Figure 7.2.	Computational Steps of the LCM . . . . .	122
Figure 7.3.	Change in the Number and Composition of a Pre-recruit Community . . . . .	130
Figure 7.4.	Computational Logic of the Pre-recruit Life Simulation . . .	131
Figure 7.5.	Effects of Various Entrainment Levels on <i>Mullus</i> <i>Barbatus</i> Population of the Gencelli Harbor . . . . .	143
Figure 7.6.	Effects of Various Entrainment Levels on <i>Sparus</i> <i>aurata</i> Population of the Gencelli Harbor . . . . .	151
Figure B.1.	Tests for Discharge Depth . . . . .	185
Figure B.2.	Tests for Discharge Velocity . . . . .	186
Figure B.3.	Tests for the Degree of Stratification . . . . .	187
Figure B.4.	Tests for the $T_{90}$ Value . . . . .	188
Figure B.5.	Tests for the Discharge to Coastline Distance . . . . .	188
Figure B.6.	Tests for the Wastewater Density . . . . .	189
Figure B.7.	Tests for the Ambient Current Velocity . . . . .	190
Figure C.1.	Process of Heat Exchange at a Natural Water Surface . .	199
Figure D.1.	Comparison of Bathymetry-4 and 1 . . . . .	204
Figure D.2.	Sensitivity Tests for Bathymetry . . . . .	204
Figure D.3.	Sensitivity Tests for Chezy Coefficient . . . . .	206
Figure D.4.	Sensitivity Tests for Momentum Dispersion Coefficients .	207

Figure D.5. Sensitivity Tests Tidal Height ..... 208

Figure D.6. Sensivity Tests for Cloud Cover ..... 209

Figure D.7. Sensitivity Tests for Solar Radiation ..... 210

Figure D.8. Sensitivity Tests for Return Rate ..... 211

Figure D.9. Sensitivity Tests for Wind Speed ..... 213





## CHAPTER I

### INTRODUCTION

#### 1.1 General

About 60 % of the world's electrical energy production is based on fossil fuels. This is not only due to the fact that different sources of energy should be in balance but also to the relatively low cost of electricity production with fossil fuels. However, energy production with fossil fuels impose certain risks on the environment. This alternative may be acceptable only if these risks are predicted and minimized.

In a rapidly developing country like Türkiye, there is a high demand for energy. This results in the need of construction of new power plants, such as hydraulic, thermal or nuclear power plants. Environmental impact assessment (EIA) studies are necessary for these facilities which are potential sources of environmental impacts. EIA is a very important tool for constructing and operating these plants safely in terms of environmental impacts.

Prediction of the environmental impacts of a proposed facility will help the decision makers to minimize the possible impacts by taking early measures during the planning stage. However, such a comprehensive study is generally expensive and time consuming. Therefore, establishment of efficient algorithms is essential for the success of EIA studies.

## 1.2 Scope and Objectives

The major goal of this study is to establish a cost effective algorithm to predict and assess the impacts of a thermal power plant on marine environment. Such a procedure should be efficient in terms of cost and time. The developed procedure was applied to the case of the proposed Aliğa Thermal Power Plant (ATPP).

ATPP is a 1000 MW, coal-fired power plant, which was proposed to be built by a joint venture company including the Electric Power Development Company of Japan (EPDC) and Turkish Electrical Authority (TEK), as a build-operate-transfer facility on the Western coast of Türkiye. Condenser cooling water for the plant was proposed to be taken from the Gencelli Harbor on the Aegean Sea through a deep, extended intake structure and discharged through a submerged, multi-port diffuser. Liquid wastes of the plant were proposed to be discharged through a deep sea discharge structure following on-land treatment.

Three major steps of the present case study are given below:

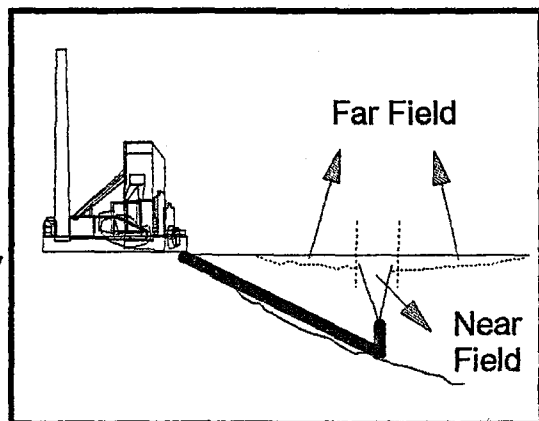
- (i) dilution prediction studies for the liquid waste discharge of the proposed ATPP
- (ii) hydrothermal modeling studies for the cooling water discharge of the proposed ATPP
- (iii) prediction and assessment of the marine biological effects of the cooling water and liquid waste discharges

The outline of the study is briefly illustrated in Figure 1.1.

### 1. LIQUID WASTE DISCHARGE

Dilution Prediction (CHAPTER 3):

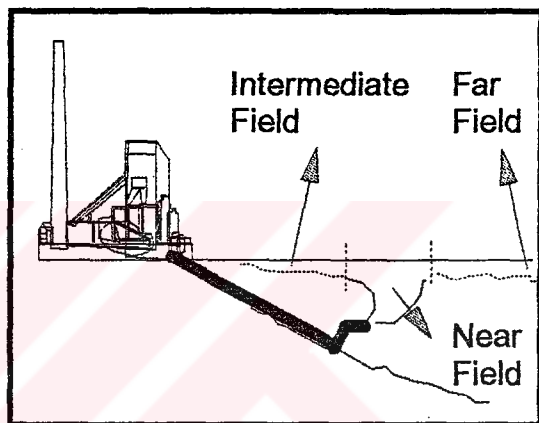
- a) Initial Dilution (Near-Field)
- b) Secondary Dilution (Far-Field)
- c) Dilution Due To Bacterial Decay



### 2. COOLING WATER DISCHARGE

Hydrothermal Modeling:

- a) Near-field (CHAPTER 4)
- b) Intermediate and Far-field (CHAPTER 5)



### 3. BIOLOGICAL IMPACTS

Prediction and Assessment:

- a) Short-term (CHAPTER 6)
- b) Long-term (CHAPTER 7)

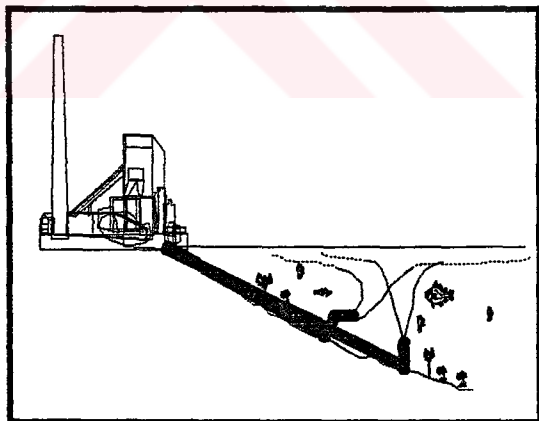


Figure 1.1. Outline of the Study

### **1.2.1 Dilution Prediction Studies for the Liquid Waste Discharge**

The liquid waste discharge analysis was made by mathematical (analytical) models to assure that the following properties of the discharge are sufficient to prevent pollution:

- initial dilution
- dilution due to dispersion
- dilution due to bacterial decay

### **1.2.2 Hydrothermal Modeling Studies for the Cooling Water Discharge**

Near, intermediate and far-field thermal plume regions were analyzed by hydrothermal modeling studies in order to assess the potential environmental impacts due to the thermal discharge. Hydrothermal modeling studies involved the following approaches:

- semi-empirical near-field analysis with models based on jet theory
- intermediate and far-field hydrothermal analysis by a three-dimensional, hydrodynamic and transport numerical model

The primary objectives of the hydrothermal studies were:

- to assure that the regulatory criterion for maximum surface water temperature rise of 1 °C will be satisfied;
- to predict the extent of the area affected by the warm plume and to estimate the surface excess temperature contourlines;
- to determine the water circulation patterns in the Gencelli Harbor;

- to investigate the possible effects of various factors, including meteorology and tides, on warm water dispersion.

### **1.2.3 Prediction and Assessment of the Biological Impacts**

The impacts of the proposed power plant on the marine organisms were predicted based on the results of the above studies. The biological effects were assessed in short and long-term time scales.

The following ecosystem components were targeted in terms of impact assessment:

- fish
- ichtioplankton (egg and larvae of fish)
- algae
- phytoplankton and protozooplankton
- zooplankton
- zoobenthose

The short-term impacts were investigated by using the results of various researches reported in the literature. For this purpose, the impacts of similar adverse conditions to those that will be created by the proposed ATPP were investigated.

An integrated approach was developed in order to predict the long-term impacts of the proposed plant on the valued ecosystem components of the Gencelli Harbor. For this purpose, several mathematical models were adapted to the case of the proposed ATPP and combined in a simple life cycle model.

## CHAPTER II

### SYSTEM DESCRIPTION AND PROBLEM DEFINITION

#### 2.1 General

The most important step of any engineering study or application is system description and problem definition. This chapter briefly describes and discusses:

- pertinent systems of the proposed ATPP which are potential sources of impact on the marine environment;
- current state of the marine environment in the vicinity of the plant;
- potential risks of a thermal power plant on marine environment; and,
- relevant environmental legislation which are used in determining the extent of potential risks imposed on the environment.

#### 2.2 Aliaga Thermal Power Plant

##### 2.2.1 General

ATPP is a proposed 1000 MW coal-fired thermal power plant. Location of the proposed plant is depicted in Figures 2.1 and 2.2. In the case of the

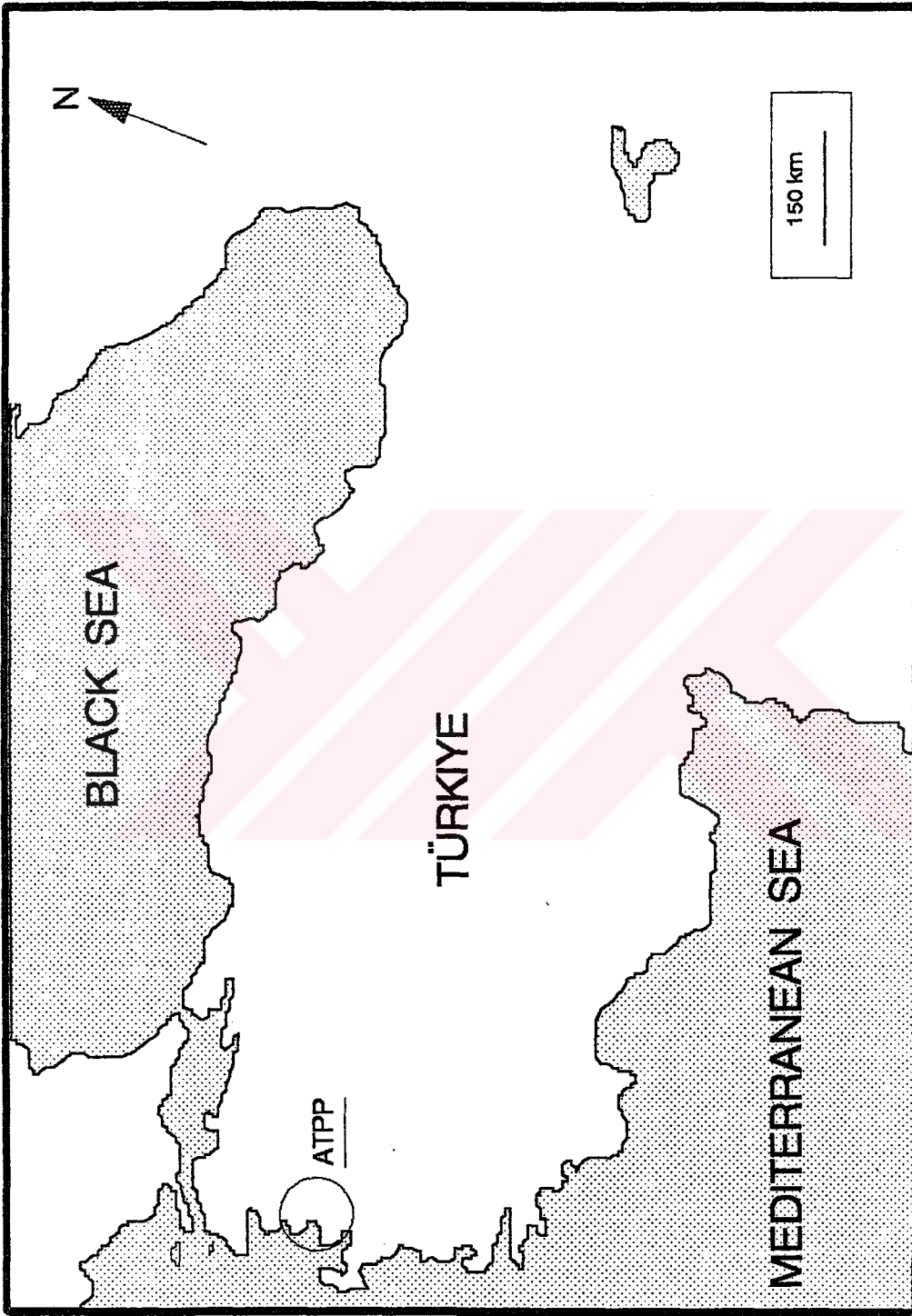


Figure 2.1. Location of the Proposed ATPP in Türkiye

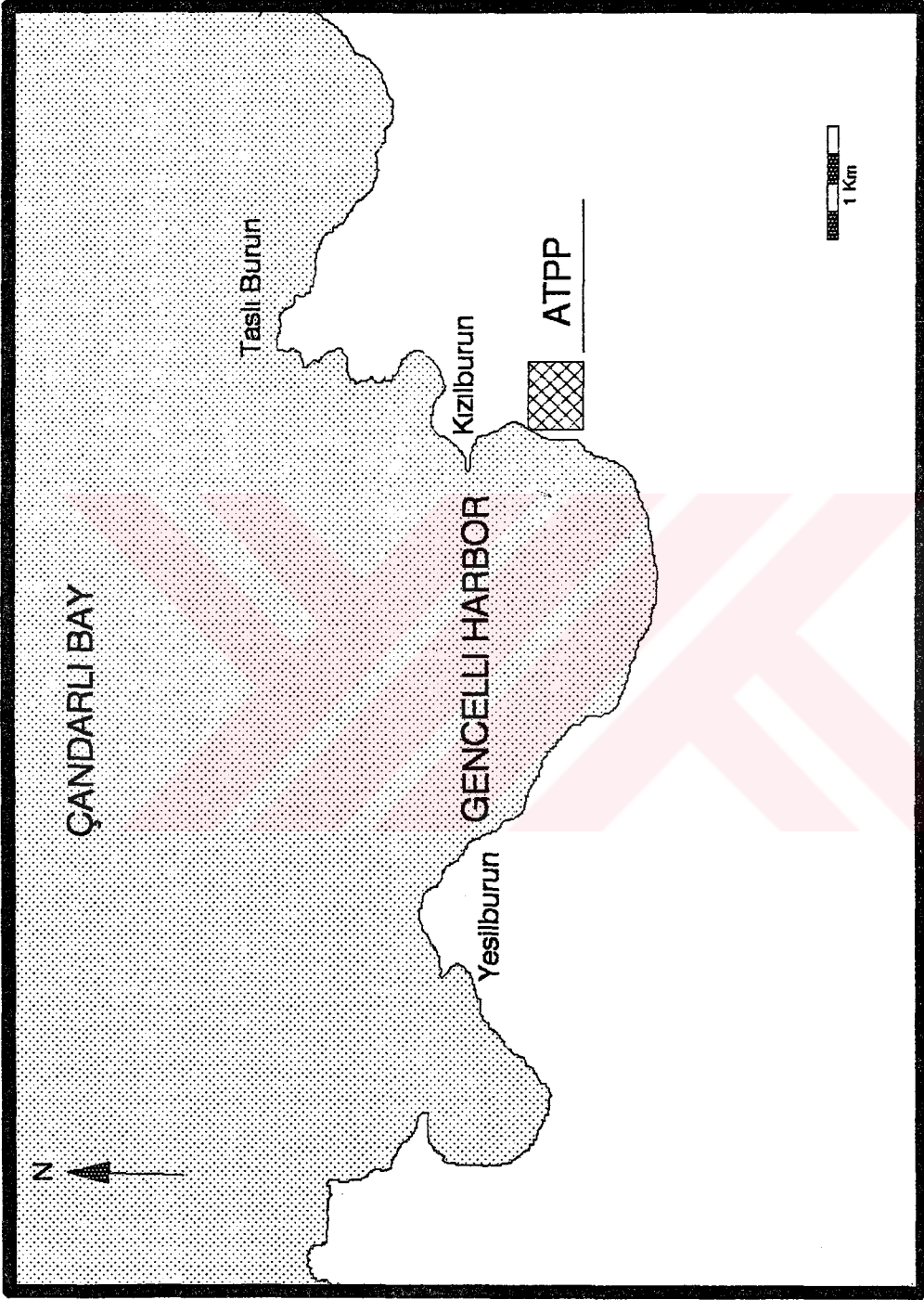


Figure 2.2. Location of the the Proposed ATPP in the Gencelli Harbor



proposed ATPP, low-sulfur coal will be used as fuel. Fluidized bed combustion system will be used to produce heat. A once-through system will be used for plant cooling and sea water as cooling medium. Deep water intake and discharge structures will be used for cooling water circulation. NaOCl will be used to prevent biofouling in the cooling water system. Liquid wastes will be discharged to the sea following an on-land treatment. Navigation lines will also be used for transportation of raw and construction materials.

### **2.2.2 Cooling Water System**

The proposed ATPP consists of two, 500 MW units, each with a separate cooling water intake and discharge system. The separate intake and discharge structures for each unit are located immediately adjacent to each other. The intake structure is located at the northwest and the discharge structure at the southwest of the proposed plant site. Important features of the cooling water system are:

- relatively deep location of the intake and discharge structures;
- relatively large separation of the intake and discharge (400 m); and,
- orientation of the discharge away from the intake.

The general lay-out of the cooling water system of the ATPP is depicted in Figure 2.3. The major components of the cooling water system are:

- cooling water intake system;
- condensers;
- cooling water discharge system; and
- antifouling system.

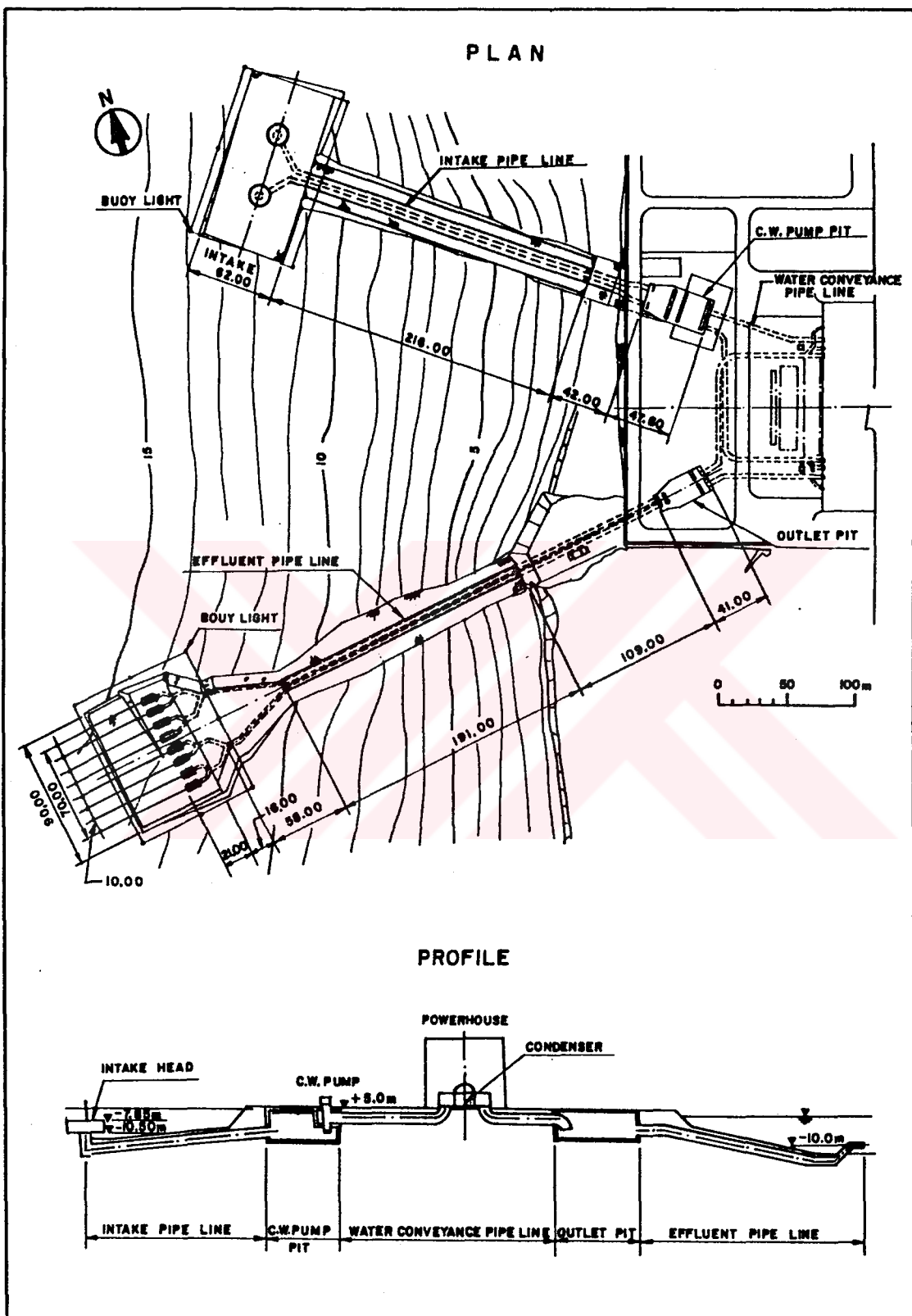


Figure 2.3. Cooling Water System of the Proposed ATPP

The major components of the cooling water system are briefly described in the following sub-sections. The generation of electricity is also briefly described in these sub-sections.

#### a. Cooling Water Intake System

The cooling water intake system of the proposed ATPP was designed to draw deep sea off-shore water from the Gencelli Harbor. Screens will be located in front of the intake heads to minimize entrapment of fish. The diameter of the intake is kept relatively large to decrease the intake velocity. The cooling water will be drawn from the lateral surfaces of the heads horizontally. The cooling water then will be pumped to the condensers. The cooling water intake system characteristics are given in Table 2.1.

Table 2.1 Cooling Water Intake System Characteristics

Parameter	Value
Total flow rate (2 units)	46.6 m <sup>3</sup> s <sup>-1</sup>
Intake to coast distance	300 m
Intake depth	8-10 m
Number of intake heads	2
Diameter of intake heads	15 m
Average intake velocity	0.2 m s <sup>-1</sup>

#### b. Condensers

The processes of a typical power plant are briefly illustrated in Figure 2.4. Vast amount of heat will be produced in the plant for electricity generation. The heat produced, first will be used in steam generation.

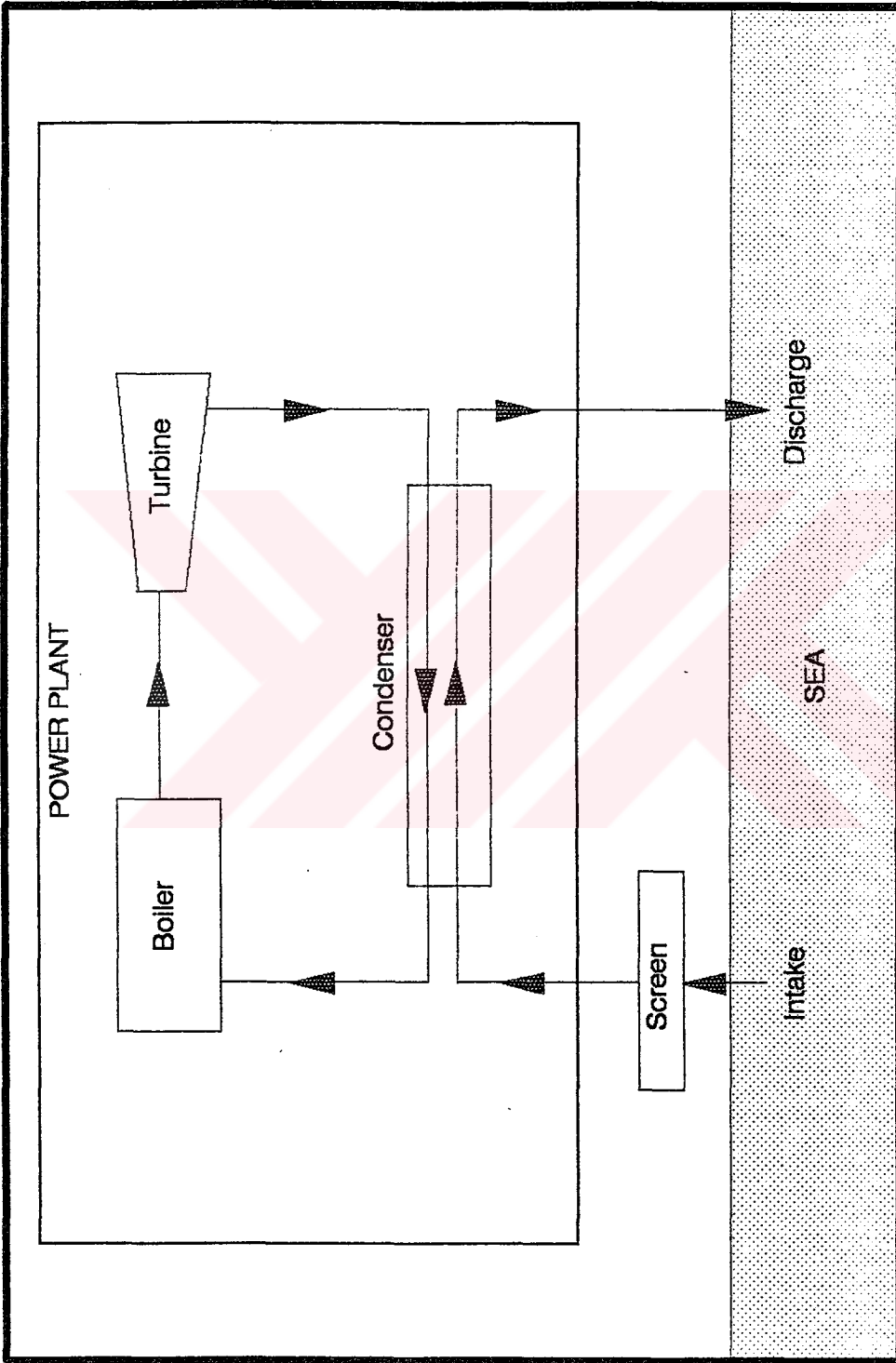


Figure 2.4. Typical Thermal Power Plant Scheme

The steam will be generated from the in-plant circulating water. The steam obtained will be used to generate electricity by means of a turbine. The cooling water will be circulated through the heat exchangers. The heat of the steam will be transferred to the cooling water and the steam will be condensed. According to the design, the temperature of the cooling water will be increased by 7 °C.

**c. Cooling Water Discharge System**

The heat released during the condensation of the steam will be discharged to sea. The cooling water will be discharged horizontally through a submerged, multi-port discharge structure in order to provide sufficient dilution for preventing thermal pollution or heat accumulation at the discharge area. The ports will be located on a concrete platform in order to prevent resuspension of bottom sediments. The characteristics of the cooling water discharge system are given in Table 2.2.

**Table 2.2 Cooling Water Discharge System Characteristics**

Parameter	Value
Total flow rate (2 units)	46.6 m <sup>3</sup> s <sup>-1</sup>
Discharge to coast distance	290 m
Discharge depth	10 m
Number of ports	8
Port spacing	10 m
Diameter of ports	1.6 m
Average discharge velocity	2.9 m s <sup>-1</sup>
Length of diffuser	70 m

#### **d. Antifouling System**

NaOCl (sodium hypochlorite) will be used to prevent the fouling of the intake and subsequent pipelines by organisms. NaOCl will be generated at the intake by means of electrolysis. The NaOCl concentration will be about 1 mg l<sup>-1</sup> at the intake and below 0.01 mg l<sup>-1</sup> at the discharge point.

### **2.2.3 Liquid Waste Treatment and Discharge System**

#### **a. Liquid Waste Treatment**

The industrial and domestic wastewaters and runoff waters resulting from the operation of the proposed ATPP will be collected, treated and discharged to sea. The treatment system of the proposed plant is composed of the plant wastewater treatment unit; domestic wastewater treatment unit; plant runoff treatment unit; and, ash disposal area runoff and leachate treatment unit.

The treated effluents of the first three units listed above will be collected and discharged to sea. The effluent characteristics of the treatment system are summarized in Table 2.3. It was stated that all the parameters which are not listed in Table 2.3 will comply with the current regulations (ATPP EIA Phase-2 Report, 1992). The plant wastewater will be treated by coagulation, sedimentation and neutralization. Domestic wastewaters will be biologically treated via an activated sludge treatment unit of extended aeration type. The ash disposal area runoff and leachates will be collected, treated and disposed separately at the ash disposal site. Wastewaters that will result from the construction works will be first subjected to settling and disposed to the surrounding medium.

## b. Liquid Waste Discharge

The treated effluents from various treatment units will be combined and discharged to sea via a deep sea discharge system at a depth of 20 m. The effluent will be discharged from a pipe of diameter 0.125 m at a rate of about  $0.015 \text{ m}^3 \text{ s}^{-1}$ . Pumps with a capacity of about  $0.016 \text{ m}^3 \text{ s}^{-1}$  will be used for discharging effluents to sea. The features of the liquid waste structure are given in Figure 2.5 and Table 2.4 (ATPP EIA Phase-2 Report, 1992).

Table 2.3. Liquid Waste Characteristics

Item	Effluent
Discharge Rate ( $\text{m}^3 \text{ d}^{-1}$ )	1200
pH	6-9
COD (mg/l)	<30
SS (mg/l)	<100
Mg (mg/l)	500
Ca (mg/l)	500
Fe (mg/l)	<5
F (mg/l)	<10
CN <sup>-</sup> (mg/l)	<0.5
Oil (mg/l)	<10

Table 2.4. Liquid Waste Discharge Features

Parameter	Value
Flow rate ( $\text{m}^3 \text{ s}^{-1}$ )	0.016
Port diameter (m)	0.125
Discharge velocity ( $\text{m s}^{-1}$ )	1.3
Discharge depth (m)	20
Discharge to coastline distance (m)	500

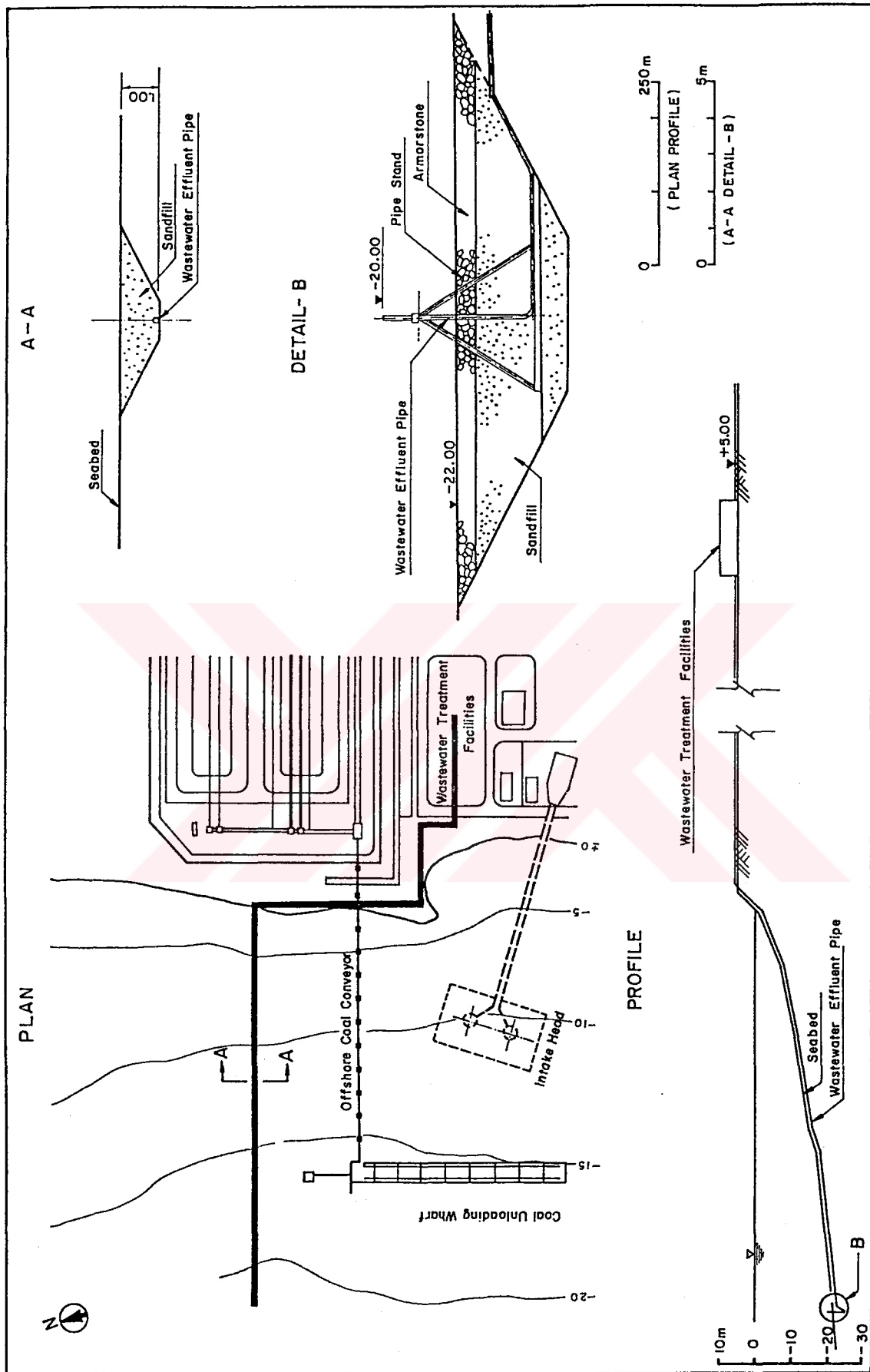


Figure 2.5. Liquid Waste Discharge System



## 2.3 Plant Site Physical Environment

### 2.3.1 General

Çandarlı Bay is located in the eastern Aegean Sea. The bay has depths up to 90 m in the vicinity of the ATPP. Çandarlı Bay is broken into a number of embayments. The ATPP was proposed to be located on one of these embayments, which is known as the Gencelli Harbor (also called Horozgediği Harbor). Gencelli Harbor can be defined as being south of a line drawn from Yeşilburun on the west and Kızılburun on the east, as shown in Figure 2.2. In the description of the current state of the physical marine environment, the data provided by several studies carried out within the context of the ATPP EIA studies. The data was provided from the studies of the following institutions:

- Dokuz Eylül University (DEU), Marine Sciences and Technology Institute;
- Navigation, Hydrography and Oceanography Department of Turkish Navy; and
- Ege University (EU), Biology Department.

### 2.3.2 Bathymetry

Gencelli Harbor has a uniform bathymetry with a maximum depth of 50 m and a mean depth of about 22.5 m. The part of the Gencelli Harbor near the plant site has an approximate sea bottom slope of 1/20. The depth contours of the harbor are shown in Figure 2.6.

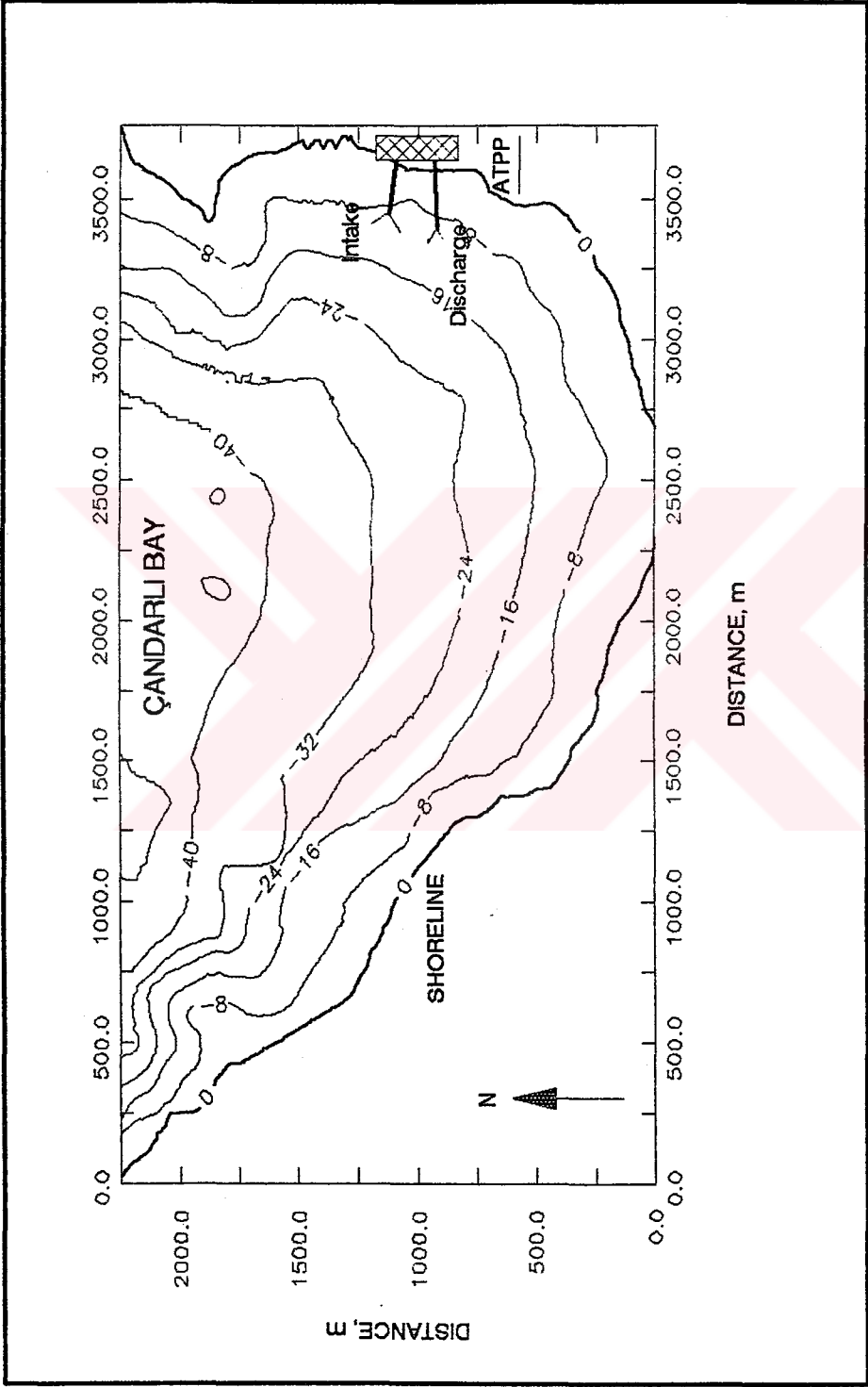


Figure 2.6. Observed Bathymetry of the Gencelli Harbor

### **2.3.3 Flow Characteristics**

#### **a. Tides**

Tides in the Gencelli Harbor and the eastern Mediterranean are quite small, with a range of 60 cm between the mean low water surface (MLWS) and mean high water surface (MHWS) (Akyarlı and Arısoy, 1988). The tides have a period of 8.5 h (Defant, 1958).

#### **b. Waves**

The calculated wave heights of 0.5 m or less and 1.0 m or less have frequencies of 82.07 and 98.65 percent, respectively (ATPP EIA Phase-1 Report, 1990).

#### **c. Currents**

Based on the field surveys of DEU, it was found that the dominant current direction was almost parallel to the shoreline (ATPP EIA Phase-2 Report, 1992). The relatively dominant current direction was observed to be Northeast to North by Northwest. Current velocities below  $4 \text{ cm s}^{-1}$  were frequent (ATPP EIA Phase-2 Report, 1992). The current characteristics are given in Figure 2.7.

### **2.3.4 Meteorology**

Meteorological data were obtained from a nearby station in Aliğa. The Aliğa Meteorological Station was about 10 km away from the plant site. A summary of the meteorological data obtained from this station is presented in Table 2.5.

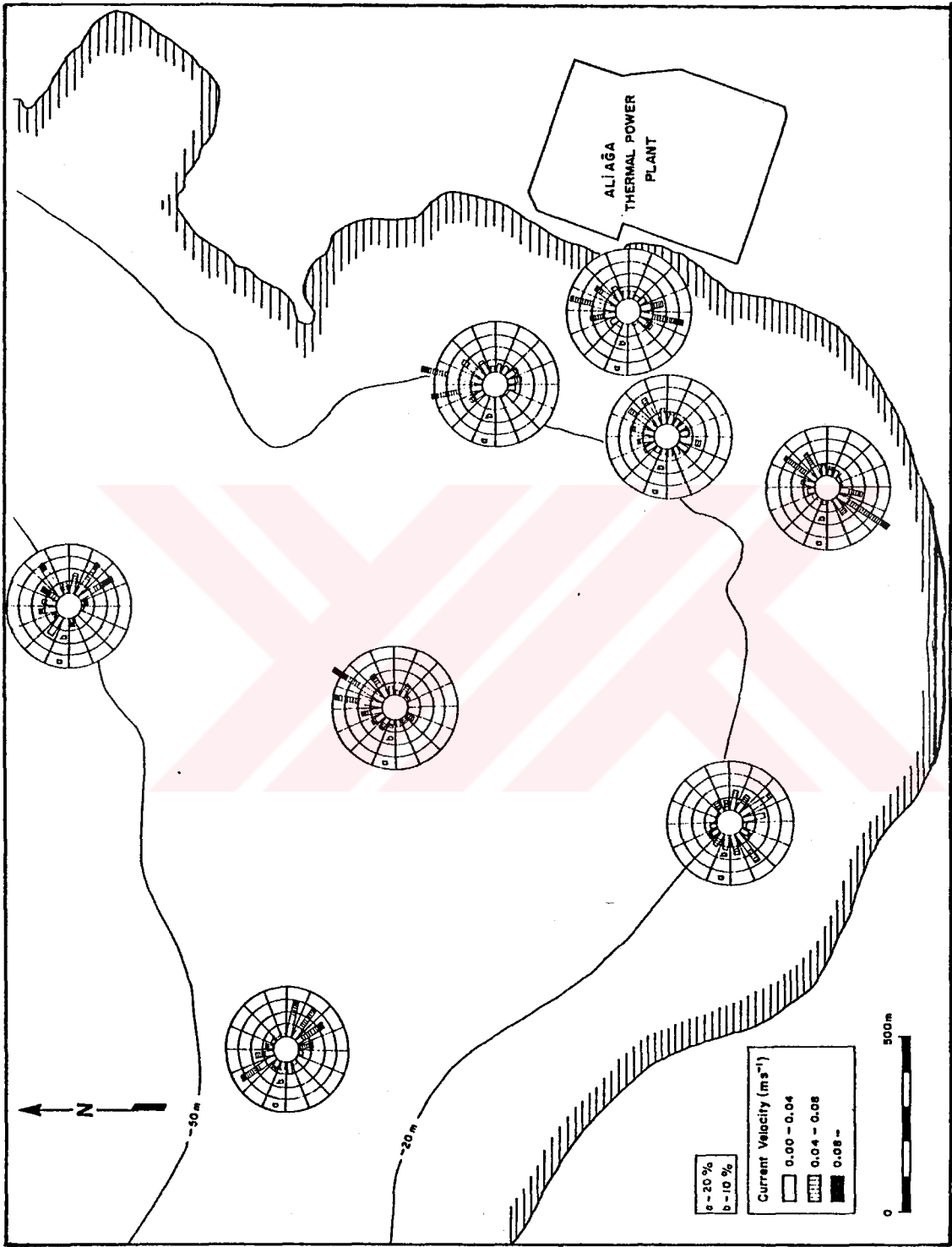


Figure 2.7. Sea Current Characteristics of the Gencelli Harbor

**Table 2.5. Annual Percentage Frequency of Wind Speed Classes and Directions (1988-1989)**

	Wind Direction							
Wind Speed	N	NE	E	SE	S	SW	W	NW
0.9-1.5	1.1	1.3	2.3	4.2	0.9	2.3	2.4	1.6
1.5-2.0	1.5	3.3	6.0	4.0	2.5	2.5	2.6	2.5
2.0-3.0	2.4	6.4	6.3	2.9	2.1	1.8	1.8	2.4
3.0-4.0	1.1	5.7	3.5	1.7	1.4	1.3	1.2	1.4
4.0-6.0	0.7	7.5	2.3	0.6	0.6	1.0	0.6	0.6
6.0-10.0	-	0.9	-	0.2	0.1	0.3	-	-
TOTAL	6.8	25.1	20.4	13.6	7.6	9.2	8.6	8.5

### 2.3.5 Sea Water Quality

The sea water quality data of the Gencelli Harbor was obtained from the surveys conducted by Dokuz Eylül University (DEU), Marine Sciences and Technology Institute and Ege University (EU), Biology Department. The former study was conducted between 1988 and 1991. The later study was conducted between June and September of 1991. The details and methodology of the surveys were given in the reports relevant to the surveys (Akyarlı, 1990,1991).

For the purpose of dilution and dispersion modeling, the most important physical parameters are salinity and temperature of sea water. There is no important freshwater runoff into this embayment. Salinity in the Gencelli Harbor is about ‰ 39. In the summer months, sea water temperature can rise upto 22-23 °C. Furthermore, there is little or no salinity and temperature stratification (Akyarlı and Arısoy, 1988). The sea water quality characteristics of the Harbor are summarized in Table 2.6.

Table 2.6. Sea Water Quality Parameters of the Gencelli Harbor

Parameter	Observed Range	Value at 20 m Depth
pH	8.23-8.32	8.28-8.31
DO (mg l <sup>-1</sup> )	7.2-8.5	8.0-8.5
SS (mg l <sup>-1</sup> )	9.6-15.9	10.5
Oil and other floatables (mg l <sup>-1</sup> )	≤ 0.009	-
Turbidity (NTU)	1.4-5.1	1.5-1.6
Phenol (mg l <sup>-1</sup> )	0.0-6.2	4.6
Hg (ng l <sup>-1</sup> )	0.0-67.0	67.0
Cr (µg l <sup>-1</sup> )	Not detected	-
Pb (µg l <sup>-1</sup> )	2.8-8.7	5.6
Zn (µg l <sup>-1</sup> )	20.0-70.0	47.0
Ni (µg l <sup>-1</sup> )	3.6-6.7	-
Cu (µg l <sup>-1</sup> )	1.4-8.3	4.1
As (µg l <sup>-1</sup> )	4.0-8.0	-
Fe (µg l <sup>-1</sup> )	101.0-159.0	159.0
Mn (µg l <sup>-1</sup> )	66.9	66.9
Petroleum Hydrocarbons (µg l <sup>-1</sup> )	2.1-9.8	-
Orthophosphate (µg l <sup>-1</sup> )	0.8-2.1	1.6
Nitrate-N (µg l <sup>-1</sup> )	2.0-4.3	3.9
Nitrite-N (µg l <sup>-1</sup> )	< 1.0	0.08
Ammonia-N (µg l <sup>-1</sup> )	< 1.0	-
Total organic Nitrogen (µg l <sup>-1</sup> )	2.5-4.8	-
Faecal coliforms (#/100 ml)	18-250	-

The values in the table are a combination of the surveys conducted by DEU and EU. The minimum and maximum values measured in the Harbor are given in the table. All the sea water quality parameters measured in the Gencelli Harbor were typical for an unpolluted marine environment (ATPP EIA Phase-2 Report, 1992). Nevertheless, as can be seen from the table at certain points of the harbor (ATPP EIA Phase-2 Report, 1992):

- Phenol concentrations were just above the value of 5µg/l stated in Turkish standards.
- Hg concentrations were above the typical Mediterranean level of 10 ng/l.
- Pb concentrations were above the typical Mediterranean level of 0.05 µg/l.
- Zn concentrations were above the expected background levels of 1-2 µg/l.
- Ni concentrations were above the values stated in the literature.

#### **2.3.6 Bottom Sediment Quality**

According to the studies of EU, conducted in June to September of 1992, the sea bottom foundation rock near the plant site is tuff covered with marine sand and gravel near the shoreline and with marine mud at offshore areas. Sediment samples were collected from 5 different points and subjected to heavy metal analysis. The targeted metals in the analyses include Fe, Zn, Cu, Pb, Cd, Mn. The results of the analysis are summarized in Table 2.7.

**Table 2.7. Sediment Quality of the Gencelli Harbor (Heavy metal dry weight, µg/g)**

	Sample No.					
Metal	1	2	3	4	5	Ave.
Fe	6699.0	13478.4	6252.00	16604.5	15631.0	11732.8
Zn	40.53	40.53	42.15	38.60	40.53	40.47
Cu	10.36	7.40	4.62	1.49	4.44	5.66
Pb	23.33	25.82	18.66	19.41	21.08	21.66
Cd	1.595	1.283	1.276	4.644	0.640	1.887
Mn	174.6	311.0	119.9	132.4	225.5	192.7

## **2.4 Plant Site Biological Environment**

### **2.4.1 General**

One of the key points of a marine impact assessment study is the collection of baseline data on the marine biology. For this purpose, two on-site surveys were conducted by Ege University, Biology Department. These surveys were conducted between 6<sup>th</sup> and 11<sup>th</sup> June of 1990, and, between July and September of 1991.

The study area for the marine biology baseline studies were limited to the area below the hypothetical line drawn from Taşlı Burun to Yesilburun. This area covers the Gencelli Harbor. Locations of the sampling stations are depicted in Figures 2.8, 2.9, 2.10, and 2.11.



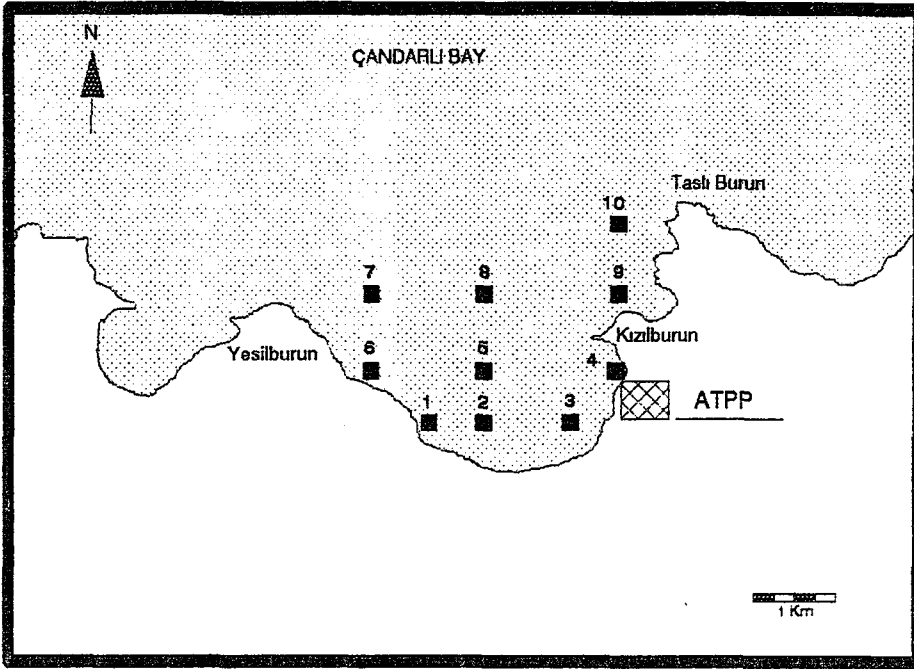


Figure 2.8. Locations of Marine Biology Sampling Stations of 1990 Spring Studies

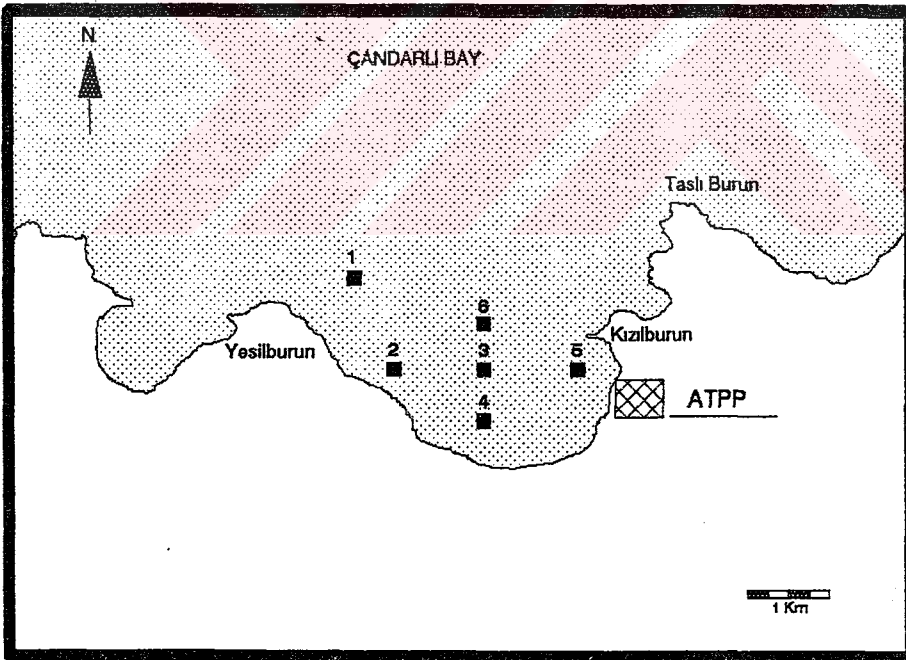


Figure 2.9. Locations of Marine Biology Sampling Stations of 1991 Autumn Studies

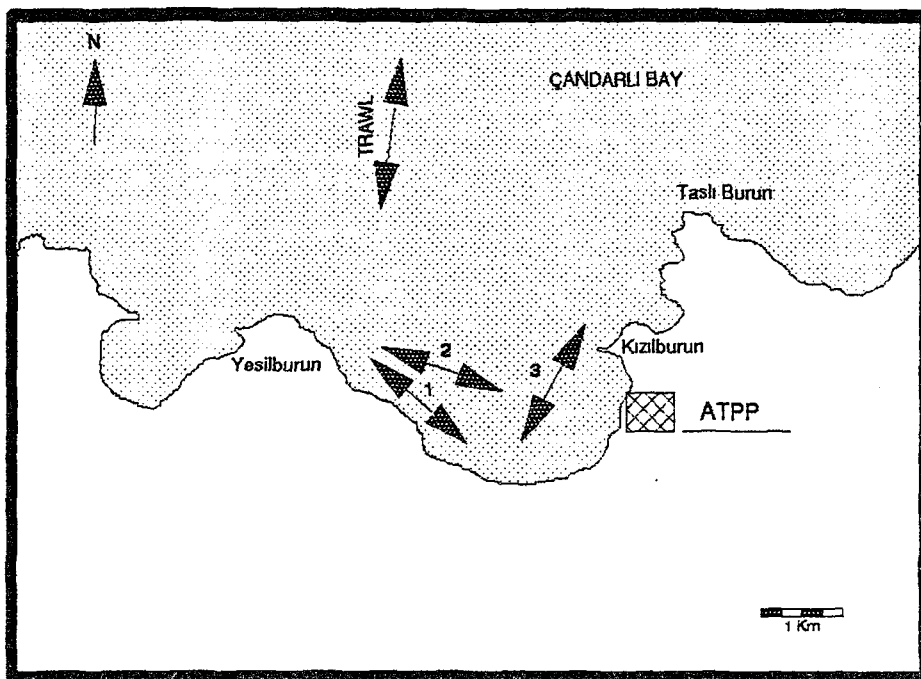


Figure 2.10 Trawl Routes (1991)

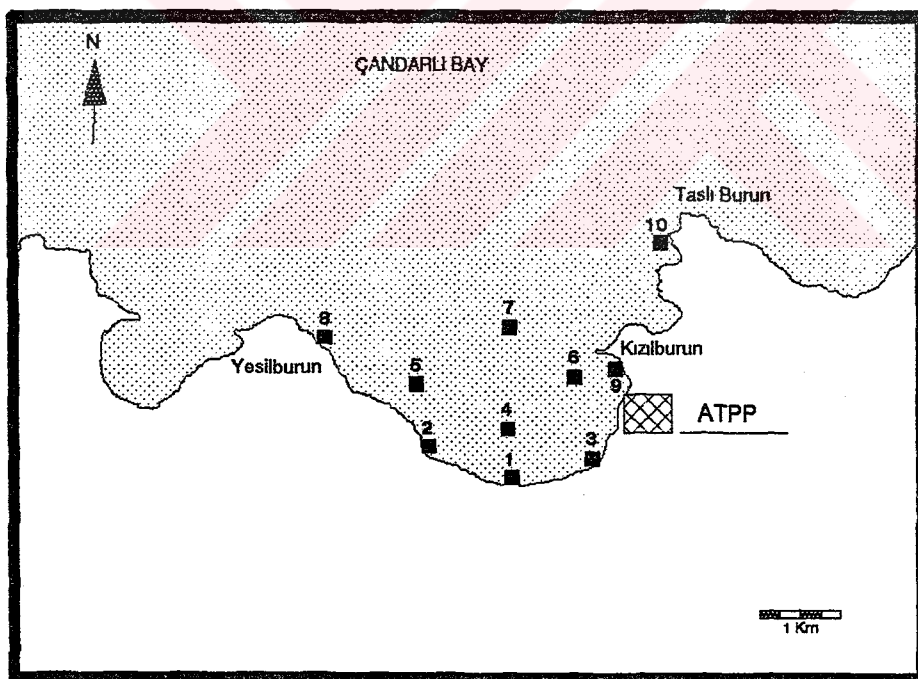


Figure 2.11 Location of Zoobenthos Sampling Stations (1991)

The studies concentrated on the determination of the species and their distribution in the Gencelli Harbor. The studies also included the measurements of heavy metal concentration in certain indicator species. The following ecosystem components were targeted in the surveys:

- fish
- ichtioplankton
- algae
- phytoplankton and protozooplankton
- zooplankton
- zoobenthose

Full details of the studies, the methods and equipments used were given in ATPP EIA Phase-2 Report (1992).

#### **2.4.2 Fish Species of the Gencelli Harbor**

A total of 77 species of fish were observed during the studies. These species are listed in Table A.1 of Appendix A. The trawl and beam trawl routes used for determination of fish species are depicted in Figure 2.10. The sampled fish species are good examples for a typical Mediterranean fish fauna. It is possible that the number of some benthic and pelagic species in the Gencelli Harbor might have been underestimated because of the facts that:

- the sea bottom was not suitable for bottom trawl except some places; and
- the duration of survey was relatively short.

### 2.4.3 Ichtioplankton Species of the Gencelli Harbor

Ichtioplankton (egg and larvae of fish) sampling studies were conducted at the stations depicted in Figures 2.8 and 2.9. The list of the fish larvae and eggs observed in the Gencelli Harbor are given in Tables A.2 and A.3 of Appendix A, respectively. The results of the study conducted in 1991 are summarized below (See Figure 2.9):

- Larvae of 28 different fish species were collected in the June-September period and 18 of these were teleost larvae.
- Richest station in terms of number of eggs was No. 6 (120 eggs).
- Richest station in terms of number of larvae was No.2 (49 individuals).
- Richest stations in terms of diversity of eggs were those that were located at the middle of the Harbor.
- Richest in terms of diversity of larvae were those that were located on the shallow regions close to the western shore of the Harbor.

Based on the results listed above it was concluded that the shallow regions were used by larvae for breeding. The only exception of this conclusion was the station No.5 which was on the proposed location of the intake and discharge structures. This condition may be attributed to the fact that eastern region was relatively poor in terms of both food and number of individuals. The following results were also obtained in the surveys:

- The most dominant species in terms of eggs were *Diplodus annularis* (annular gilthead), *Arnoglossus laterna* (scaldfish) and *Engraulis encrasicolus* (anchovy).

- The most dominant species in terms of larvae were *D. annularis*, *E. encrasicolus* and *Gobius niger* (black goby).

Most probably, the dominance of *D. annularis* and *A. laterna* eggs and larvae in the study area resulted from the fact that the study region served as ideal biotope for these species and that Autumn was their spawning season (ATPP EIA Phase-2 Report, 1992). Very few eggs could be collected in Autumn belonging to the school-forming pelagic fish. The only species observed of this type was *E. encrasicolus*. The eggs of this species were rarely observed in spite of the fact that it was its spawning season. This implies that *E. encrasicolus* species spawn in deeper regions around 30-100 m depth out of the study area (ATPP EIA Phase-2 Report, 1992).

The species discussed above were not primarily important in terms of commercial value. The ichtioplankton of two relatively important species from the commercial point of view, *Sparus aurata* (gilthead) and *Dicentrarchus labrax* (bass) were not observed in the study area. This is probably due to the fact that the spawning period of these fishes is the winter months (ATPP EIA Phase-2 Report, 1992).

#### 2.4.4 Benthic Algal Species of the Gencelli Harbor

The benthic algal species of the Gencelli Harbor are presented in Table A.4 of Appendix A. It was observed that the most abundant species in the study area was the *Posidonia oceanica* (sea grass). Sea grass, being extremely sensitive to any form of pollution, serves as an excellent indicator of impacts on coastal marine environments. Maximum and minimum number of taxa were sampled at station 10 and 5, respectively (see Figure 2.9).

#### 2.4.5 Phytoplankton and Protozooplankton of the Gencelli Harbor

36 species of Dinophyceae, 23 species of Bacillariophyceae, 5 species of Ciliata and 2 species of Radiolaria were observed in the Gencelli Harbor during the surveys. The phytoplankton and protozooplankton species observed in these surveys are presented in Table A.5 of Appendix A.

The results of the field surveys showed that there was partial eutrophication in the study area. It was reported that no anthropogenic effects were observed in the system which was in equilibrium (ATPP EIA Phase-2 Report, 1992). No toxic species were observed except for *Nocticula scintillans* which is not a major source of risk in terms of biotoxicity.

Some *Gonyaulax* cysts were observed in the planktonic samples in the surveys. This showed that the benthic structure was suitable for rising of the benthic cysts in the water column by a turbulence effect. It was pointed out that in the case of a destruction of the planktonic equilibrium phase there existed a risk for such catastrophic conditions as red-tide (ATPP EIA Phase-2 Report, 1992).

It was also reported that there was little, if any, variation in species diversity with depth and station location (ATPP EIA Phase-2 Report, 1992). The planktonic community structure observed in the area was a typical example for the Aegean Sea.

#### 2.4.6 Zooplanktons of The Gencelli Harbor

The zooplanktonic species of The Gencelli Harbor are tabulated in Table A.6 of Appendix A. The results of the surveys are summarized below:

- In terms of number of species, the most dominant groups were Copepoda, Decapoda, Hydrozoa, Appendicularia and Cladocera in descending order.
- In terms of number of individuals, richest stations were No.3, 2, 6, 5, 4 and 1.
- In terms of number of individuals, the most dominant groups were Copepoda, Cladocera and Mollusca in descending order.
- In terms of number of individuals, the most dominant species were *Oncaea sp.*, *Podon polyphemoides*, *Clausocalanus furcatus*, *Paracalanus parvus*, *Euterpina acutifrons*, *Oithona plumifera* and *Centropages typicus*.

During the surveys, it was observed that the number of species increased at deeper parts probably due to the nutrient-rich off-shore currents.

#### 2.4.7 Zoobenthic Fauna of the Gencelli Harbor

The zoobenthic species observed in the surveys are given in Table A.7 of Appendix A. The following results were obtained during the surveys (see Figure 2.11):

- The most dominant groups were Polychaeta and Crustacea.
- In terms of number of species, the richest station was No. 10.
- In terms of number of species, the poorest station was No. 3 which was located near the proposed plant site.
- A total of 166 species were sampled at the central stations No. 4, 5, 6 and 7, which represent sandy and muddy biotopes covered with *Posidonia* (sea grass).

- A total of 173 species were sampled at the coastal stations which represent rocky, stony and often gravel biotopes covered with *Cystoseria* and *Padina* species dominated algae species.
- On the stony parts of the coastal regions *Posidonia oceanica* and *Zoostera sp.* communities were observed.

It may be concluded that the biotopes of the Gencelli Harbor are suitable for zoobenthic organisms. Several fouling organisms were also observed in the study area. Among these were, *Pomatoceros triquetus*, *Hydroides pseudouncinata*, *Spirobranchus polytrema*, *Vermilopsis infundibulum*, *Balanus perforatus*, *Balanus sp.*, *Chthamalus stellatus*, *Mytilus galloprovincialis*, *Modiolus barbatus*, *Sertella sp.*, *Membranipora sp.*, *Cyrtosula sp.*, *Porella sp.*, *Cellopora cf. pumicosa*, *Tubucellaria opuntioides*, *Ascidia sp.* and *Botryllus schlosseri* (ATPP EIA Phase-2 Report, 1992).

#### 2.4.8 Heavy Metals in the Marine Organisms of the Gencelli Harbor

The concentrations of such heavy metals as Cu, Fe, Zn, Cd, Pb, Mn and Hg were measured by EU in some algal, fish and benthic invertebrate species. The results of these measurements are given in Table 2.8.

It can be concluded that all the metal concentrations except of Fe (iron) was around the values obtained in unpolluted coastal areas (ATPP EIA Phase-2 Report, 1992). As in the case of sediments, the Fe concentration is relatively high in some species like *Patella sp.* and *Monodonta sp.* This is most probably due to the activities of the existing metal works and ship dismantlers located in the vicinity of the proposed plant site.



Table 2.8 Heavy Metal Concentrations in Some Species of the Gencelli Harbor

Species	Metal Concentration ( $\mu\text{g g}^{-1}$ - wet weight)						
	Fe	Zn	Cu	Pb	Cd	Mn	Hg-t
<i>C. barbata</i>	114.190	14.690	12.170	9.110	0.750	2.840	n. d.
<i>C. fimbriata</i>	9.590	6.180	8.850	4.200	0.750	4.130	n. d.
<i>Patella sp.</i>	116.725 - 220.230	9.705 - 27.860	1.790 - 6.050	1.535 - 5.185	0.178 - 0.750	0.710	0.030 - 0.265
<i>Ulva sp.</i>	89.970	22.690	12.930	8.970	1.230	38.830	n. d.
Mackarel	2.280 - 18.365	2.960 - 10.615	0.355 - 1.400	0.190 - 3.990	0.013 - 0.340	n. d.	0.080 - 0.223
<i>Sardina pilchardus</i>	3.025 - 87.275	5.050 - 17.015	0.375 - 1.400	0.100 - 0.210	0.035 - 0.210	n. d.	0.063 - 0.410
<i>Monodonta turbinata</i>	59.425 - 458.450	10.120 - 20.195	9.775 - 20.910	4.935 - 10.215	0.225 - 0.745	n. d.	0.020 - 0.118
<i>Mytilus galloprovincialis</i>	35.060 - 93.205	16.630 - 42.445	0.845 - 3.200	1.100 - 6.490	0.055 - 0.463	n. d.	0.025 - 0.178
<i>Trachurus trachurus</i>	4.315 - 38.300	3.300 - 6.675	0.455 - 2.215	0.310 - 1.400	0.015 - 0.165	n. d.	0.030 - 0.225

n.d. : not determined

## **2.5 Potential Risks and Their Sources**

### **2.5.1 General**

A brief schematical representation of the hydrobiological effects of thermal power plants are given in Figures 1.1 and 2.12. The effects may appear due to the following operations:

- cooling water operations;
- liquid waste discharge; and
- marine transportation facilities.

These operations may change the physical and chemical properties of the marine environment. (see Chapters 3 to 5). A change in the physical and chemical properties of sea water may affect marine biology negatively or positively. Potential biological effects are discussed in Chapters 6 and 7.

### **2.5.2 Effects Due to Cooling Water Operations**

In electric power generation with once-through cooling system, vast amount of water is drawn from sea. The cooling water is returned back to sea with a relatively higher temperature and antifouling chemicals. Marine species may be affected by a once-through cooling system of a thermal power plant in one or more of the following ways:

- entrapment
- impingement
- entrainment
- intermittent contact with thermal plume
- far-field exposure to altered sea water quality

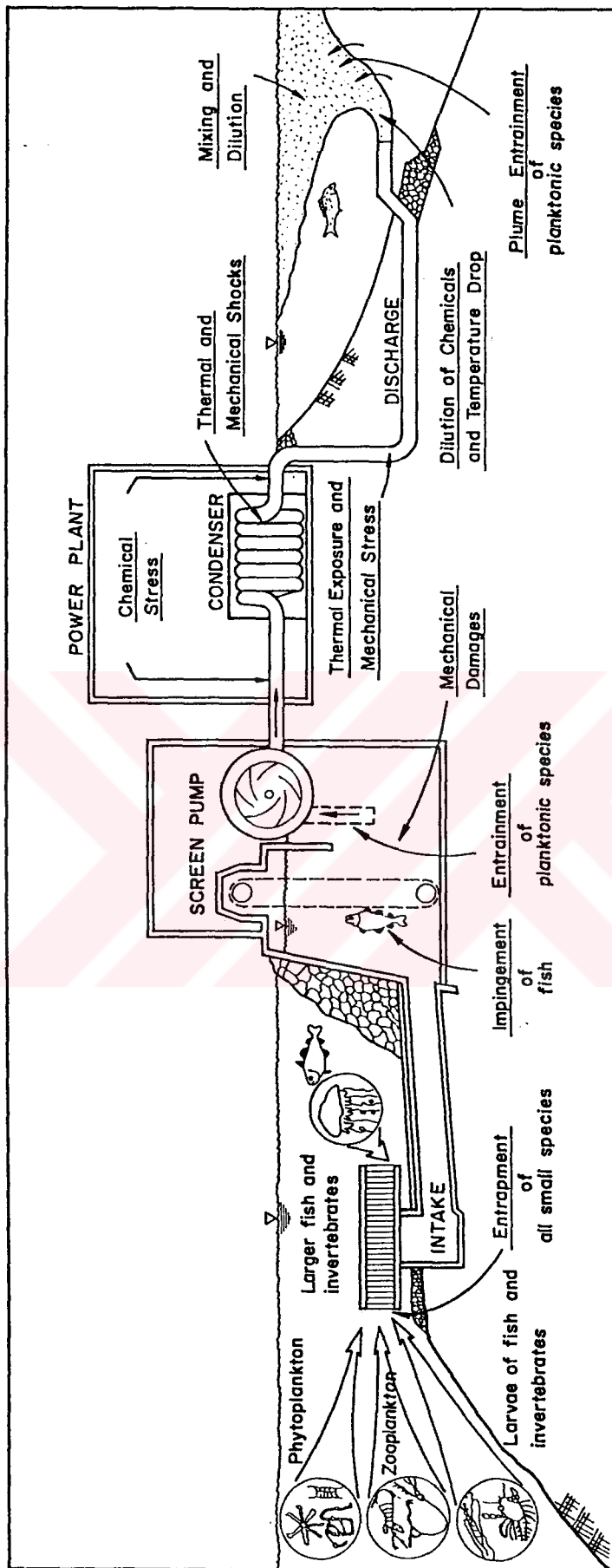


Figure 2.12. Effects of Thermal Power Plants on Marine Environment

(reproduced from Kirk, 1981)

#### **a. Entrapment**

Smaller organisms including planktonic organisms and small fish can be drawn into the condenser with the cooling water (see Figure 2.12). This process is called entrapment. The fish species large enough to withstand the inflow can return back to the marine water-body.

#### **b. Impingement**

The smaller of the entrapped fish species which cannot withstand the inflow are drawn onto the fine screens and subjected to physical stress. As illustrated in Figure 2.12, this direct action of hitting to the fine screens and experiencing physical damage is termed as impingement.

#### **c. Entrainment**

Planktonic species can pass through the fine screens of the plants. These species are drifted with the cooling water and are subjected to mechanical, thermal and chemical stresses in various points of the cooling water system. This action is called entrainment (see Figure 2.12). The stresses and the effects experienced by the entrained organisms are discussed in Chapter 6, in detail.

#### **d. Intermittent Contact With the Thermal Plume**

Aquatic organisms may also be affected by cooling water operations without being entrained or entrapped. They can come in contact with either the elevated temperature or chemicals in the plume discharged into the receiving environment (see Figures 1.1 and 2.12).

#### **e. Far-field Exposure to Altered Sea Water Quality**

Warming of the receiving waterbody may affect the metabolic reactions of the organisms in the environment. Further, some species may be under the risk of cold-shock, after the plant shut downs. The antifouling chemicals used to prevent biofouling in the cooling water system, if not sufficiently diluted, may also affect the sea water quality and hence various organisms. The details of such effects are given in Chapter 6.

All of the risks summarized above and the contribution of various stresses to those risks greatly vary due to the design features of different systems and the characteristics of site.

#### **2.5.3 Liquid Waste Discharge**

The industrial and domestic wastewaters of thermal power plants include many chemical and biological pollutants. Depending on the degree of treatment, discharge of these wastewaters is a potential risk to the marine environment.

#### **2.5.4 Marine Transportation**

The major and auxiliary fuels needed for power generation (coal, heavy and light oils) are usually delivered via marine shipping to an off-shore wharf. In such cases, marine vessels are a potential risk, if appropriate measures are not taken for spills and wastewater discharges which are very variable in content. In addition, appropriate measures should be taken while constructing off-shore wharfs.

## CHAPTER III

### LIQUID WASTE DILUTION AND DISPERSION MODELING STUDIES

#### 3.1 General

Wastewater disposal into marine environment is a potential risk especially for coastal areas. However, the discharged wastewater can be sufficiently diluted so that the concentration of pollutants at the potentially sensitive areas will not exceed certain critical levels stipulated by standards or guidelines. The degree of dilution and dispersion should be predicted, for a proper design of disposal facilities.

Liquid waste dilution and dispersion modeling studies of the proposed ATPP include the estimation of certain criteria required by the Turkish Water Pollution Control Regulation (TWPCR) (Official Gazette # 19919, dated 4.9.1988). For deep-sea discharges, the TWPCR states that:

- initial dilution,  $S_1$ , should preferably be higher than 100 but not less than 40;
- minimum discharge depth should be 20 m
- $T_{90}$  value should be taken as at least 1.5 hours for the Aegean and the Mediterranean Sea, and, 2 hours for the Black Sea in the summer months; and,
- $T_{90}$  values can be taken as 3 to 5 hours on the average in the winter months.

In the Administrative Procedures Notice of the TWPCR (Official Gazette # 20106, dated 12.3.1989), it is required that all the project characteristics including the values of initial dilution ( $S_1$ ), dilution due to dispersion ( $S_2$ ) and due to bacterial decay ( $S_3$ ), and,  $T_{90}$  should be included in the application documents.  $T_{90}$  is defined as the time elapsed until 90 % of bacteria in a certain amount of wastewater disappears.

The treated liquid wastes of the proposed ATPP will be discharged into the Gencelli Harbor via a deep-discharge structure. The liquid wastes include power house general wastewater, effluent from the flue gas desulfurization unit, domestic sewage, and runoffs from the plant yard, and, coal storage area.

Two alternatives were considered for the discharge type; namely, horizontal and vertical. Three near and far-field models were used for the purpose of predicting the  $S_1$ ,  $S_2$ ,  $S_3$  and  $S_{total}$  values for the liquid waste discharges of the proposed ATPP. These models were:

- a near-field model developed by Cederwall to predict  $S_1$  for horizontal discharges (Cederwall model);
- a near-field model developed by Hayashi and Ito to predict  $S_1$  for vertical discharges (Hayashi and Ito model);
- a far-field model, developed by Brooks to predict  $S_2$  (Brooks model); and,
- first-order decay kinetics to predict  $S_3$ .

Both near-field models are applicable in stagnant environment. Such a condition will yield minimum initial dilution and, therefore, conservative results. For the sake of convenience, a computer program was developed to apply these models more efficiently.

## 3.2 Theoretical Background

### 3.2.1 General

When discharged into a marine environment from a submarine outfall, wastewater is usually in the form of a turbulent jet. This jet have momentum due to the discharge velocity, as well as buoyancy due to the difference between the densities of the ambient sea water and the wastewater.

The momentum and buoyancy decreases as the jet rises to the sea surface. During this motion, the ambient sea water mixes with the wastewater due to free turbulence which is a result of the shear stresses at the boundary between the jet and the ambient sea water. As the ambient water is entrained into the jet, the pollutants in the wastewater become diluted.

At the point where the density of the jet is nearly equal to that of the ambient water, upward motion of the jet is completed and a wastewater field starts to developed. Initial dilution,  $S_1$ , is the dilution process occurred at the trajectory of the jet until the rising motion of the jet is completed.

Due to the degree of density stratification in the marine environment, a wastewater field may develop at the surface or below the surface. The field is further diluted and dispersed by the natural turbulence and currents of the receiving environment. Further dilution due to natural turbulence and currents is termed as "secondary dilution" or "dilution due to dispersion" ( $S_2$ ).

Liquid wastes, domestic wastes in particular, include high concentrations of coliform bacteria. The concentration of bacteria in the plume decreases due to diffusion, die-away, flocculation and sedimentation processes.



The dilution resulting from the change in the concentration of coliform bacteria is termed as dilution due to bacterial decay ( $S_3$ ).  $S_3$  is a function of both time and the parameter  $T_{90}$ .

### 3.2.2 Initial Dilution ( $S_1$ )

Both models use the jet Froude number as the determining factor of the trajectory or the curvature of jet, by neglecting the zone of flow establishment (Cederwall, 1968). The jet Froude number (for a non-stratified environment) is given by the following formula (Cederwall, 1968):

$$F = \frac{u_o}{\sqrt{\frac{|\rho_a - \rho_o|}{\rho_o} \cdot g \cdot D_o}} \quad (3.1)$$

where;

- $F$  : jet Froude number (dimensionless)
- $u_o$ : discharge velocity ( $\text{m s}^{-1}$ )
- $\rho_a$ : ambient water density ( $\text{kg m}^{-3}$ )
- $\rho_o$ : initial density of jet fluid ( $\text{kg m}^{-3}$ )
- $g$  : gravitational acceleration ( $\text{m s}^{-2}$ )
- $D_o$ : diameter of the discharge ports (m)

Stratified environments, on the other hand are represented by superimposed, homogenous layers which have distinct mean density values. The modified Froude number for a stratified environment is given by the following formula (Cederwall, 1968):

$$F_I = u_o \sqrt{\frac{i \cdot \rho_o}{\sum_{j=1}^i |(\rho_{a,j} - \rho_o)| \cdot g \cdot D_o}} \quad (3.2)$$

where;  $i$  : layer number

$\bar{\rho}_{a,i}$ : mean ambient density of layer  $i$   
( $\text{kg m}^{-3}$ )

$F_i$  : modified Froude number for layer  $i$

The density of the jet at the axis of each layer can be calculated by the following equation (Cederwall, 1968):

$$\rho_{m,i} = \bar{\rho}_{a,i} - \frac{S_{m,i-1}}{S_{m,i}} \cdot (\bar{\rho}_{a,i} - \rho_{m,i-1}) \quad (3.3)$$

where;  $S_m$  : centerline (minimum) dilution at layer  $i$

$\rho_{m,i}$ : jet fluid density at centerline of layer  $i$  ( $\text{kg m}^{-3}$ )

The formulation used in the estimation of the centerline dilution (also called minimum dilution,  $S_m$ ) for the horizontal and vertical discharges is given below:

#### a. Horizontal Discharge (Cederwall Model)

The centerline dilution formulation for a non-stratified environment is given below (Cederwall, 1968):

$$S_m = 0.54 \cdot F \cdot \left( \frac{z}{D_o \cdot F} \right)^{7/16} \quad \text{if } \frac{z}{D_o} < 0.5 \cdot F \quad (3.4)$$

$$S_m = 0.54 \cdot F \cdot \left( 0.38 \cdot \frac{z}{D_o \cdot F} + 0.66 \right)^{5/3} \quad \text{if } \frac{z}{D_o} \geq 0.5 \cdot F \quad (3.5)$$

where;  $S_m$ : centerline (minimum) dilution

$z$  : vertical distance from discharge (m)

The centerline dilution formulation for a stratified environment is given below:

$$S_{m,i} = 0.54 \cdot F_1 \cdot \left( \frac{z_1}{D_o \cdot F_1} \right)^{7/16} \quad \text{if } \frac{z_1}{D_o} < 0.5 \cdot F_1 \quad (3.6)$$

$$S_{m,i} = 0.54 \cdot F_1 \cdot \left( 0.38 \cdot \frac{z_1}{D_o \cdot F_1} + 0.66 \right)^{5/3} \quad \text{if } \frac{z_1}{D_o} \geq 0.5 F_1 \quad (3.7)$$

where;  $S_{m,i}$ : centerline dilution at layer i  
 $z_1$  : vertical distance from discharge to top of layer i (m)

In constructing the computer program for the prediction of  $S_1$ , a uniform stratification was assumed and its degree was represented by a slope term. As a rule of thumb, the plume width is generally assumed to be 1/3 of the discharge depth for a non-stratified environment.

#### b. Vertical Discharge (Hayashi and Ito Model)

In the case of a vertical discharge, a different model is necessary. For this purpose, it was decided to use a model which was developed by Hayashi and Ito (1974). The main equation used in the model is given below (Hayashi and Ito, 1974):

$$S_m = \beta \left( \frac{2\beta F^2}{16\beta F^2 - 3} \right)^{-1/3} \left( \frac{z}{D_o} + \frac{1}{4\beta} \right) \left( 1 + \left( \frac{48\beta^2}{16\beta F^2 - 3} \right) \left( \frac{z}{D_o} + \frac{1}{4\beta} \right)^2 \right)^{1/3} \quad (3.8)$$

where;  $D_o$ : diameter of discharge port (m)  
 $S_m$ : centerline (minimum) dilution  
 $z$ : vertical distance from discharge (m)  
 $F$ : jet Froude number  
 $\beta$ : an empirical coefficient

According to Hayashi and Ito (1974),  $\beta$  can be assumed as 0.084. The plume width is then given by the following equation (Hayashi and Ito, 1974):

$$b=2\beta H \quad (3.9)$$

where;      b: width of plume (m)  
                $\beta$ : a coefficient  
               H: discharge depth (m)

### 3.2.3 Dilution Due to Dispersion ( $S_2$ )

A two-dimensional, steady-state far-field model which was developed by Brooks (Brooks model), was selected to predict the dilution due to dispersion ( $S_2$ ) for the proposed ATPP. The major assumptions of this model are summarized below (Grace, 1978):

- Vertical mixing is negligible.
- Mixing in the direction of current is negligible.
- The effluent has the same density with the ambient sea water.
- The lateral dispersion coefficient term is proportional to the 4/3 th power of the nominal plume width, L.

The main equation of Brooks model is given below (Grace, 1978):

$$S_2 = \frac{C_0^*}{C(x_1, 0)} = \frac{1}{\text{erf} \left( \sqrt{\frac{3/2}{(1 + \frac{2}{3}\beta \frac{x_1}{b})^3 - 1}} \right)} \quad (3.10)$$

where;  $S_2$  : ratio of dilution due to dispersion  
 $C_0^*$  : initial concentration of pollutant ( $\text{kg m}^{-3}$ )  
 $C(x_1,0)$ : pollutant concentration at any point along  $x_1$   
( $\text{kg m}^{-3}$ )  
 $x_1$  : spatial coordinate  
 $\beta$  : a dimensionless coefficient  
 $b$  : initial plume width (m)

The parameter,  $\beta$ , is given by the equation:

$$\beta = 12\epsilon_2^0 / u_1 b \quad (3.11)$$

where;  $\epsilon_2^0$ : initial dispersion coefficient at  $x=0$  ( $\text{m}^2 \text{s}^{-1}$ )  
 $u_1$ : current velocity along  $x_1$  direction  
( $\text{m s}^{-1}$ )

Based on Richardson's Law, the equation for initial dispersion coefficient is given as below (Grace, 1978):

$$\epsilon_2^0 = \alpha b^{4/3} \quad (3.12)$$

where;  $\alpha$  : a coefficient  
 $b$  : initial width of jet (m)

The approximate range for  $\alpha$  is in between  $0.0015$  and  $0.049 \text{ cm}^{2/3} \text{s}^{-1}$  (Koh and Brooks, 1975). For practical purposes,  $\alpha$  was taken as  $0.01 \text{ cm}^{2/3} \text{s}^{-1}$ , as recommended by various researches (Grace, 1978).

### 3.2.4 Dilution Due to Bacterial Decay ( $S_3$ )

The dilution due to bacterial decay ( $S_3$ ) is calculated by the following formula (Grace,1978):

$$S_3 = \frac{C_0^*}{C(x_1, 0)} = e^{-k \frac{x_1}{u_1}} \quad (3.13)$$

where;  $k$  : bacteria disappearance rate constant ( $\text{day}^{-1}$  or  $\text{hour}^{-1}$ )

In the case of coliform bacteria, the design value,  $k$ , can obtained from the  $T_{90}$  data.  $T_{90}$  value depends primarily on temperature, sunlight and salinity.  $T_{90}$  values range between 2 and 6 hours (Metcalf and Eddy, 1979). The relationship between  $k$  and  $T_{90}$  is given below (Grace, 1978):

$$k = \frac{2.3}{T_{90}} \quad (3.14)$$

## 3.3 Results

The details of the ATPP liquid waste discharge system are given in Figure 2.5 and Table 2.4. Based on the design parameters and sensitivity tests (see Appendix-B), the predictions of the dilution ratios,  $S_1$ ,  $S_2$  and  $S_3$  were made with the parameters listed in Table 3.1. Conservative values were selected for each parameter. The results of the modeling studies are summarized in Table 3.2. The conditions which will result in the highest pollution in the coastal region is represented with the term worst case. The predictions were made for both horizontal and vertical discharge alternatives. The parameters,  $S_2$  and  $S_3$ , were calculated for both the coastline and a distance of 200 m away form the coastline. Most of the recreation and sports

the conceptual line 200 m away from the coastline. There are different reported definitions and values for the extent of this zone (Sorensen and McCreary, 1990). In the case of Gencelli Harbor, the value of 200 m was selected.

Table 3.1. Prediction Parameters of Liquid Waste Discharge

Parameter	Summer	Winter
Flow rate ( $\text{m}^3 \text{s}^{-1}$ )	0.016	0.016
Port diameter (mm)	125	125
Discharge velocity ( $\text{m s}^{-1}$ )	1.3	1.3
Discharge depth (m)	20	20
Discharge to coastline distance (m) ( $x_1$ in Eqn. 3.13)	500	500
Measured average ambient sea water temperature ( $^{\circ}\text{C}$ )	22	14
Measured ambient sea water salinity (‰)	38	39
Estimated ambient sea water density ( $\text{kg m}^{-3}$ )	1026.5	1029.3
Assumed wastewater density ( $\text{kg m}^{-3}$ )	1000	1000
$T_{90}$ (hr)	1.5	4
Worst case current velocity ( $\text{m s}^{-1}$ )	0.1	0.1
Worst case current direction	East	East

**Table 3.2. Predicted Values for the Dilution Ratios for Liquid Waste Discharge**

Parameters	Summer		Winter	
Discharge Type	H'	V''	H'	V''
$S_1$	154.2	138.6	158.6	143.3
$S_2$ (Coast)	11.3	20.4	11.3	20.4
$S_2$ (200m)	6.1	10.6	6.1	10.6
$S_3$ (Coast)	8.4	8.4	2.2	2.2
$S_3$ (200m)	3.6	3.6	1.6	1.6
$S_{total}$ (Coast)	13550	22000	3500	5700
$S_{total}$ (200m)	3400	5300	1550	2400

\* H: Horizontal discharge

\*\*V: Vertical discharge

Two discharge alternatives for liquid wastes were investigated in this study. The results of the predictions showed that the initial dilution,  $S_1$ , achieved by a hypothetical horizontal discharge was slightly higher than that of a vertical discharge alternative. The secondary dilution,  $S_2$ , values of the hypothetical alternatives, however, were notably different. The estimated  $S_2$  values of the vertical discharge were about two times that of horizontal alternative. This was partially due to the the difference in the initial plume width (b) parameter predicted by the models. The plume widths were estimated with different approaches. The plume width of a hypothetical vertical discharge was lower than that of the horizontal alternative. As can be seen in Equation 3.11, the only parameter representing discharge characteristics is the plume width. Therefore, a smaller plume width represents:



- a smaller wastewater field, which is easy to be diluted; and,
- a higher ratio between the "contact area" and the "wastewater field volume", which results in a relatively rapid dilution.

However, in the assessment of the individual and total dilution ratios conservative results were used. In the case of the proposed ATPP, the advantage of a vertical discharge over a horizontal one is the flexibility of the former one under different sea current conditions. A horizontal discharge usually achieves a higher initial dilution. However, currents in opposite directions of the orientation of diffusers, significantly decrease the dilution efficiency of the discharge. Nevertheless, a vertical discharge structure is nearly free of the current direction effects. In the case of the ATPP, both types of discharge structures seem to be equally suitable.

### 3.4 Summary

As stated in Chapter 2, the liquid wastes of the proposed ATPP will be collected, treated and disposed to the Gencelli Harbor. The initial dilution ( $S_1$ ), dilution due to dispersion ( $S_2$ ) and bacterial decay ( $S_3$ ) of the wastewater deep sea discharge of the proposed ATPP were predicted for the purpose of impact assessment of the proposed plant.

The concentrations of all materials in the liquid wastes were proposed and stated to comply with the Turkish water quality standards (ATPP EIA Phase-2 Report, 1992). Using the proposed design parameters, it was found that the dilution ratios achieved by the liquid waste discharge system comply with the requirements in the Turkish environmental regulations. Therefore, no further investigation for the fates of pollutants was made in this study.

Several sensitivity runs were performed to test the sensitivity of the targeted parameter (dilution) to the variations in the input parameters (see Appendix B). Based on the results of the sensitivity tests, it can be concluded that the values of the parameters listed in Table 3.1 are conservative.

It was estimated that the minimum initial dilution,  $S_i$ , would be about 140. This value was an acceptable value according to the TWPCR. The total dilution was estimated for both at the coastline and a distance of 200m from the coastline. This distance was assumed to be the hypothetical border of a recreation zone. It was estimated that domestic wastewater would be diluted at least by a factor of 1550 at a distance of 200m away from the coastline, if discharged under the conditions presented in Table 3.1. To achieve the sea water quality standards in the area, the number of total coliforms in liquid waste effluents should not be above  $1.55 \times 10^6/100$  ml. Considering the conservative nature of the selected model parameters, the degree of treatment needs a further assessment following the plant start-up. Based on field measurements and statistical analysis of effluent characteristics, necessary precautions should be taken in the case of a violation of water quality standards.

## CHAPTER IV

### HYDROTHERMAL MODELING STUDIES: NEAR-FIELD

#### 4.1 General

Analyses of the near, intermediate and far-field thermal plume regions, by hydrothermal modeling studies, is necessary to assess potential environmental impacts due to waste heat discharge. Hydrothermal modeling studies of the proposed ATPP environmental impact assessment (EIA) study involved the following approaches:

- near-field analysis using semi-empirical models based on jet theory
- intermediate and far-field hydrothermal analysis using a three-dimensional, hydrodynamic and transport numerical model

The selection of the models used in this study were based on a criteria that the models should be well-accepted, field-tested and applied to similiar cases. This chapter outlines the application of two near-field dilution models to the case of the proposed ATPP.

Based on the orientation of the cooling water discharge structure of the proposed ATPP with respect to the coastline and the dominant currents, the diffuser of the ATPP can be considered as a tee diffuser. Various types of diffusers are depicted in Figure 4.1.

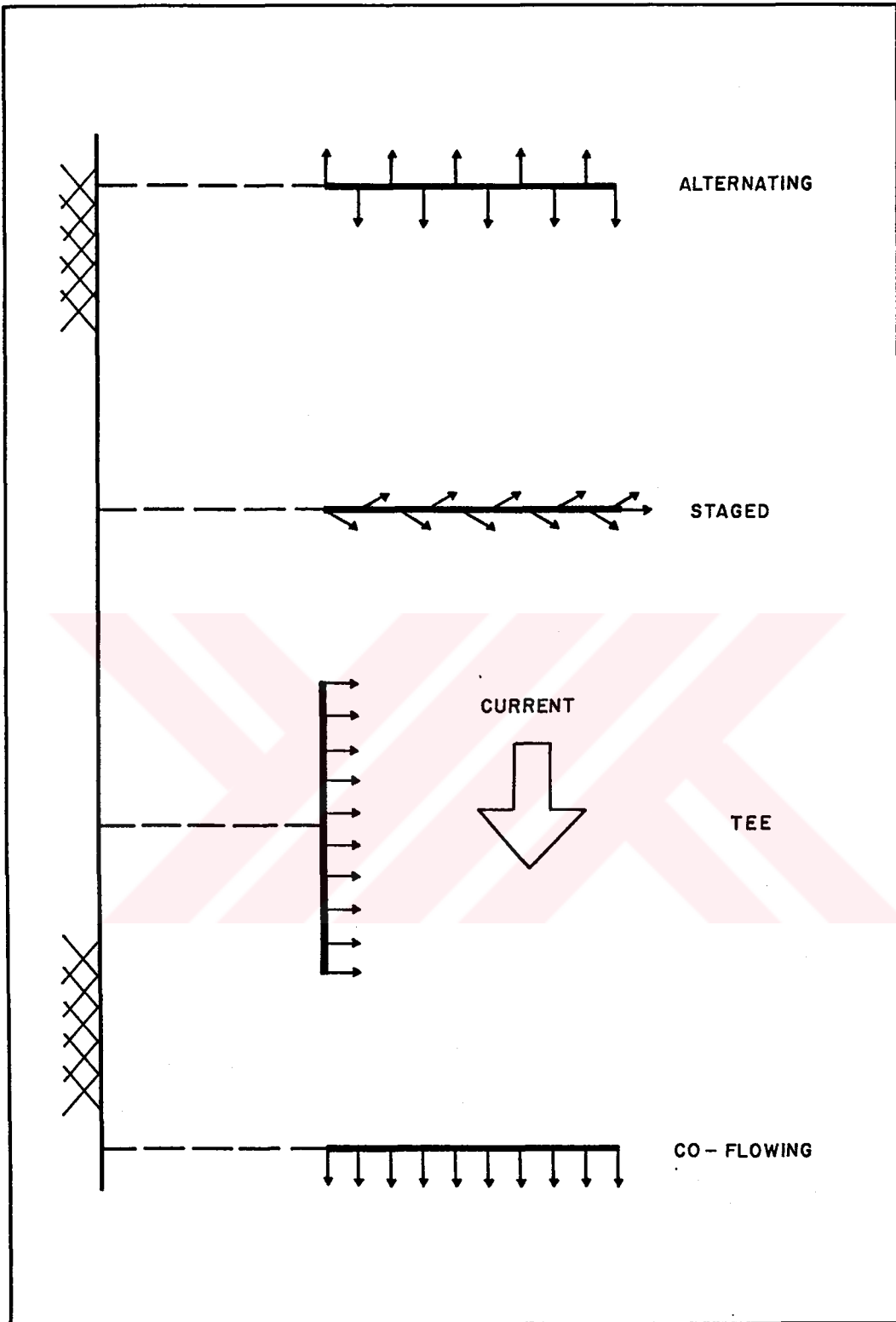


Figure 4.1. Diffuser types

The ports of a tee diffuser are oriented in a single direction normal to the dominant coastal current. In general, this is called cross-flowing orientation. The bidirectional current characteristics parallel to coastline at the proposed discharge area are given in Figure 2.7. Tee diffusers are more appropriate for such field conditions.

It is reported for tee diffusers in cross-flows that the increasing ambient current velocity has a reducing effect on the dilution of the jet (Adams and Stolzenbach, 1977; Stolzenbach et al., 1976; Adams, 1982). Regarding this fact, the near-field analyses were conducted for both:

- stagnant water; and,
- flowing water.

Two models were selected for the near-field analyses of the thermal discharge for these cases. The models were:

- a semi-empirical model developed by the Japanese Central Research Institute of Electric Power Industry (CRIEPI) for stagnant environment; and,
- a semi-empirical model developed by Adams for flowing environment (Adams model).

## **4.2 Prediction of Dilution in Stagnant Environment (CRIEPI Model)**

### **4.2.1 General**

The semi-empirical CRIEPI model has been used for various cases of single and horizontal warm jets in stagnant water. If the ports are sufficiently distinct so that no merging of the jets occurs, the analysis of a multi-port

discharge can be conducted on a single-port basis. The distance between the ports of the proposed ATPP cooling water discharge system are proposed to be 10 m. Based on the criteria given in Chapter 3, the individual plume widths were estimated to be about 3 m. Under these conditions, the CRIEPI model was deemed applicable to the case of the proposed ATPP. The model details of which is given elsewhere (ATPP EIA Phase-2 Report, 1992) can be used to predict:

- the dilution ratio (or temperature decay ratio) along the jet axis;
- the jet trajectory;
- spread width of the jet;
- thickness of the thermal field; and,
- maximum surface current velocity.

#### 4.2.2 Dilution Ratio Along the Jet Axis

The dilution of a warm jet along the jet axis,  $S_m$ , is a function of the amount of ambient water mixed into the jet.  $S_m$  depends on the ratio of vertical distance (from the point of discharge) to nozzle diameter ( $z/D_o$ ) and the jet densimetric Froude number ( $F$ ). Based on the regression analysis of the results of the experiments, the dilution ratio can be found by using the following expressions (ATPP EIA Phase-2 Report, 1992):

$$\log Y = -0.0346(\log X)^3 - 0.2155(\log X)^2 + 0.3202(\log X) + 0.1061 \quad (4.1)$$

where;  $X = (Z/D_o).F^{-1}$

$Y = (Z/D_o).S_m^{-1}$

$z$  : vertical distance from the point of discharge (m)

$F$  : jet Froude number

$S_m$ : the dilution ratio along jet axis

$$F = \frac{u_o}{\sqrt{\frac{\Delta \rho_o}{\rho_o} \cdot g \cdot D_o}} \quad (4.2)$$

where;

- $u_o$  : discharge velocity ( $\text{m s}^{-1}$ )
- $g$  : gravitational acceleration ( $\text{m s}^{-2}$ )
- $\Delta \rho_o$ : difference in densities of ambient water and wastewater at nozzle ( $\text{kg m}^{-3}$ )
- $\rho_o$  : initial density of wastewater ( $\text{kg m}^{-3}$ )
- $D_o$  : port diameter (m)

In terms of temperature, the dilution ratio,  $S_m$ , is given as follows (ATPP EIA Phase-2 Report, 1992):

$$S_m = \frac{(T_o - T_a)}{(T_m - T_a)} = \frac{\Delta T_o}{\Delta T_m} \quad (4.3)$$

where;

- $T_o$ : temperature of jet discharge ( $^{\circ}\text{C}$ )
- $T_m$ : temperature of jet along the jet axis ( $^{\circ}\text{C}$ )
- $T_a$ : temperature of ambient water ( $^{\circ}\text{C}$ )
- $\Delta T_m$ : difference between  $T_m$  and  $T_a$  ( $^{\circ}\text{C}$ )
- $\Delta T_o$ : difference between  $T_o$  and  $T_a$  ( $^{\circ}\text{C}$ )

#### 4.2.3 The Jet Trajectory

The horizontal and vertical coordinates of the jet trajectory can be found using Equation 4.4. The trajectory of the axis of a horizontal warm jet reaches further when the jet densimetric Froude number is larger.

$$z/D_o = 0.0493 (x/D_o)^3 F^{-2} \quad (4.4)$$

where;  $x$  : horizontal coordinate (m)

#### 4.2.4 Spread Width of the Jet

The width of a jet, discharged from a nozzle, increases gradually as the ambient water is entrained and mixed into the jet. The spread width of a jet can be defined from the velocity or temperature distributions in the direction normal to the jet axis.

Figure 4.2 shows the data plotted with  $x/D$  in the abscissa and the ratio of nominal half width to nozzle diameter,  $b'/D_o$ , in the ordinate. The nominal half width of  $b'$ , is the value of the characteristic length,  $b$ , multiplied by  $\sqrt{2}$ .

#### 4.2.5 Thickness of the Thermal Field

The thickness of the thermally stratified layer (thermal field), which develops when a warm jet reaches the surface, can be determined from vertical water temperature distribution. The thickness of the thermal field tends to increase as the jet densimetric Froude number gets larger and the submerged depth gets deeper.

Based on experiments, the relationship between the non-dimensional parameters of  $H/D_o$  and  $(h_w/D_o) \cdot F^{-0.5}$  are given by the following equation:

$$(h_w/D_o) F^{-0.5} = 0.09(H/D_o) \quad (4.5)$$

where;  $h_w$  : the thickness of the thermal field (m)



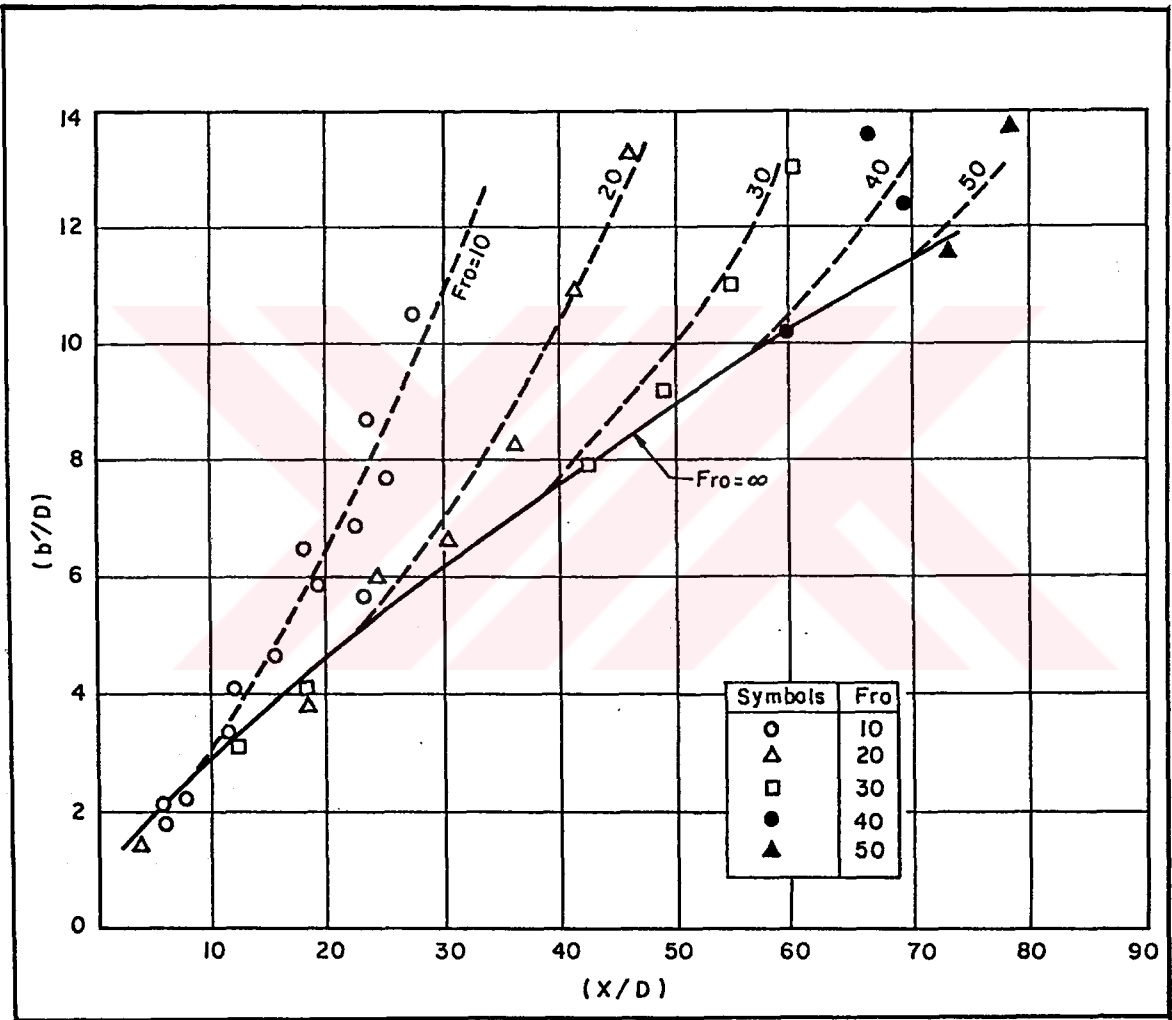


Figure 4.2 Spread Width ( $b'$ ) of Horizontally-Issued Warm Jet

#### 4.2.6 Maximum Horizontal Velocity at the Surface

The maximum surface velocity of the horizontal flow which develops when the warm jet reaches the surface, is given by the following equation (ATPP EIA Phase-2 Report, 1992):

$$\frac{u_s}{u_o} = 2.16 (H/D_o)^{-0.28} F^{-0.72} \quad (4.6)$$

where;  $u_s$  : maximum surface current velocity( $\text{m s}^{-1}$ )  
 $u_o$  : average discharge flow velocity ( $\text{m s}^{-1}$ )

### 4.3 Prediction of Dilution in Flowing Water (Adams Model)

#### 4.3.1 General

The predictions of dilution under the action of ambient currents were based on a semi-empirical model developed by Adams (1982). The discharge area was relatively shallow. The salinity and temperature measurement studies conducted in the Gencelli Harbor showed that the vertical and horizontal distribution of these physical parameters were uniform. It was therefore concluded that the proposed discharge area is well-mixed. The currents on the discharge area were bidirectional and parallel to the coastline and relatively weak, between  $0.0$  and  $8.0 \text{ cm s}^{-1}$  (ATPP EIA Phase-1 Report, 1990).

#### 4.3.2 Theoretical Background

Adams model is applicable to the unidirectional diffusers located in a relatively shallow and well-mixed environment (Adams, 1982). The shallow and well-mixed conditions are represented by a criterion,  $\Phi$  (Adams, 1982).

$$\Phi = \frac{HL^{1/3} \left[ \frac{g(\rho_a - \rho_o)}{\rho_a} \right]^{2/3}}{Q_o^{1/3} u_o} \quad (4.7)$$

where;       $\Phi$  :    a parameter used as a criterion for shallow water  
                   $H$  :    discharge depth (m)  
                   $L$  :    diffuser length (m)  
                   $Q_o$ :    volumetric flow rate of discharge  
                          (m s<sup>-3</sup>)

The critical value of  $\Phi$  is 0.5 (Adams, 1982; Almquist and Stolzenbach, 1980), below which a marine environment may be accepted as shallow and well-mixed. In such an environment, the buoyancy effect on the jet may be neglected. The major assumptions of Adams Model are summarized below:

- Flow is incompressible and inviscid.
- Discharge depth is relatively shallow ( $\Phi \leq 0.5$ ).
- Diffuser is relatively long ( $L/H \geq 10$ ).
- Ambient flow is vertically well-mixed.
- Buoyancy effect on the jet is negligible.
- Dilution due to lateral entrainment of ambient fluid is negligible.

The model and the data used in its validation are applicable to relatively long diffusers, where  $L/H$  ratio is greater than or equal to 10 and the dilution due to lateral entrainment is negligible. It is reported that fractional increase in dilution due to lateral entrainment is about 10 % (Adams, 1982). For relatively short diffusers, (i.e.,  $L/H \leq 10$ ), the effect of lateral entrainment may be significant (Adams, 1982).

It is stated that the diffuser discharge momentum induces a flow and creates a uniform head difference,  $\Delta h$ , between the zones just behind and in front of the diffuser (Adams, 1982). The combined effect of the ambient current and the diffuser flow results in the water surface to shift upwards by an amount of  $\Delta h_d$ , due to the establishment of a high pressure region. This situation is shown in Figure 4.3, as adapted from Adams (1982).

Under these conditions, Adams model analyzes the flow within a control volume bounded with two streamlines using the Bernoulli and momentum equations at certain sections behind and in front of the diffusers, for predicting the dilution of the jet discharged from a tee diffuser. The equations of the model are given below (Adams, 1982):

$$\frac{S_t}{S_o} = 1 - \frac{c_d u_a^2 A}{Nu_o^2 a_o} \quad (4.8)$$

$$S_o = \left( \frac{A}{2Na_o} \right)^{1/2} \quad (4.9)$$

where;	$S_t$ :	dilution for tee diffuser in a current
	$S_o$ :	dilution for the tee diffuser in stagnant water
	$c_d$ :	empirical drag coefficient associated with the tee diffuser in cross-flow
	$u_a$ :	ambient current velocity ( $\text{m s}^{-1}$ )
		$= (u_{a,x} + u_{a,y})^{0.5}$
	$A$ :	diffuser area ( $\text{m}^2$ ) = LH
	$N$ :	number of diffuser ports
	$a_o$ :	individual port area ( $\text{m}^2$ )

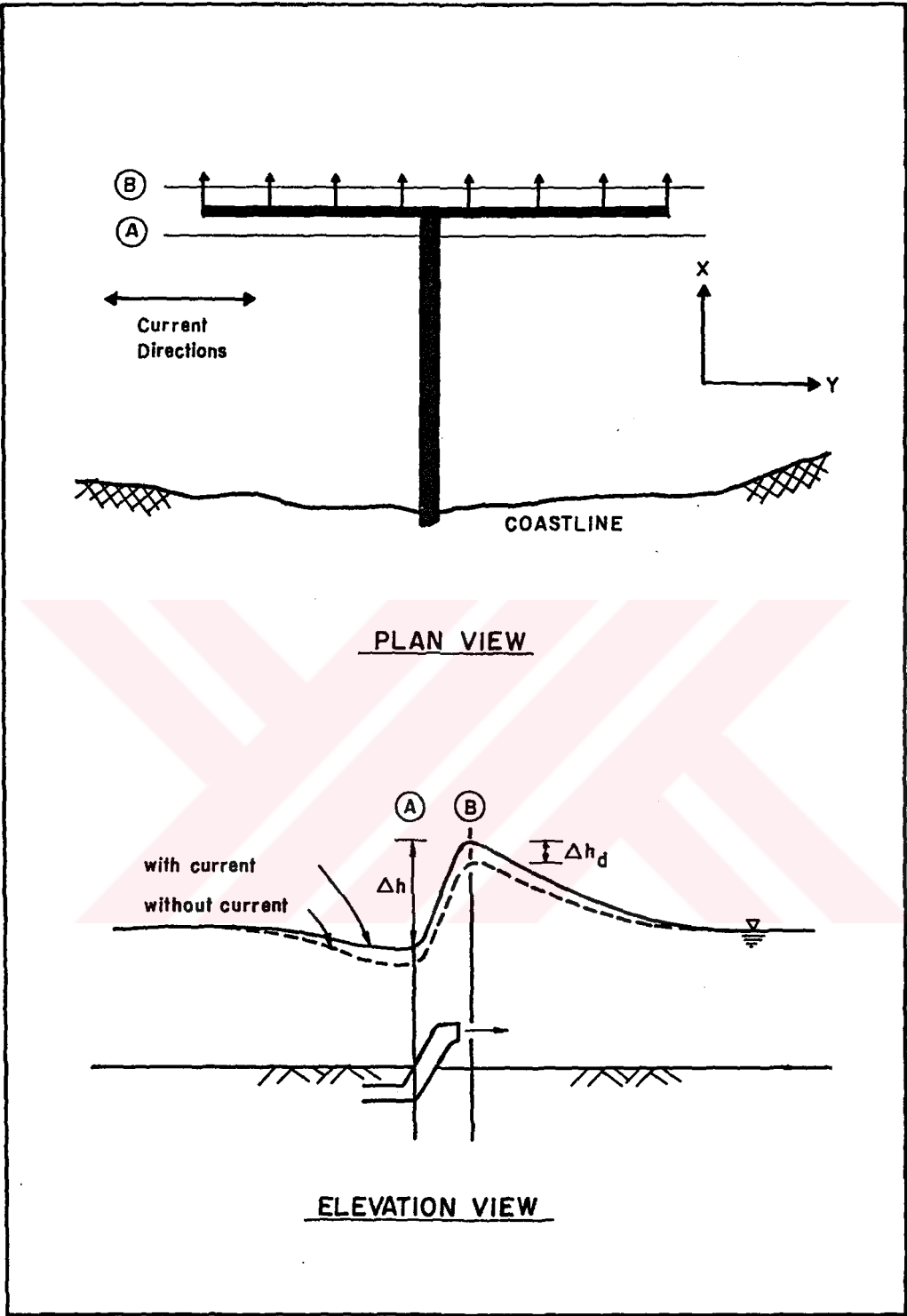


Figure 4.3. Details for Adams Model

4.4 Results and Discussion

4.4.1 Design Features of the Cooling Water Dicharge Structure

The cooling water of the proposed ATPP will be discharged from a submerged, multi-port tee diffuser. The design features of the cooling water discharge structure are summarized in Table 4.1. The details of the discharge facilities are shown in Figure 2.3. The sea current characteristics are depicted in Figure 2.7.

Table 4.1. Features of the Discharge Structure and Area

Parameter	Value
Discharge to coast distance	290 m
Discharge depth	10 m
Orientation of ports	Towards WSW
Total flow rate	46.6 m <sup>3</sup> s <sup>-1</sup>
Number of ports	8
Port spacing	10 m
Diameter of ports	1.6 m
Average discharge velocity	2.9 m s <sup>-1</sup>
Length of diffuser	70 m
Observed current velocity range	0.00-0.08 m s <sup>-1</sup>
Dominant current directions	NNE and SSW
Excess temperature	7 °C

#### 4.4.2 Dilution in Stagnant Environment

A computer program was constructed to apply the CRIEPI model to the case of the proposed ATPP. The results are summarized in Table 4.2. In this table, the values are given as a function of depth and horizontal distance from the discharge.

Table 4.2. Dilution and Surface Velocity in Stagnant Conditions

	Values				
z (m) - depth	28	36	41	45	49
x (m) - horz. dist.	2	4	6	8	10
S (CRIEPI)	3.47	4.49	5.36	6.15	6.91
$u_m$ (m s <sup>-1</sup> )	0.75	0.66	0.62	0.59	0.56

As can be seen from Table 4.2, the jet was estimated to reach to the surface at a point about 50 m away from the ports. The estimated thickness for the thermal field established at the surface,  $h_w$ , was about 3.5 m. The values for nominal half width,  $b'$ , obtained from the graph in Figure 4.1 vary between 5 to 10. Such values were relatively high for a marine environment of 10 m depth. This may be due to the rapid entrainment of the ambient fluid into the jet and rapid dispersion of the jet within the near-field.

The estimated maximum surface velocity, which occurs at the point where the centerline of the jet reaches to the surface, was about 0.50 m s<sup>-1</sup>. Based on the intermediate and far-field hydrothermal studies, it is expected that this relatively high velocity will rapidly diminish to values in the order of 0.05 m s<sup>-1</sup> at the surface (See Chapter 5).

The dilution ratio necessary to decrease the excess temperature of 7°C to about 1°C, is 7. Based on the results of the CRIPEPI model, it was estimated that the diffuser will achieve the required dilution in a stagnant environment.

#### 4.4.3 Dilution in Cross-Flowing Environment

The  $\Phi$  parameter used as a criterion for shallow water, was estimated to be 0.32 for the case of the proposed ATPP. This value, which is below the critical value of 0.50, represents a shallow and well-mixed waterbody. In the case of the proposed ATPP, the L/H ratio was about 7. This means that the model underestimated the dilution by about 10 % or more (see Section 4.3.2). This condition was conservative, in terms of impact assessment.

The dilution for the tee-diffuser system in stagnant water,  $S_o$ , was estimated to be 4.7. This value is lower than the values predicted by the CRIEPI model. As calculated from Equation 4.8, the estimated dilution values for different drag coefficients and ambient current velocities are given in Table 4.3.

Table 4.3. The results of the Near-Field Hydrothermal Studies for Cross-Flow Conditions

	Drag Coefficient, $C_d$					
	0.5		1.0		2.0	
Current Velocity $u_a$ (m s <sup>-1</sup> )	0.04	0.08	0.04	0.08	0.04	0.08
Dilution, $S_t$	4.68	4.62	4.66	4.54	4.62	4.38



The relatively low values of dilution in Table 4.3 were due to:

- the neglect of the lateral entrainment effect on dilution; and
- the decreasing effect of cross-flows on dilution.

Under field conditions, these conservative dilution values are expected to be greater by at least %10. This, in turn, is in agreement with the dilution prediction obtained for stagnant environment.



## **CHAPTER V**

### **HYDROTHERMAL MODELING STUDIES: INTERMEDIATE AND FAR-FIELD**

#### **5.1 General**

This chapter outlines the results obtained from the application of a three-dimensional, time-varying, hydrodynamic and transport model to the case of the proposed ATPP. The primary objectives of the hydrothermal modeling study were:

- to assure that the criterion for maximum surface water temperature rise of 1 °C will be satisfied;
- to predict the extent of area affected by the warm plume and to estimate the surface excess temperature contourlines;
- to determine the water circulation patterns in the Gencelli Harbor;
- to investigate the possible effects of various factors, including meteorology and tides, on warm water dispersion.

#### **5.2 Study Approach**

An intermediate and far-field hydrothermal modeling approach is applied to the case of the proposed ATPP. Near-field models, such as the ones discussed in Chapters 3 and 4, concentrate on the immediate vicinity of the discharge and are based on the theory of plume, as stated in those chapters.

These models are mostly applicable for such cases as steady conditions of ambient density and flow (Buchak et al., 1992). Such models simplify mixing and dispersion in the far-field, since they rely on a single, time-invariant set of ambient conditions (Buchak et al., 1992). In the intermediate and far-fields, recirculation may be important and the ambient velocity field may vary in time. For such cases, three-dimensional, time-varying, numerical models are more appropriate to illuminate the following points:

- availability of sufficient water exchange at the boundary to provide the necessary dilution
- existence of shoreline-effects
- effects of wind speed and direction as well as tides
- possibility of recirculation of warm water and a subsequent heat accumulation

In the case of the proposed ATPP, a time-varying, three-dimensional model, GLLVHT (generalized, longitudinal - lateral - vertical hydrodynamics and transport), was used. The theory of GLLVHT is briefly discussed in the following sections.

### 5.3 Description of GLLVHT

#### 5.3.1 Background of GLLVHT

GLLVHT is a commercial model originally developed by Edinger and Buchak (1980 and 1985). The model can provide three-dimensional, time-varying simulations of rivers, lakes, impoundments, estuaries and coastal waterbodies. GLLVHT is an extensively tested and applied one. GLLVHT has been applied to numerous cases similar to that of ATPP and has also been

subjected to real-time verification studies many times (see Section 5.3.3). As an example, Figure 5.1 shows a comparison of predicted and observed water temperatures for the case of the Chalk Point Steam Electric Station (Edinger et al., 1988). In the application of a numerical model such as GLLVHT, the following factors may majorly affect the results:

- assumptions and equations of the model
- solution techniques of the equations
- boundary conditions
- input data

### 5.3.2 Assumptions, Equations and Solution Techniques

The GLLVHT model is based on the longitudinal, lateral and vertical equations of momentum, continuity and constituent transport. The model can provide simulations of constituent transport, ranging from temperature and salinity to fish eggs and larvae, as well as the hydrodynamics of rivers, lakes, impoundments, estuaries and coastal waterbodies. The formulation of the GLLVHT includes:

- vertically varying longitudinal and lateral momentum balances, the vertical momentum being in the form of the hydrostatic approximation;
- local continuity;
- free-water surface condition based on vertically integrated continuity;
- longitudinal, lateral and vertical transport of constituents;
- an equation of state which relates momentum to constituents that determine density such as temperature and salinity.

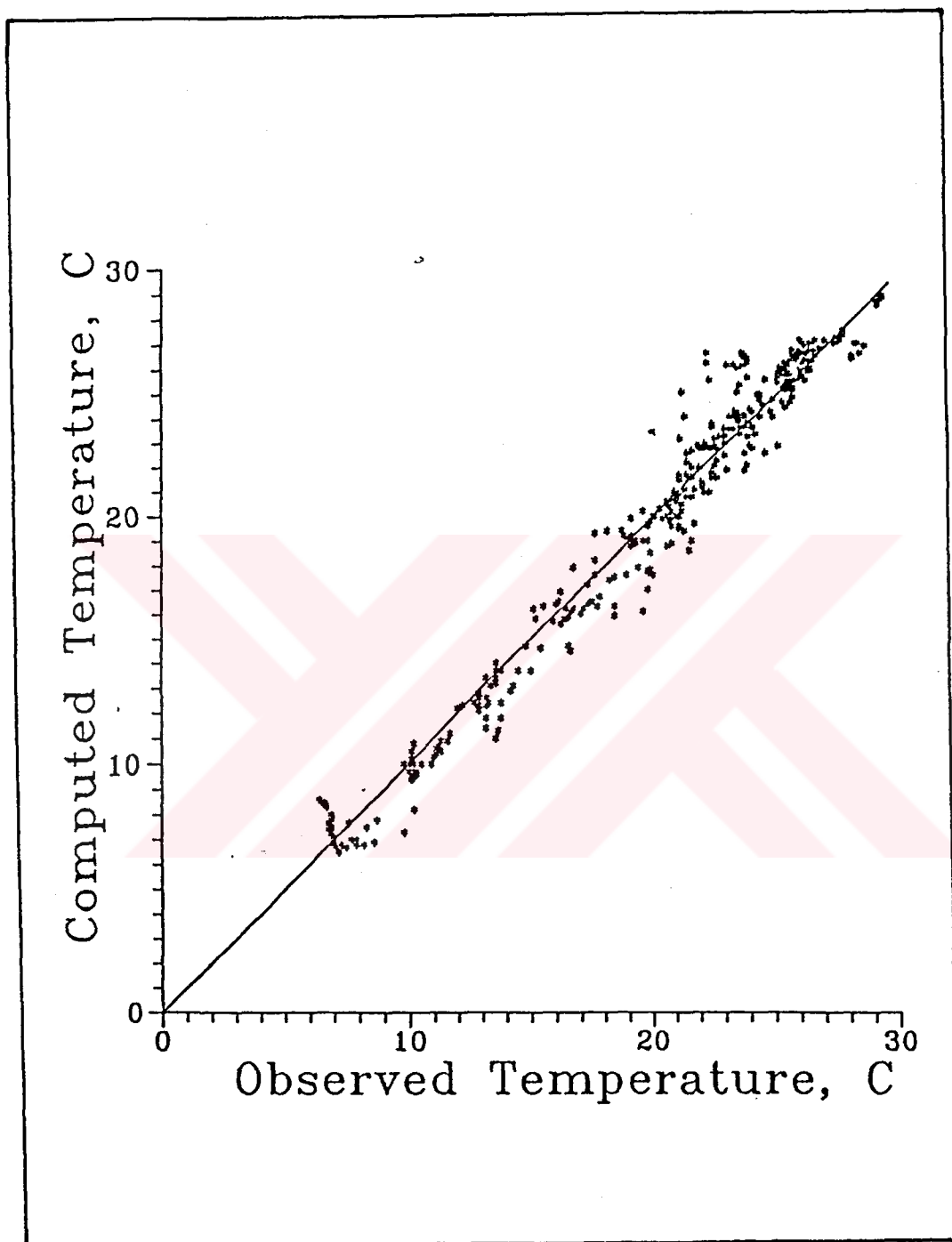


Figure 5.1. A Comparison of Observed Sea-Water Temperatures With the Values Predicted by GLLVHT (Edinger et al., 1988)

The vertically varying longitudinal and lateral momentum balances include local acceleration of horizontal velocity, horizontal and vertical advective momentum transfer, the horizontal pressure gradient, and horizontal and vertical shear stress. Included in the latter are the surface wind stress and the bottom stress due to friction. The horizontal pressure gradient includes the barotropic surface slope and the baroclinic vertical integral of the horizontal density gradient which is the dominant term of density-induced convective circulation.

The relevant equations of the model and technical information pertinent to the numerical solution techniques are given in Appendix C. However, it should be noted that the discussion presented in Appendix C is limited with commercial restrictions.

### 5.3.3 Boundary Conditions

The selection and availability of the data which will be input as initial and/or boundary conditions are among the key points in model applications. In the case of GLLVHT, using boundary condition data, the model can be applied in either "real-time" or "stationary-state" simulations.

Real time simulations are based on time variant field data, continuously recorded over a real period of time. They require a considerable amount of data which should be measured or, if available, compiled from existing data sources. For this reason, they are expensive and time-consuming. Furthermore, real time simulations are of a lesser value for a proposed facility, since extrapolation of field data will be necessary, which requires modeling in any event.

Stationary-state simulations, on the other hand, are based on time invariant data, such as, water inflows, surface wind stress and meteorological conditions which are assumed to be constant over a given period of simulation. In the stationary-state simulations, the only time-variant data is the tidal height which can be used as an infinitely repeating series. The data necessary to set up the stationary-state simulations are given below (Buchak et al., 1992):

- bathymetry
- tidal components
- boundary salinities
- ambient temperatures
- freshwater inflows (if exist)

A stationary-state simulation setup can only be verified by determining if the results are in agreement with available data and their orders are the same.

If real time data are insufficient and difficult to obtain on both financial and temporal basis, stationary-state simulations are preferred in descriptive and comparative studies.

In the case of the proposed ATPP, real-time simulations were not considered as applicable for the following reasons:

- The time variant and synoptic real-time data, such as wind speed, tidal height, wave height, current velocity, water salinity and temperatures, air temperature, cloud cover, atmospheric pressure were not available.
- The available data were, generally, in the form of daily or monthly averages.

- The available data were not coincident and the plant was not operative.

If a real-time simulation was to be applied, the real-time data listed above should be obtained from the following sources (Buchak et al., 1992):

- water surface elevation gauges
- salinity and temperature recorders at the open boundary of the Gencelli Harbor
- meteorological recorders located on-site or near-site
- velocity recorders located at various points including the proposed outfall of the ATPP

#### 5.3.4 Input Data for the Model Parameters

One of the most important features of the ATPP hydrothermal modeling studies is the "worst case" approach. In this approach, using field data and sensitivity tests, the values of the model parameters are selected such that they represent the worst conditions most likely to occur. Even with these worst-case conditions, if the results are environmentally acceptable and comply with the standards, being on the safe side, it can be concluded that the plant operation will not create any significantly adverse effects on the water quality and the ecology of the modeled marine environment.

Three preliminary stages were completed before applying the GLLVHT model to the case of the proposed ATPP. These stages are given below:

- model setup
- setup validation
- sensitivity tests



## 5.4 Model Setup

### 5.4.1 Grid System

To construct the grid system of the Gencelli Harbor, the bathymetry was examined first. Average depths were interpolated for each of the resulting grid cells by means of a package program (SURFER). The depths on the national bathymetric map shown in Figure 5.2, were used as inputs with the format presented in Appendix E. The approximation to the actual depth contours was achieved by the krigging interpolation method. A separate pre-processing computer program, BATH.FOR developed by J.E. Edinger Associates, Inc. (Buchak et al.,1992), was used in computing the number of layers in each cell and also the resulting elevation-area-volume table. BATH.FOR also utilizes the available bathymetric information as input.

As a result of preliminary runs, a finite difference grid of  $\Delta x = \Delta y = 250\text{m}$ , and,  $\Delta z = 2\text{ m}$  was used in the simulations and tests. The x-axis of the model was oriented approximately along an east-west line, positive east and the y-axis was oriented approximately on a north-south line, positive north. The finite difference representation of the Gencelli Harbor is shown in Figure 5.3. The codes I, J, and K were used for x, y, and z coordinates, respectively. These grids were abstracted into the hypsograph given in Table 5.1. The portion of the Gencelli Harbor modeled encompasses about 5.9 million  $\text{m}^2$  and has a volume of about 133.5 million  $\text{m}^3$ . The mean depth is about 22.5 m.

To orient the grid, so that windshear can be correctly applied from wind speed and direction observations, the relationship of the grid axes to compass was also determined.  $\Phi_{ix}$ , the angle the positive x-axis makes with north (tail of the x-axis at the compass origin), was determined to be 87.5 degrees with

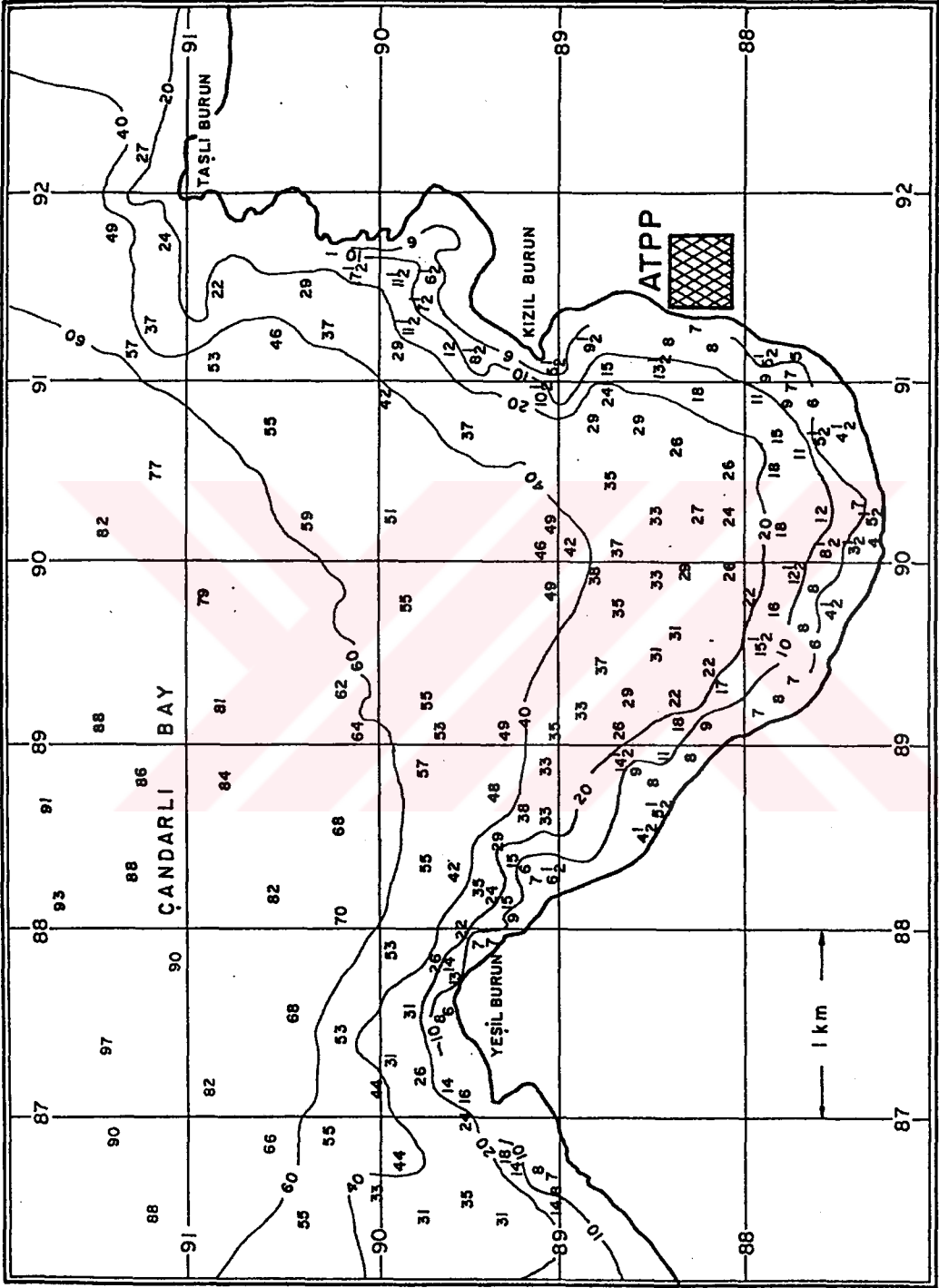


Figure 5.2 National Bathymetric map

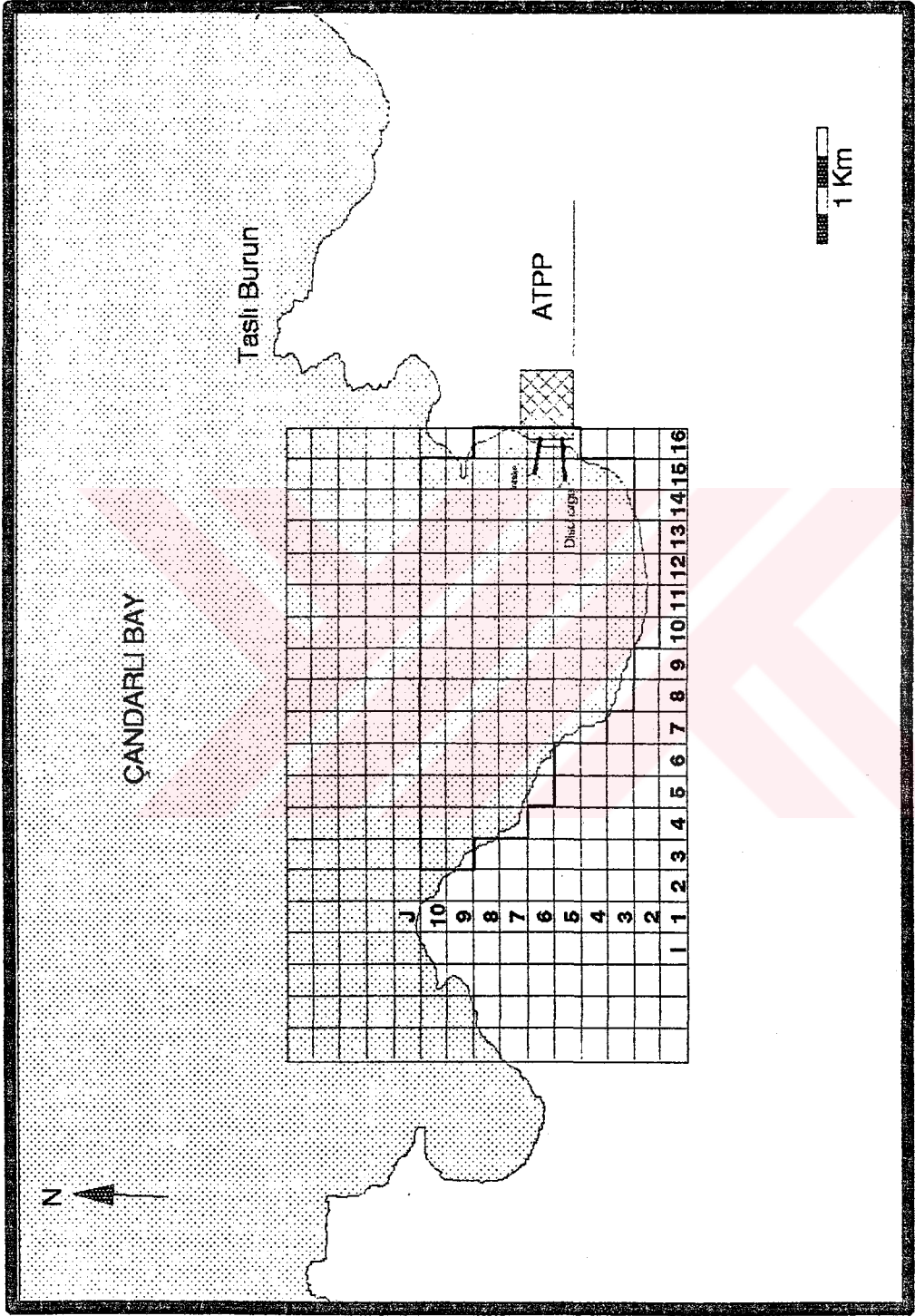


Figure 5.3. Finite Difference Discretization of the Study Area

**Table 5.1      Hypsometric Data for the Modeled Portion of Gencelli Harbor**  
**(area and capacity (values are for the top layer K))**

K	Thickness m	Depth m	Area 10 <sup>6</sup> m <sup>2</sup>	Cum. volume 10 <sup>6</sup> m <sup>3</sup>	Mean depth m	Number of Active Cells
2	2.00	0.00	5.938	133.500	22.48	95
3	2.00	-2.00	5.938	121.625	20.48	95
4	2.00	-4.00	5.250	109.750	20.90	84
5	2.00	-6.00	4.875	99.250	20.36	78
6	2.00	-8.00	4.625	89.500	19.35	74
7	2.00	-10.00	4.375	80.250	18.34	70
8	2.00	-12.00	3.813	71.500	18.75	61
9	2.00	-14.00	3.750	63.875	17.03	60
10	2.00	-16.00	3.438	56.375	16.40	55
11	2.00	-18.00	3.000	49.500	16.50	48
12	2.00	-20.00	2.938	43.500	14.81	47
13	2.00	-22.00	2.813	37.625	13.38	45
14	2.00	-24.00	2.625	32.000	12.19	42
15	2.00	-26.00	2.188	26.750	12.23	35
16	2.00	-28.00	2.188	22.375	10.23	35
17	2.00	-30.00	1.688	18.000	10.67	27
18	2.00	-32.00	1.625	14.625	9.00	26
19	2.00	-34.00	1.500	11.375	7.58	24
20	2.00	-36.00	1.125	8.375	7.44	18
21	2.00	-38.00	1.063	6.125	5.76	17
22	2.00	-40.00	0.938	4.000	4.27	15
23	2.00	-42.00	0.500	2.125	4.25	8
24	2.00	-44.00	0.500	1.125	2.25	8
25	2.00	-46.00	0.063	0.125	2.00	1

north.  $\Phi_{iy}$ , the angle that the positive y-axis makes with north, was determined to be 357.5 degrees.

#### 5.4.2 Meteorological Conditions

In hydrodynamic and transport modeling, meteorological data are used for both computation of surface heat exchange and for generation of the surface wind stress. For the case of the Gencelli Harbor, simplified methods of heat exchange analysis employing the equilibrium temperature concept was used. The equilibrium temperature, is defined as the hypothetical water surface temperature at which no plant heat rejection would occur and the net rate of heat exchange would be zero (Edinger et al., 1974). In this case no heat storage would occur. The surface heat exchange computations were run for the steady meteorological conditions that result in a constant ambient temperature. These meteorological conditions are summarized in Table 5.2.

Table 5.2. Meteorological Data Used in the Runs and Simulations

Parameter	Value
Dry bulb temperature	21 °C
Dew point temperature	13 °C
Wind speed at 2 m height	2 m s <sup>-1</sup>
Cloud cover	0.2
Shortwave solar radiation	120 W m <sup>-2</sup>

When used in conjunction with the wind speed function given by Adams et al. (1990), the resulting water temperature that balances incoming and outgoing heat exchange processes was found to be 20 °C. Under such conditions, the coefficient of surface heat exchange can be taken as 25 W m<sup>-2</sup>

°C<sup>-1</sup> (Edinger et al., 1974). Using the above measurable data, the heat exchange components were evaluated (see Appendix C) and the surface heat exchange processes were simulated. As can be seen from Table 5.2, the meteorological parameters are constant (time-invariant) throughout the simulation period. This assumption is applicable only to the case of a non-existing facility where real-time simulations are not meaningful. In the case of a proposed facility, the problem can be analyzed conceptually. Beginning with an equilibrium condition, in terms of heat balance, a constant amount of heat is continuously input to the system and a new equilibrium condition with a relatively higher temperature is achieved. The simulations can be performed in order to predict the distribution of the excess temperatures (increase in water temperature due to plant heat rejection), in the harbor, with their values at certain locations.

The simulations were started with the above steady meteorological conditions which yield to an equilibrium temperature of 20 °C. As the plant heat rejection was added to the heat budget components, the relevant components were re-evaluated and the excess temperatures were computed until a new stationary state was reached (see Section 5.5). In terms of temperature, the time to reach the stationary state can be defined as the amount of time required to build up heat in the modeled region such that heat additions from the power plant equalled heat removed due to circulation at the boundary and due to surface heat exchange. At this state, a new equilibrium state and a new water temperature (equilibrium temperature + excess temperature) is obtained.

As summarized in Table 2.5 of Chapter 2, the most frequent wind direction and speed range is northeast at 4-6 m s<sup>-1</sup> (7.5 percent). The other two most frequent combinations are east at 2-3 m s<sup>-1</sup> (6.3 percent) and southeast at 0.9-1.5 m s<sup>-1</sup> (4.2 percent). These three cases, along with a calm condition, were used in the simulations.

### 5.4.3 Ambient Temperatures and Salinities

Initial and boundary conditions need to be set for the transport of two constituents, temperature and salinity. Because of the lack of stratification in either parameter, the boundary values were made vertically homogenous. Furthermore, the initial values for the interior points were also set to these same values. For salinity, the initial and boundary value was selected to be 39 ppt. The initial and boundary value for temperature was selected to be compatible with the meteorological data set used for surface heat exchange.

### 5.4.4 Boundary Conditions

A tidal boundary condition was applied to the open boundary of the Gencelli Harbor. The boundary condition was relatively simple and reproduced the varying water surface elevation using a sine function with an amplitude of 30 cm and a period of 8.5 h. The excess temperatures were set along the open boundary which is coded with  $J=10$ , as shown in Figure 5.3. It was conservatively assumed that the amount of excess temperature returned on an incoming tide was equal to 50 percent of the value inside the model grid. For this purpose, as a boundary condition, the value of any constituent at the open boundary ( $J=10$ ) was set to half of that of the inner grid adjacent to the open boundary ( $J=9$ ).

### 5.4.5 Current Velocities

The initial values of the current velocities were set to zero. With this condition, the currents rapidly develop by the effects of tides, wind shear and bottom stress as the simulation proceeds.

#### 5.4.6 Intake and Outfall Conditions

The separate intake and discharge structures for each unit of the ATPP are located immediately adjacent to each other. Therefore, for the purposes of modeling, both intake and outlet structures of each individual unit could be considered as single systems. As noted in Figure 5.3, the intake and outlet were located onto finite difference grid system at the following locations:

intake codes: I=15, J=6, K=6

outlet codes: I=15, J=5, K=6

The pumping rate for the two-unit operation,  $Q_p$ , will be  $46.6 \text{ m}^3\text{s}^{-1}$ , with a temperature rise of  $7^\circ\text{C}$ . The model was set up such that the excess temperature of the intake water is added to the temperature rise to account for recirculation and buoyancy at the discharge, correctly. Finally, the specific momentum of discharge ( $SM_x$  and  $SM_y$ ) can be computed as follows (see Appendix C):

$$SM_y = (Q_p \cdot v) / (\Delta x \cdot \Delta y \cdot \Delta z \cdot 1.732) \quad (5.1)$$

$$SM_x = (2 \cdot Q_p \cdot v) / (\Delta x \cdot \Delta y \cdot \Delta z \cdot 1.732) \quad (5.2)$$

where,  $v$  is the discharge velocity, which has a value of  $2.89 \text{ m s}^{-1}$ . The correct direction of the momentum of discharge orifice relative to the grid, was represented, by the ratio between the  $SM_x$  and  $SM_y$ .

#### 5.5 Setup validation

Preliminary simulations were made with the boundary and initial conditions discussed in Section 5.4. The first sets of simulations were made to evaluate run times, to check the correctness of the set up and to determine



the length of simulation required to initialize the computation. It was found that a reasonable simulation length was four days. This was determined by monitoring the build-up of excess temperature at a location in the grid far from the discharge over the simulation and recognizing the onset of a repeating cycle corresponding to the tidal period of 8.5 h. All the subsequent simulations were run for the four day period.

In order to check the correctness of the model setup, each feature of the Gencelli Harbor and ATPP was added sequentially to the model. Preliminary simulations for setup validation started with the following conditions:

- calm environment
- no surface heat exchange
- no intake/discharge
- no tide

As each feature was added to the computation, the results were examined and validated. When the tide was considered in the computations, it was found that computed velocities were in the order of  $2\text{--}4\text{ cm s}^{-1}$ . These values were compared with the observed currents, which has an average of  $2\text{ cm s}^{-1}$  or less (Akyarlı et al., 1988). The agreement between the computed and observed values was deemed satisfactory for the validation study.

A second comparison was made with the results of near-field hydrothermal modeling studies. These results showed that the maximum surface water temperature just above the outfall is  $1\text{ }^{\circ}\text{C}$ . As will be discussed in the subsequent sections, these results are compatible with the results of three-dimensional GLLVHT model results. Output from GLLVHT consisted of the following information:

- longitudinal-lateral snapshots of velocity and excess temperature at the surface, at the level of the intake and the level of the discharge, collected at required intervals (i.e. once a day through the simulation)
- snapshots of a longitudinal-vertical slice through the boundary, collected at required intervals (i.e. once a day)
- time series of temperatures at  $I=8, J=10$ ;  $I=14, J=10$ ;  $I=12, J=5$ ; and at  $I=11, J=8$ , collected every hour through the simulation
- data for velocity vector plots and contours of excess temperature at the surface, collected at the same frequency as the snapshots

The setup simulations are defined in Table 5.3. Runs 2.15, 3.01, 3.09 and 3.10 were the series used for validation, with each successive run adding an additional forcing function. The simulations resulted in maximum surface excess temperatures between 0.65 and 1 °C. In the absence of momentum terms in the calculations, maximum surface excess temperature values of about 1.40 °C were calculated.

**Table 5.3 The Setup Simulations of the GLLVHT**

Run	Momentum	Tide	Wind
2.15	does not exist	does not exist	calm
3.01	exists	does not exist	calm
3.09	exists	does not exist	NE at 4.5 m s <sup>-1</sup>
3.10	exists	exists	NE at 4.5 m s <sup>-1</sup>

5.6 Model Simulations for Excess Temperature

5.6.1 General

Four cases were selected for the final simulations, based on wind data set summarized in Table 2.5. These cases were the most probable conditions that could be experienced. In the simulations, for a frequent wind speed range, the value which will result in the worst case was preferred in the light of the sensitivity runs. The base case parameters given in Appendix D were used in the final simulations, except for Simulation 5 which is the simulation of a hypothetical case of surface discharge. The presented excess temperature values represent the predicted values after reaching the stationary state, at the end of four-day simulation period. The model simulations are defined in Table 5.4.

Table 5.4. Simulations for the Proposed ATPP

Simulation	Discharge Type	Wind Direction	Wind Speed (m s <sup>-1</sup> )
1	Deep	Northeast (NE)	4.5
2	Deep	East (E)	2.0
3	Deep	Southeast (SE)	2.0
4	Deep	Calm	-
5	Surface	Northeast (NE)	4.5

### 5.6.2 Simulation 1

Using the meteorological data set presented Table 2.5, it was observed that, the most frequent wind direction is Northeast (NE) with an annual frequency of 25.1 percent. The wind speed range  $4\text{--}6\text{ m s}^{-1}$  in that direction was observed with an annual frequency of 7.5 percent. The wind speed value  $4.5\text{ m s}^{-1}$  was used in the simulation. Under these conditions, the predicted maximum stationary sate surface excess temperature was  $0.63\text{ }^{\circ}\text{C}$ . The stationary sate surface excess temperature distribution is depicted in Figure 5.4.

### 5.6.3 Simulation 2

The annual frequency of winds from east (E) was observed to be 20.4 percent. The frequency of the wind speed range  $2.0\text{--}3.0\text{ m s}^{-1}$  in this direction was 6.3 percent. The calculated maximum stationary sate surface excess temperature was  $0.77\text{ }^{\circ}\text{C}$ . The stationary sate surface excess temperature distribution is depicted in Figure 5.5.

### 5.6.4 Simulation 3

The annual frequency of winds from southeast (SE) was 13.6. The frequency of the wind speed ranges  $0.9\text{--}1.5\text{ m s}^{-1}$  and  $1.5\text{--}2.0\text{ m s}^{-1}$ , in this direction, were 4.2 and 4.0 percent, respectively. The sensitivity runs showed that, for the southeast wind direction, as the wind speed increased the maximum surface excess temperature also increased.  $2.0\text{ m s}^{-1}$  wind speed was selected to be on safe side. The calculated maximum stationary sate surface excess temperature was  $0.78\text{ }^{\circ}\text{C}$ . The stationary sate surface excess temperature distribution is depicted in Figure 5.6.



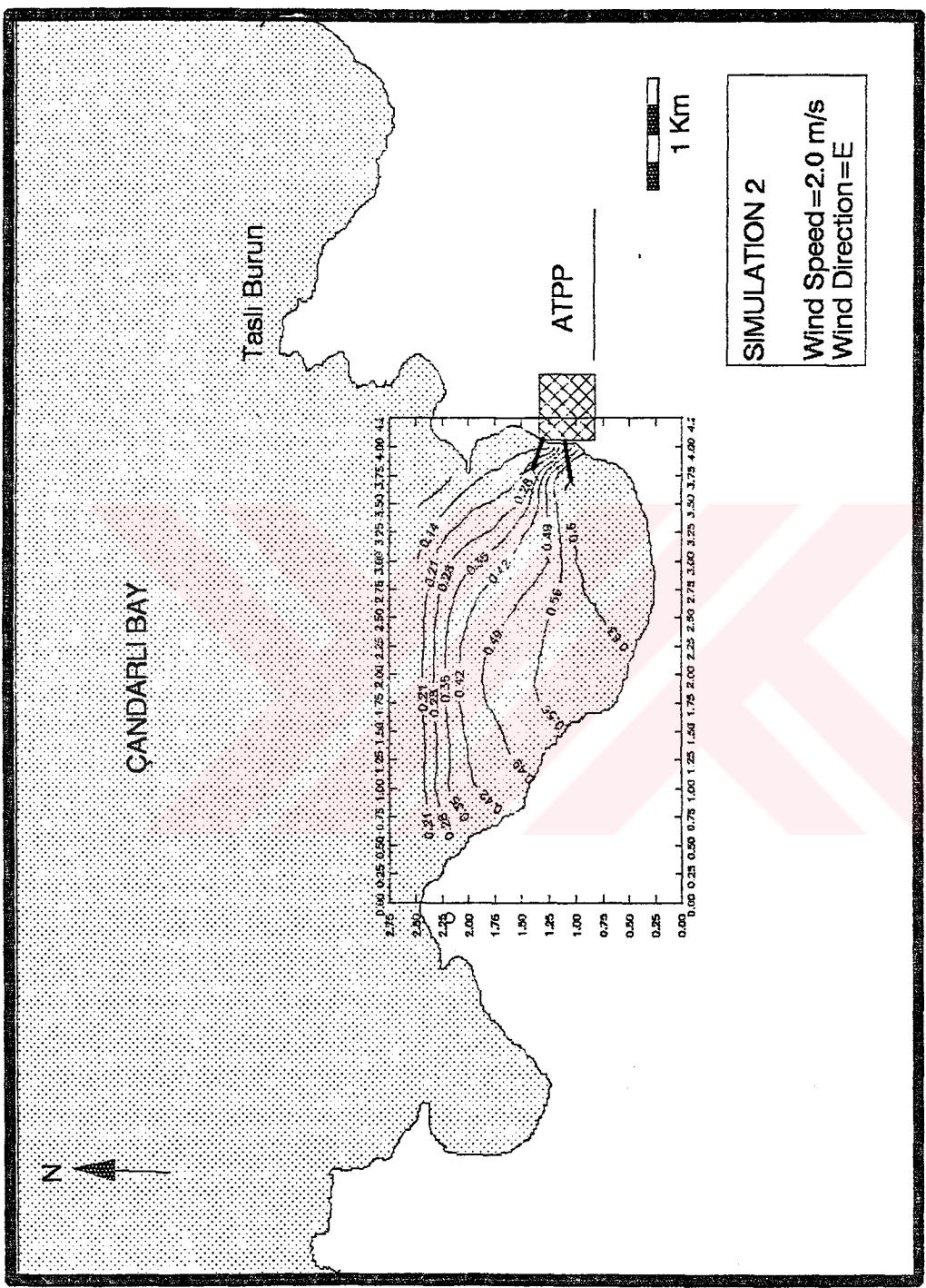


Figure 5.5. Surface Excess Temperature Distribution for Simulation 2



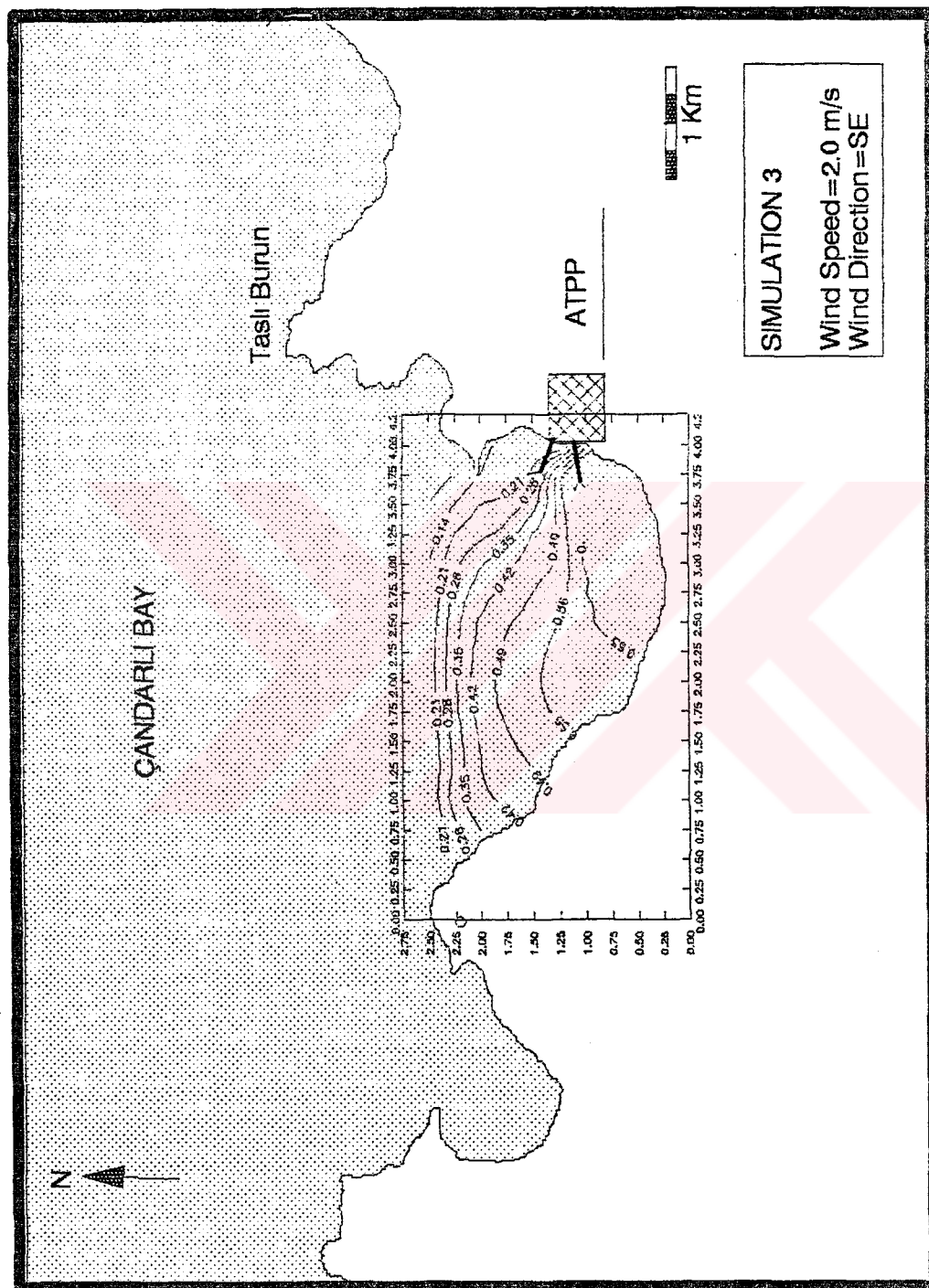


Figure 5.6. Surface Excess Temperature Distribution for Simulation 3

#### 5.6.5 Simulations 4

In the meteorological conditions, calm case is also a possible case. The sensitivity test and simulation results showed that a maximum stationary sate surface excess temperature of 0.79 °C might be experienced, in the case of calm conditions. The stationary sate surface excess temperature distribution is depicted in Figure 5.7.

#### 5.6.6 Simulation 5

To emphasize the advantage of deep sea discharge over surface discharge alternative, in terms of mixing and pollution control, a simulation for a case of surface discharge with a wind speed of 4.5 m s<sup>-1</sup> in the northeast (NE) direction was performed. The calculated maximum stationary sate surface excess temperature was 6.53 °C. The stationary sate surface excess temperature distribution is depicted in Figure 5.8.

### 5.7 Model Simulations for Water Circulation

Several runs were performed in order to determine the water circulation patterns in the Gencelli Harbor and to investigate the possible effects of various factors, including meteorology and tides, on warm water dispersion. In the Figures 5.9 to 5.12, the water circulation patterns of the Gencelli Harbor with and without cooling water operations are illustrated, for commonly observed northeastern wind and calm cases. In the case of a moderate wind and the current velocities estimated by using GLLVHT were:



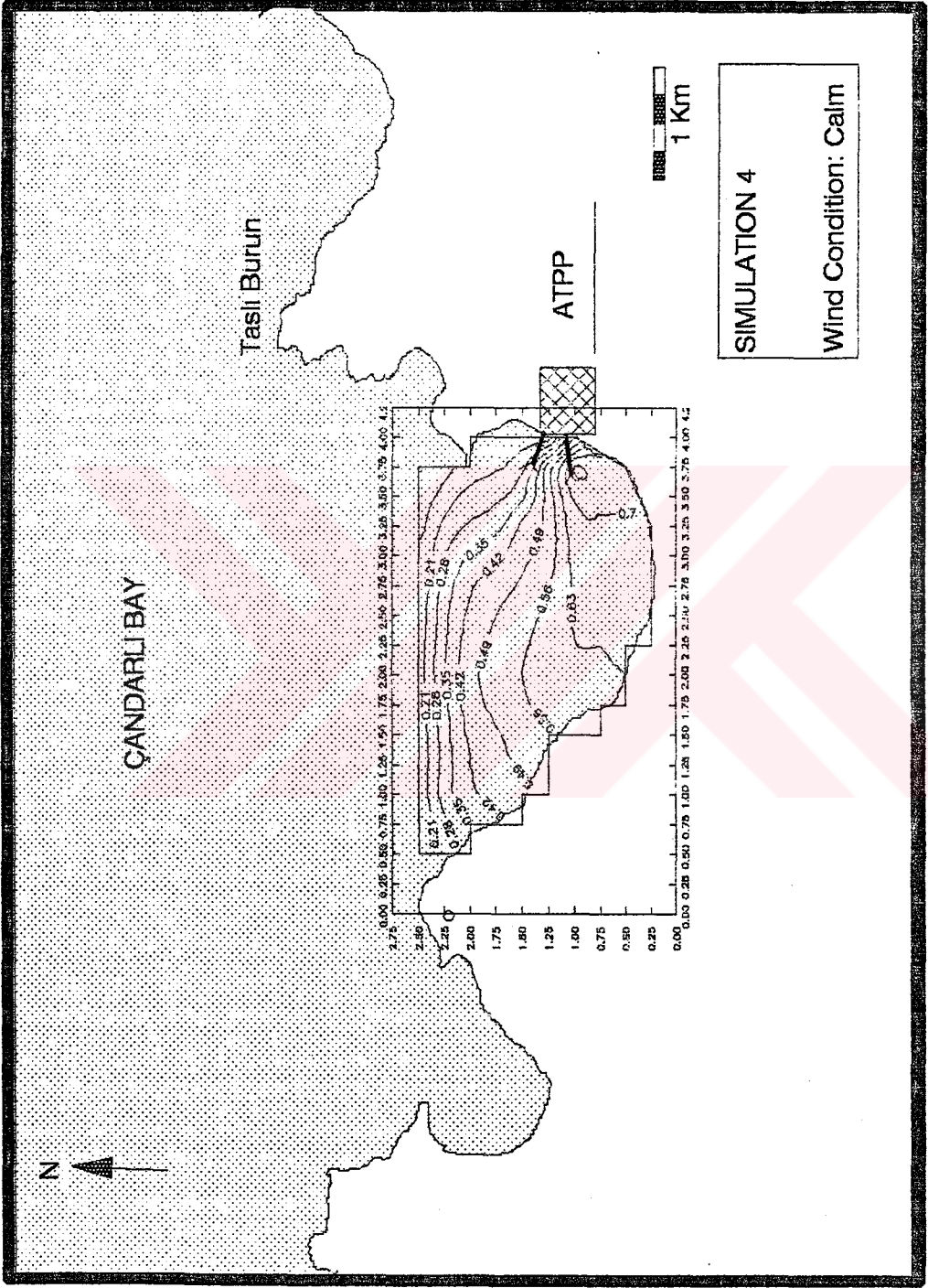


Figure 5.7. Surface Excess Temperature Distribution for Simulation 4

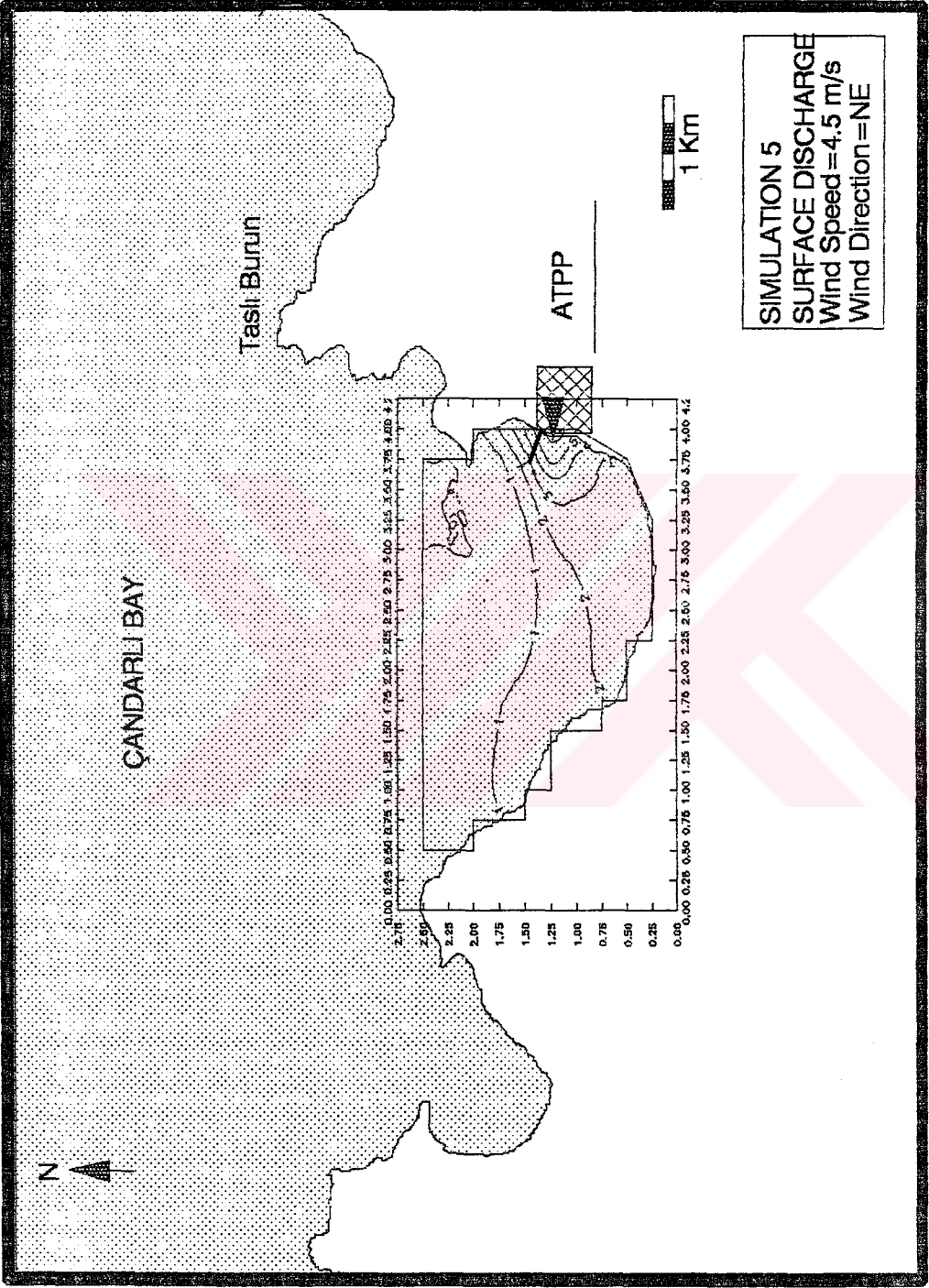


Figure 5.8. Surface Excess Temperature Distribution for Simulation 5

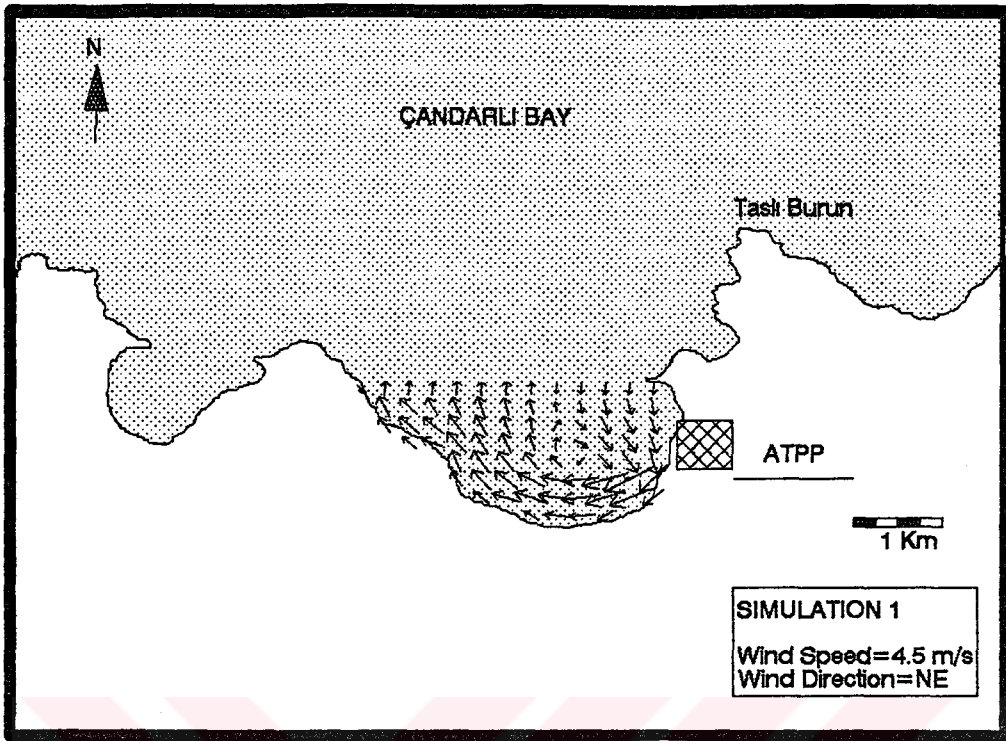


Figure 5.9. Surface Circulation With Plant (Wind)

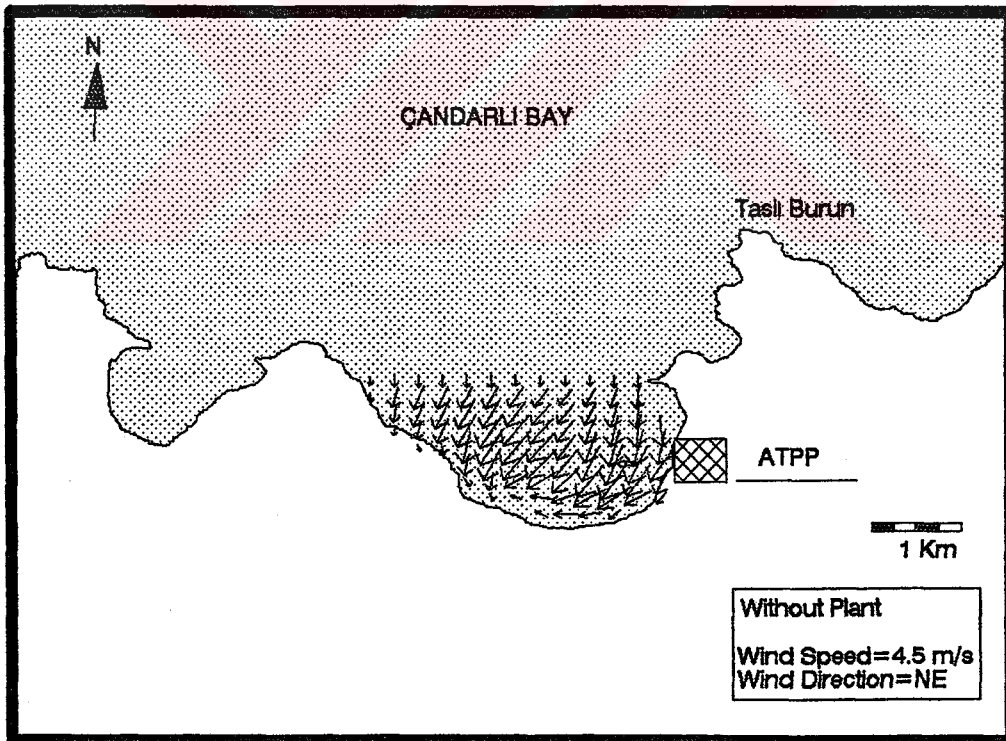


Figure 5.10. Surface Circulation Without Plant (Wind)

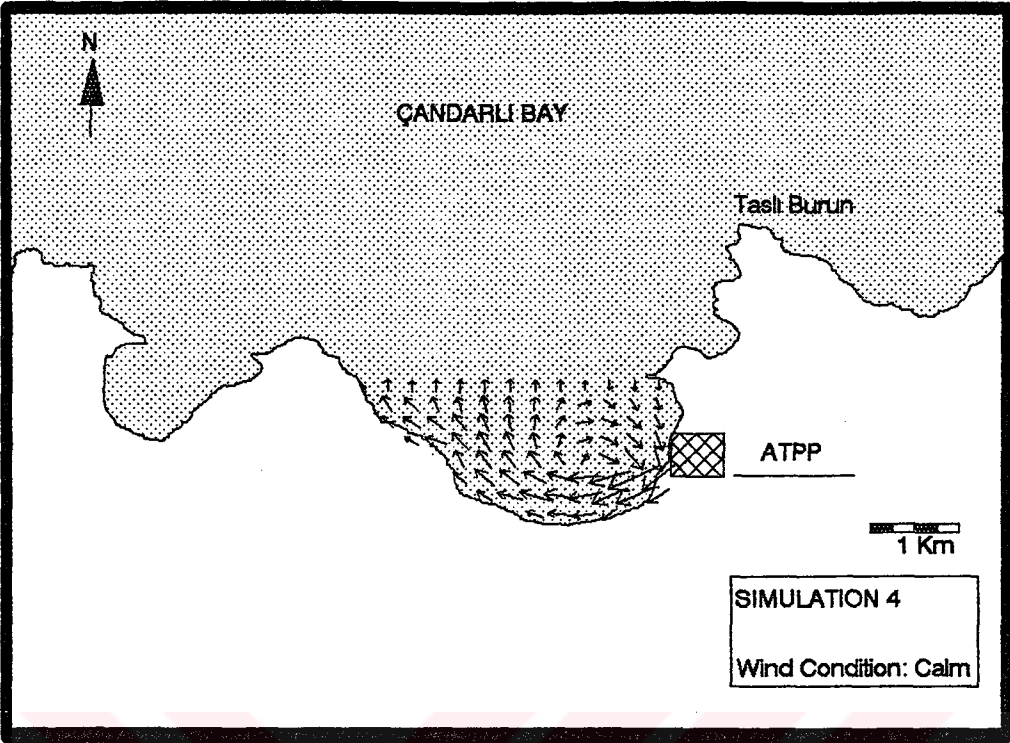


Figure 5.11. Surface Circulation With Plant (Calm)

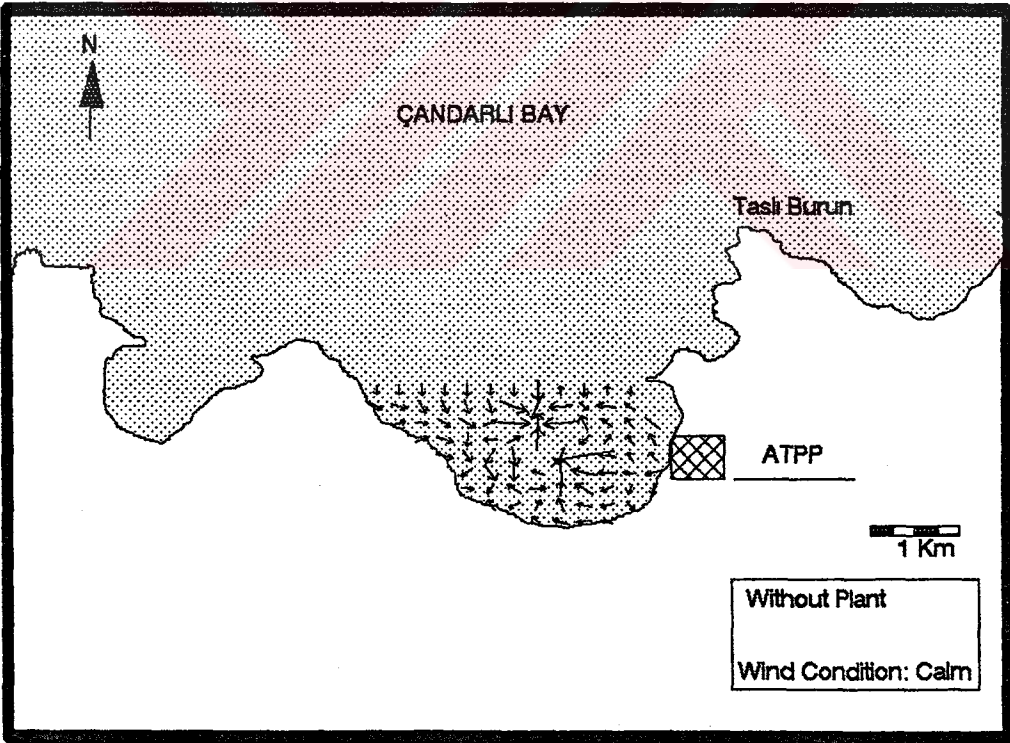


Figure 5.12. Surface Circulation Without Plant (Calm)

- in the order of  $0.01 \text{ m s}^{-1}$  on the coastal surface waters;
- in the order of  $0.02 \text{ m s}^{-1}$  on the open boundary surface waters;
- about  $0.02$  to  $0.08 \text{ m s}^{-1}$  at the middle parts.

In the hypothetical case of a moderate wind and operating plant, the estimated current velocities were:

- in the order of  $0.05 \text{ m s}^{-1}$  on the coastal surface waters; and,
- in the order of  $0.1 \text{ m s}^{-1}$  on the open boundary surface waters.

In the hypothetical case of calm conditions, the estimated surface current velocities were below  $0.01 \text{ m s}^{-1}$ , generally in the order of  $0.002 \text{ m s}^{-1}$ . In the hypothetical case calm conditions and operating plant, the predicted current velocities were slightly lower than that of the windy case. For both the windy and calm cases with plant operation, the maximum current velocity was not higher than  $0.45 \text{ m s}^{-1}$ , which was achieved only in the grid where the discharge was located. Tide, wind and plant operation were concluded to be effective on the circulation in the Gencelli Harbor, the latter being significantly dominant.

## 5.8 Summary and Conclusions

The effects of the operation of the proposed ATPP cooling water system on the Gencelli Harbor was evaluated using a three-dimensional, time-varying hydrodynamic and transport model, GLLVHT. Simulations with this numerical model were made in order to examine recirculation effects and the effects of various sustained wind events that would place the thermal plume on potentially sensitive shoreline areas. Comparison was made to the results of the near-field hydrothermal modeling studies. In general, a slight discrepancy



was observed between the GLLVHT model predictions and those of the near-field thermal plume analysis.

The simulation results indicate small surface temperature rises (below 0.8 °C) after reaching the stationary state, for a worst case of calm weather. Steady northeasterly (NE) winds (most frequent direction) had some effect on the shape of the surface plume, while easterly (E) winds (second most frequent direction) had very little effect.

The simulation results indicated very little recirculation at the intake. An extra rise of 0.07 °C due to recirculation was estimated for a worst case of calm weather. This rise in the excess temperature is due to the insignificant short circuiting of cooling water between the discharge and the intake.

The excess temperatures predicted by the intermediate and far-field modeling studies are quite lower than that of the near-field modeling studies. The discrepancy between the results can be attributed to the different natures of the models used in the studies. Near-field models, being based on the theory of plume, are used to predict the excess temperature on the jet trajectory. For this reason, the excess temperature values predicted by these models will be the maximum values at a certain horizontal plane. However, in the application of a three-dimensional numerical model, the excess temperature of a cell in the grid system is represented by a single value. Considering the dimensions of a cell (250x250x2 m), it can be stated that the value of excess temperature in a cell is an average value through the volume of the cell.

The cooling water operations of the proposed ATPP were predicted to affect the circulation in the Gencelli Harbor significantly. However, the expected current velocities are not expected to result in any shoreline-effects.

## **CHAPTER VI**

### **MARINE BIOLOGICAL IMPACTS OF THE ATPP: SHORT-TERM**

#### **6.1 General**

In this chapter, the expected and predicted short-term biological impacts of construction and operation of the proposed ATPP on the marine environment are discussed. The potential impacts of the proposed ATPP on marine biology are analyzed in both short and long-term time scales.

A brief review of the potential impacts and relevant concepts are given in Section 2.5. Here, the focus is on potential effects of cooling water operations on various marine organisms including fish, ichtioplankton, algae, phytoplankton, protozooplankton, zooplankton and zoobenthose.

The following possible short-term effects of the proposed plant on the marine life are also addressed:

- effects of the thermal discharge on heavy metal toxicity
- effects of liquid waste discharge
- effects of the construction phase

## 6.2 Effects on Fish

In general terms, freely-swimming fish are affected only if they are in the immediate vicinity of the discharge. It is possible to categorize the effects of a thermal power plant on marine fish as follows:

- thermal effects due to the rapid change in sea water temperature
- chemical effects related to antifouling agents
- mechanical effects due to entrapment and impingement

### 6.2.1 Thermal Effects on Fish

The potential thermal effects on fish can both be beneficial or detrimental. These effects include:

- advanced spawning times;
- improved growth rates;
- accumulation fish populations near the outlet area;
- mortality due to intolerable water temperatures by intermittent contact with the thermal plume; and,
- mortality due to intolerable decreases in water temperatures (cold shock) following plant shut-downs.

The predicted temperature rise in the Gencelli Harbor due to the operation of the proposed ATPP in the intermediate and far-field of the plant discharge was less than 1 °C. This condition was in compliance with the requirements of the Aquatic Products Regulation of the Aquatic Products Act and those of Water Pollution Control Pollution Regulation (Official Gazette # 19919, Dated 4.9.1988). Such a temperature rise in the harbor, is not expected



to have adverse effects on the benthic and the pelagic fish populations. In contrast, insignificant improvements in both spawning and growth rates are expected.

It is well known that fish can move into and out of heated plume on their own and concentrate in the discharge area (Hadderingh, 1979). Upto a critical point, which is between 30 and 35 °C, the fish can tolerate and sometimes prefer temperatures higher than they are acclimated. However, most of the temperal species are non-resident above 30 °C (GESAMP, 1984). The upper lethal temperatures of commercially important fish species found in the Gencelli Harbor are listed in Table 6.1 as adapted from a series of reference material (Chervinsky, 1978; Barnabe, 1976; Fonds, 1976 and Thomson, 1963).

Table 6.1 Critical Sea Water Temperatures for the Commercially Important Fish Species of the Gencelli Harbor (°C)

Species	Upper Lethal Temperature	Optimum Growth Temperature	Lower Lethal Temperature
<i>Sparus aurata</i>	34	25	3
<i>Dicentrarchus labrax</i>	34	22-24	1
<i>Solea vulgaris</i>	31	20-25	3
<i>Liza ramada</i>	31	22	3.5

Tolerance limits of some species observed in the Gencelli Harbor are given in Table 6.2 as adapted from several publications. (Langford, 1983; de Sylva, 1969; GESAMP, 1984; Akşiray, 1954).

Table 6.2. Tolerance Limits of Some Species Observed in the Gencelli Harbor (°C)

Species	Tolerance Limits
<i>Mullus surmuletus</i>	30-31
<i>Mullus barbatus</i>	32
<i>Gobius paganellus</i>	32
<i>Scorpaena porcus</i>	32
<i>Mugil cephalus</i> (adult)	38
<i>Mugil cephalus</i> (post larvae and prelarvae)	32
<i>Engraulis encrasicolus</i>	> 30
<i>Solea solea</i>	35

Based on the long and short term water temperature data, the expected maximum water temperature in Gencelli Harbor is about 23 °C, which most probably will occur in the month of July (Akyarlı, 1990-1991). The nearest meteorological station with long-term sea-water temperature data is the Dikili Meteorological Station. The Dikili water temperature data was analyzed in detail. The frequency distribution of the 1963-1985 data reveals that the monthly average water temperature is the highest in July, being 23.1 °C, and lowest in February, being 13.2 °C. And, on the average, the sea water temperature will be higher than 23 °C in about 32 days per year. However, the sampling conditions of this station cannot be considered appropriate. The reason for this is the selection of the measurement point located in a fishery harbor which has relatively low depths and very low water exchange capacity. Under these conditions, the temperature of the sea water is controlled by meteorological processes rather than oceanographic processes. In this regard, short-term field measurements indicated that the maximum sea-water temperature is less than 23 °C (Akyarlı, 1990-1991).

Under the conditions given above, with the addition of an excess temperature of 7 °C, the expected maximum water temperature is 30 °C, which will occur in the condenser. After the discharge, the dilution process of the plume will immediately start and the excess temperature of 7 °C will be diluted to about 0.8 °C at the water surface.

It is also expected that the fish entering the plume, in the near-field of the discharge, will be affected by the rapid temperature rise but no significant thermal mortalities of fish due to the operation of the proposed ATPP are expected.

No significant fish mortalities are expected due to so-called cold shocks experienced during plant shut-downs. It is reported that a temperature drop of less than 10 °C had insignificant effects on *Mugil cephalus*, which is observed and assumed to represent the fish community in the Gencelli Harbor (Lamadrid-Rose and Boehlert, 1988).

#### 6.2.2 Chemical Effects on Fish

Chemical effects include the possible adverse effects of antifouling agents on certain sensitive species. The concentration of the antifouling agent, NaOCl (sodium hypochlorite), which will be used in the ATPP, will be less than 0.01 ppm at the discharge point. Under the circumstances of such a low concentration, no adverse effects on fish are expected due to the antifouling chemicals.

#### 6.2.3 Mechanical Effects on Fish

Mechanical effects include the physical damages due to entrapment. The organisms which are drifted into the intake structure with the cooling water

are said to be entrapped. The term, impingement, refers to the direct action of being drawn onto the fine screens and hitting them (see Section 2.5).

The potential for impingement mortality strictly depends on the size of the fish and the physical characteristics of the intake area. Studies on impingement show that, young fish of small size, belonging to such species as *Torpedo marmorata* and *Atherina boyeri* are most susceptible to be entrapped but have the chance to survive if their size and intake parameters are proper (Moazzam and Rizvi, 1980; Turnpenny et al., 1980). Both of these species are observed in the Gencelli Harbor. It was observed that as the length of fish decreased from a range of 10-40 cm to a range of 4-7 cm, the impingement mortality rate increased from 0 to 95 % (Hadderingh, 1979). It is also reported that by a proper design of the intake structure and barriers, it is possible to achieve impingement survival rates of up to 100 % (Hadderingh, 1979).

Due to their completely unknown patterns of behaviour, it is not possible to predict the number of fish species that will be entrapped and face impingement mortality. However, assessment of the mitigation measures to reduce the impingement mortality of fish will provide valuable information about the impingement potential of power plant on fish population. The most effective measures in controlling impingement of fish are:

- appropriate location of the intake systems;
- restriction of cooling water flow; and
- barriers to stop fish from entering the intake.

The intake structure of the proposed ATPP was located on the eastern coast of the Gencelli Harbor. The results of the field surveys conducted by Ege University revealed that this area was relatively poor in terms of ichtioplankton concentrations and food for fish (ATPP EIA Phase-2 Report, 1992). Low larval

and egg, hence fish populations near the intake area are expected to result in a decrease in the impingement potential of the proposed plant.

In general, the impingement potential can be significantly reduced by a proper screen design and limiting the approach velocities in the intake channel to about  $0.15 \text{ m s}^{-1}$ . Moazzam and Rizvi (1980) reported a tendency of fish to impingement with a withdrawal velocity of  $0.13 \text{ m s}^{-1}$  or greater.

The cooling water of the proposed ATPP will be taken from the Gencelli Harbor with a velocity of about  $0.2 \text{ m s}^{-1}$ . This value is in agreement with the above guideline values. However, screen design parameters of the proposed ATPP have not been decided upon at the present time.

### 6.3 Effects on Ichtioplankton

Ichtioplankton, may be affected by the cooling water system of a thermal power plant in the following ways:

- entrainment
- warming of the receiving waterbody
- decrease in dissolved oxygen levels
- contamination of the waterbody by chemicals

#### 6.3.1 Effects on Ichtioplankton Due to Entrainment

Planktonic organisms, which are drifted into the condensers passing through the fine screens are termed as entrained organisms (See Section 2.5). In this regard, the ichtioplankton may be entrained into the condensers of the plant with the cooling water. The entrained ichtioplankton are then exposed to:

- a relatively high and rapid temperature rise;
- significant mechanical and chemical stresses; and,
- a rapid decrease in ambient temperature, following the discharge.

The thermal, mechanical and chemical stresses on the entrained ichtioplankton are discussed in the sub-subsequent sections.

#### a. Thermal Stresses on the Entrained Icthioplankton

As almost all other effects, the entrainment effects of a thermal power plant are case specific. The existence and/or degree of thermal effects on the entrained ichtioplankton depend on design parameters, as well as environmental conditions. In particular, the most significant adverse entrainment effects are observed, in the following cases:

- temperature rises of more than 10 °C in the condensers;
- long exposure times to thermal stresses; and
- in plants which use long discharge channels where the larvae are exposed to thermal shocks for relatively long time periods, in the order of hours.

It is reported that larvae can generally withstand excess temperatures around 12 °C for at least 40 minutes without any significant increases in mortality (Schubel, 1975). In the case of the proposed ATPP, the exposure time of ichtioplankton to various stresses is in the order of a few minutes. This exposure time is the time elapsed between the condensers and a point at the surface where an excess temperature of less than 1 °C is reached. Once released back to the sea, surviving organisms are exposed to gradually decreasing temperatures and in some cases to cold shock.

#### **b. Mechanical Stresses on the Entrained Ichtioplankton**

Based on several studies, it can be stated that the contribution of mechanical stress to the entrainment mortality ranges between 8.5 to 100 % (Majewski and Miller, 1979; Crippen and Fahmy, 1981). As given by Marcy (1973), the generally accepted value for the contribution of mechanical stress is about 80 %. Mechanical stresses include:

- mechanical shocks due to turbulence;
- mechanical shocks and abrasions due to collision with screens, walls and equipment parts; and,
- pressure changes due to pumping.

#### **c. Chemical Stresses on the Entrained Ichtioplankton**

The chemicals used to prevent biofouling is one of the major factors contributing to the entrainment mortality. In the case of the proposed ATPP, the antifouling agent that will be used is NaOCl (sodium hypochlorite). The concentration of NaOCl at the intake head will be 1.0 mg l<sup>-1</sup>, gradually decreasing to a value less than 0.01 mg l<sup>-1</sup> at the discharge point. No suitable data could be found in literature in order to assess the effect of a 1.0 mg l<sup>-1</sup> NaOCl concentration on ichtioplankton. However, conservative assumptions were made in the entrainment modeling studies considering this point.

#### **d. Entrainment Modeling**

To estimate the effects of entrainment, the three dimensional hydrodynamics and constituent transport model (GLLVHT) was used. In field studies, tracers are generally used to observe dilution and dispersion processes in marine environment. For this purpose, a dye can be released as

a slug or a continuous source. Equivalent to the "dye" of a field study, a "numerical dye" concept can be used in numerical modeling studies. With this intention, the numerical dye is introduced at a given location and time. Then the fate of this hypothetical substance is observed by means of model expressions simulating such processes as diffusion and dispersion.

In the entrainment modeling studies, a numerical dye was used in the GLLVHT model to represent the ichtioplankton. The initial number of the numerical dye was set to a value of 100 in each modeling grid of 250x250x2 m. The major assumptions of this approach are summarized below:

- The ichtioplankton is uniformly distributed in the harbor.
- All the ichtioplankton in the modeling grid, where the intake is proposed to be located, will be entrained with the cooling water.
- All of the entrained organisms will be lost during passage through the cooling system (100 % entrainment mortality rate).
- The production of eggs is continuous and homogenously distributed over the spawning time.

It is hard to predict the degree of the effects of the thermal, mechanical and chemical stresses discussed in the previous sub-sections. In this regard, assuming a 100 % mortality, all these stresses were taken into account in a conservative manner.

Two numerical dyes were used to predict the effect of entrainment on the ichtioplankton population in the modeled area. Using GLLVHT, one of the two numerical dyes, of the same properties, was mathematically subjected to entrainment while the other was kept free of the entrainment effect. At any instant, the cases with and without entrainment were compared by comparing the total amounts of the two dyes, one continuously being entrained and the



other not. The difference between the amounts of dyes or the entrainment effect was expressed as percent decrease in the amount of dye and termed as the instantaneous entrainment ratio.

With the intention of minimizing the entrainment impact, this modeling approach was used to investigate the effects of flow rate on entrainment. The variation of the instantaneous entrainment ratio with flow rate is shown in Figure 6.1. As can be seen in the figure, stationary-state conditions are reached at the end of second day of the simulation. As expected, the effect of entrainment increases significantly with increasing flow rate. The estimated instantaneous entrainment ratios for the flow rates 23.3, 46.6 and 93.2  $\text{m}^3 \text{s}^{-1}$  are 1.5, 2.0 and 2.5 % respectively.

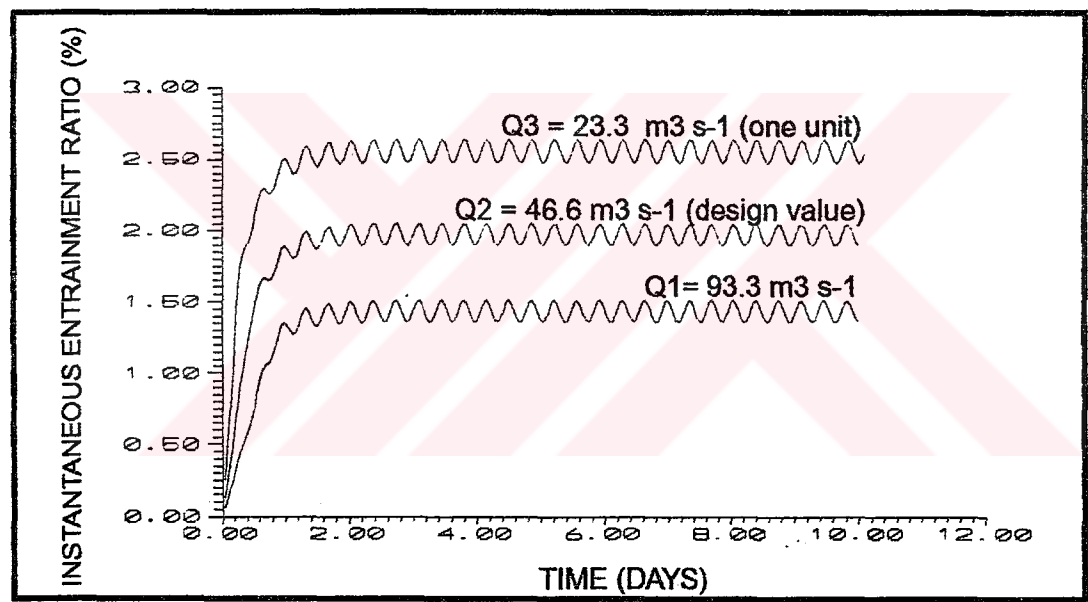


Figure 6.1. Entrainment Ratios for Various Flow Rates

In entrainment modeling, the entrainment problem was treated without differentiating between egg and larvae. In other words, the Ichtioplankton, whether it is in the form of egg or larvae, is treated as one. However, in the long-term modeling studies they were considered separately (see Chapter 7). Larvae are most susceptible to entrainment in the first three months of their

lives. Since both eggs and larvae are drifted with dominant flows, the entrainment effect is the same for the larvae at this stage and eggs. Therefore, the estimated entrainment ratios are the same for both.

Based on the field surveys conducted by Ege University, the average larval and egg concentrations at the proposed intake area were 4.75 (# of larva/m<sup>3</sup>) and 7.5 (# of eggs/m<sup>3</sup>), respectively (ATPP EIA Phase-2 Report, 1992). Using these values, it is also possible to estimate the approximate number of ichtioplankton that will be entrained by the ATPP. Considering the species observed in the marine biology survey period (see Chapter 2), it was estimated that the number of larva and egg which will be entrained by the proposed ATPP will be about  $20 \times 10^6$  and  $30 \times 10^6$  per day, respectively.

#### 6.3.2 Effects on Ichtioplankton Due to Warming of the Receiving Waterbody

Temperature rise in the intermediate and far-field of the discharge is another important factor influencing ichtioplankton. In the near-field of the discharge, the excess temperature of 7 °C was predicted to gradually decrease to about 1 °C. Compared to the Gencelli Harbor, this area is very small (with horizontal dimensions of about 100x50 m and a depth of 10 m). The hydrothermal modeling studies indicated that the temperature rise due to the plant operations will be lower than 1°C in the Gencelli Harbor, except this zone. The estimated surface excess temperature values ranged between 0.01 °C at the northern open boundary of Gencelli Harbor to 0.79 °C at the point where the discharge jet reaches the surface.

An excess temperature up to 1 °C is not expected to result in any adverse effects. On the contrary, slightly improved embryonic and larval developments are expected.

### 6.3.3 Effects on Ichtioplankton Due to Decrease in Dissolved Oxygen Level

In either fresh or saline water, increasing temperature has a decreasing effect in dissolved oxygen concentration essential for marine organisms. The maximum ambient sea water temperature in the Gencelli Harbor was about 23 °C in summer with insignificant variations with depth. In this case, a maximum water temperature of about 30 °C will be obtained in the condenser. As an example, for a typical sea water, the saturated dissolved oxygen levels for these two temperatures are 7.00 and 6.13 mg l<sup>-1</sup>, respectively. Thus, the D.O. level reduction in the Gencelli Harbor due to a temperature rise of less than 1°C is expected to be insignificant and no adverse effects on ichtioplankton are expected due to D.O. level changes in the Gencelli Harbor.

### 6.3.4 Effects on Ichtioplankton Due to Antifouling Chemicals

Another major effect of power plant cooling facilities is the contamination of the waterbody by the antifouling chemicals. According to the proposed design, concentration of the antifouling agent, NaOCl, will be less than 0.01 ppm at the discharge point (ATPP EIA Phase-2 Report, 1992). Under these circumstances, no adverse effects on ichtioplankton are expected due to the low concentration of the antifouling chemical.

## 6.4 Effects on Algae

Observed lethal temperatures of some algal species found in the Gencelli area are given in Table 6.3 as adapted from the data of Verlaque (1977). The tolerance limits given by Altman and Dittmer (1966) are listed in Table 6.4.

Table 6.3. Lethal Temperatures for Algal Species (Verlaque, 1977)

Species	Temperature (°C)	Duration (hour)
<b>CHLDROPHYLEAE</b>		
<i>Ulva rigida</i>	45	1-2
<i>Cladophora prolifera</i>	46	1-2
<i>C. pellucida</i>	30	12
<i>Enteromorpha compressa</i>	35	12
<i>Udotea petiolate</i>	45	1-2
<b>PHAEDPHYCEAE</b>		
<i>Cladostephus spongiosus f. verticillatus</i>	30	12
<i>Dictyota dichotoma</i>	27	12
<i>Halopteris filicina</i>	27	12
<b>RHODOPHYCEAE</b>		
<i>Laurencia obtusa</i>	27	12
<i>Nithophyllum punctatum</i>	40	1-2
<i>Ceramium rubrum</i>	46	1-2
<i>Peyssonnelia squamaria</i>	46	1-2

Table 6.4. Tolerance Limits for Algae (Altman and Dittmer, 1966)

Species	Minimum Tolerance (°C)	Maximum Tolerance (°C)
<i>Anadyomena stellata</i>	8	32
<i>Dictyota dichotoma</i>	3-5	27-32
<i>Laurencia obtusa</i>	14	35

Based on the available data, no significant adverse effects of the power plant on the algal species can be expected in the Gencelli Harbor. However, based on the values presented in Tables 6.3 and 6.4, it is expected that in the hot summer season during which the ambient sea water temperature exceeds a value of 23 °C, the algal species adjacent to the limited area of the discharge may be replaced by other more temperature tolerant species.

## 6.5 Effects on Phytoplankton and Protozooplankton

It is expected that, the relatively high growth rates and short doubling times of the phytoplankton and protozooplankton will compensate their loss due to entrainment. It is also expected that the growth of the temperature resistant species such as *Navicula sp.* may be favoured at 27-32 °C (Langford, 1983). However, other species may be reduced in numbers or eliminated in the limited area adjacent to the discharge structure. In overall, no significant adverse effects of the ATPP cooling system on the phytoplankton and protozooplankton species are expected in the Gencelli Harbor.

## 6.6 Effects on Zooplankton

Zooplanktons are the most sensitive organisms to the thermal power plant cooling operations. In the condensers, Zooplanktons are exposed to considerable mechanical, thermal and chemical stresses.

Reported lethal temperatures for the species of the Gencelli Harbor, such as *Acartia clausi*, *Centropages typicus*, *Eutepina acutifrons*, and *Clausocalanus sp.*, are between 29 and 34 °C (Benon and Gaudy, 1979). The observed mortality for some zooplankton species, including *Acartia clausi*, is

50 % at temperatures between 30 and 34 °C (Parent, 1979; GESAMP, 1984). The expected mortality rates for thermally stressed but unentrained *Euterpina* sp. and *Labidocerra* sp. are given as 12 and 20 %, respectively, at 30 °C (Alden III, 1979).

A temperature increase of less than 1 °C is not expected to result in significant effects on the zooplankton population of the Gencelli Harbor. However, it is expected that zooplankton species entrained with the cooling water will be adversely affected.

It is reported by several researchers that the temperature rise increases the effects of heavy metals and chlorine on marine organisms (Benon and Gaudy, 1979; Langford, 1983). It is possible to minimize the effects of temperature rise on chlorine toxicity by controlling the concentration of chlorine in the cooling water system. A chlorine concentration of 1.5 mg l<sup>-1</sup> resulted in 100 % mortality, whereas concentrations in the range of 0.25 to 0.75 mg l<sup>-1</sup> lead to 0 % mortality, at 33 °C (Langford, 1983).

As a result, in the area adjacent to the intake structure, local disappearance of some species may be expected. However, a temperature increase of less than 1 °C in the Harbor is not expected to result in significant effects on zooplanktons.

## 6.7 Effects on Zoobenthose

The observed effects of power plants on zoobenthic species similar to that of the Gencelli Harbor are attributed to excessively high temperature rises and long exposure durations. For instance, the upper avoidance temperature of *Gammarus* sp. is 33.8-34.3 °C for 1-hour exposure (Ginn and O'Connor,

1978). No delaying effects on reproduction of the same specie was observed at 34.3 °C for 60 minutes (Langford, 1983). Upper tolerance limits for *Poatocerus triqueter* and *Tellina tenuis* are 30 and 32-36 °C, respectively (Klöckner, 1978; Bodoy and Masse, 1978). *Mytilus galloprovincialis* has an optimum temperature range in between 15-20 °C and it is temperature-sensitive above 25 °C, for larval development (Hrs-Brenko, 1974). It was observed that the amphipods survived a 1-hour exposure to cooling water effluents with temperature rises of 7.3 - 9.3 °C and total chlorine concentrations of 0.05 mg/l (Ginn and O'Connor, 1978). A fouling organism *Balanus balanoides*, is known to spawn at 27 °C (Crips, 1957). Since such a temperature may be achieved only at a very limited area and in a limited time of the year, significant production of this specie is not expected in the harbor.

The hydrothermal modeling studies showed that the temperature increase on the southern and eastern shore areas close to the discharge structure will be lower than 0.5 °C. The excess temperature values at the other benthic areas were estimated to be insignificant. Further, the antifouling concentration in the discharge is expected to be below 0.01 ppm. Under these conditions, no significant effects of the proposed cooling water facilities on the zoobenthose community are expected, other than the limited entrainment of larvae belonging to certain species.

## 6.8 Effect on Heavy Metal Toxicity

Augmentative contribution of temperature increments to the effects of heavy metals on marine organisms are observed in many cases. For instance, Cd, Pb and Zn were observed to have increasing adverse effects with increasing temperature on *Eurydice pulchra* and *Faera nordmanni* (Jones, 1975). However, it was also observed that increasing temperature decreased Fe-59 bioaccumulation by decreasing the metabolic reactions (Fraizer, 1974).



Field observations in Gencelli Harbor showed that Cu, Zn, Cd, Pb and Mn concentrations in water samples were close to the values observed in clean waters. Of the heavy metals in the sediment samples, only Fe was in excessive amounts (see Section 2.3.6). Fe concentrations in the sediments, were attributed to the iron and steel industries in the region (ATPP EIA Phase-2 Report, 1992).

It is expected that, a temperature rise of less than 1 °C in the intermediate- and far-field of the plant will increase neither the absorption of heavy metals by the organisms nor the solubility of the heavy metals stored in the sediments.

#### 6.9 Effects of Liquid Waste Discharge

Since, the wastewaters of the proposed ATPP will be subjected to treatment and will meet the Turkish standards, no adverse and significant effects are anticipated due to liquid waste discharge to the Gencelli Harbor.

#### 6.10 Effects of Construction Facilities on Marine Life

Localized and temporary adverse effects on marine life in the Gencelli Harbor are expected due to the construction of cooling water intake and discharge structures, wharf and pipelines. Significant loss of habitat in the dredging site is expected. However, the habitat is expected to recover in the long-run. The increased turbidity and decreased light penetration may adversely effect the primary producers in the area adjacent to the dredging site. Based on measured concentrations in the sediment, except iron, no bio-accumulation of heavy metals due to the resuspension of sediments was anticipated. As a result of unfavourable conditions in the area, it is expected that the free swimming species, such as fish, will avoid the area.



## **6.11 Effects of Fuel Delivery, Conveyance and Storage**

Coal and fuel-oil needed for plant operation will be delivered via marine shipping. Depending on vessel size, coal delivery will require about 40 vessels per year; whereas, oil delivery will require approximately 20 vessels per year. In order to reduce the adverse effects of unlikely but possible accidental oil spills during oil delivery, floating oil fences will surround the oil carrier while it is anchored at the unloading wharf.

Coal will be transported to the storage area via conveyors. Appropriate dust control measures for off-loading, transport and storage are proposed for the ATPP. The coal unloading facility at the wharf is proposed to have lagging and cover to prevent generation of dusts. The conveyors are proposed to be provided with dust prevention covers. The coal in the storage yard is proposed to be provided with adequate humidity by sprinkling water to prevent dusting. The surface runoff from the coal storage area is proposed to be directed to a sedimentation basin followed by oil separation before being discharged.

In light of the proposed precautions, no pivotal adverse effects of coal and fuel-oil delivery, conveyance and storage should be anticipated under normal operating conditions.

## CHAPTER VII

### MARINE BIOLOGICAL IMPACTS OF THE ATPP: LONG-TERM

#### 7.1 General

Environmental impact assessment studies, emphasize the potential impacts on valued ecosystem components (VEC's). In general, the VEC term is used for those species which have commercial, recreational or cultural value. In this study, the commercially important fish species of the Gencelli Harbor were considered as VEC's. In this regard, the long-term impacts of the proposed ATPP on *Mullus barbatus* and *Sparus aurata* were investigated for a sufficiently long period of 100 years.

#### 7.2 Study Approach

It is a well known fact that entrainment of ichtioplankton and impingement of small fish are the two most important mechanisms for long-term impacts of cooling water operations on various types of fish populations. Similarly in this study, analysis of the short-term effects indicated that entrainment and impingement effects may lead to adverse impacts in the long run (see Chapter 6). Consequently, after quantifying the phenomenon of ichtioplankton entrainment, an integrated life cycle model (LCM) was developed to investigate the long-term effects of ichtioplankton entrainment on the overall population of selected fish species. The LCM adapted for the

ATPP, simulates the life cycles of a population by means of appropriate mathematical formulations compiled from the pertinent literature (Beverton and Holt, 1957; Hess et al., 1975; Ogawa and Mitsch, 1979; Ricker, 1975).

As discussed in the subsequent sections, the developed LCM is flexible in the sense that it is possible to estimate the long-term impacts of both entrainment and impingement mortalities. However, in the case of a proposed facility, it is not feasible to precisely quantify the impingement mortalities due to the irregular mobility and the completely unknown patterns of behavior of the fish species. Therefore, only the long-term effects of entrainment are addressed in this study.

### **7.3 Theoretical Basis and Structure of the LCM**

#### **7.3.1 Life Stages**

For a given fish population, the following life stages were considered in the LCM:

- egg
- larvae
- juvenile
- yearling (sexually mature or not)
- adult (sexually mature or not)

A schematic representation of the above life-stages is given in Figure 7.1. According to this scenario, the following events take place:

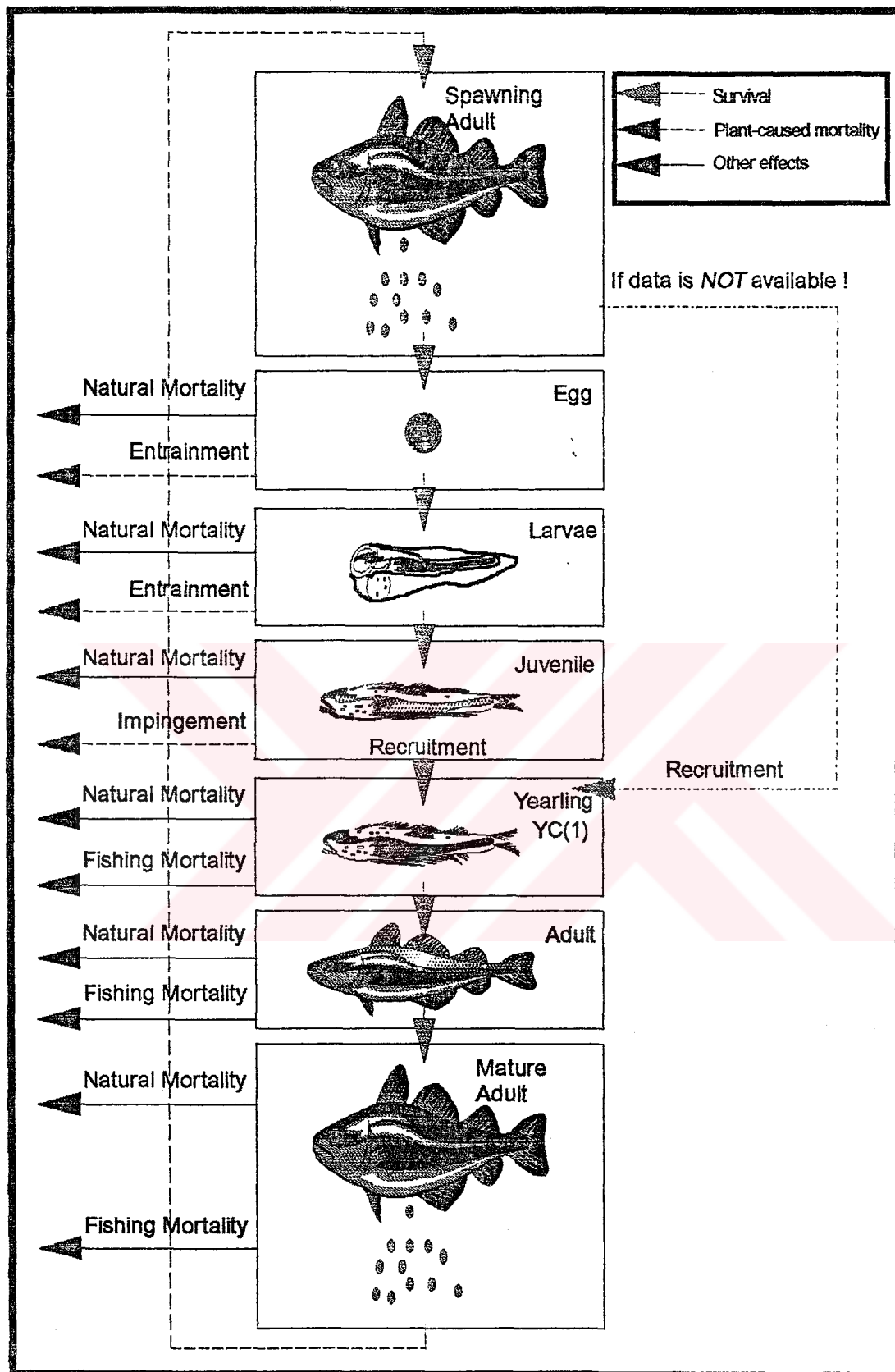


Figure 7.1. Life-cycle Scenario of Fish

- Sexually mature adult fish species produce eggs during the spawning season.
- Eggs are subjected to both natural (including prey action) and entrainment mortality.
- Larval stage begins for the surviving eggs.
- Larval species are also subjected to natural and entrainment mortality.
- Juvenile stage begins following the larval stage.
- Juveniles are capable of swimming and are relatively larger in size. For this reason, they predominantly undergo impingement mortality rather than entrainment mortality.
- Surviving juvenile species are recruited to the adult population, which covers the yearlings as well as sexually immature and sexually productive individuals.
- If the sizes of the young fish are not large enough, they may also be subjected to impingement mortality.
- Depending on the characteristics of the species and environmental conditions, a number of individuals reaches to sexual maturity.
- Once sexually productive, an individual is only subject to natural and fishing mortality.

In this approach, from a very large pool of eggs only a limited number of sexually mature adults are produced via a series of life stages each with decreasing populations.

### 7.3.2 Assumptions of the LCM

Several factors affecting the dynamics of a fish population were included in the LCM. External factors such as temperature, food availability, and

competition with other species were not directly included; but, taken into account in various rate expressions. The major assumptions of the model can be summarized as follows:

- (i) Egg production is continuous throughout the spawning period with a constant rate.
- (ii) Mortality terms for the pre-recruit species have two components; one of which is not dependent on the density of the pre-recruit population. The other component is density-dependent and induces a limited compensation of the losses due to entrainment mortality. It should be noted that a fully density-independent relationship would result in an exponential and unrecoverable decrease in the population even with a low effect of entrainment mortality.
- (iii) The mortality rates for eggs, larvae and juveniles are different but constant for each life-stage. However, in case of insufficient data, equal mortality rates for eggs and larvae can be used with a certain error.
- (iv) Pre-recruit species are most susceptible to entrainment during their egg and larva stage.
- (v) Since it is not viable to predict impingement effects in the case of a non-existing facility, juveniles are assumed to be subjected only to natural mortality.
- (vi) The pre-recruit stage lasts 365 days. At the end of this period, the surviving juveniles are recruited to the adult population.
- (vii) Adults of year-class 1 and older undergo no entrainment or impingement mortality.

- (viii) Fish of year-class 2 and older have equal and constant survival rates.
- (ix) At any instant, the population of a given life stage is obtained by multiplying the population of the previous stage with a constant less than unity. According to this assumption, the overall population structure regulates itself in the long run and remains fixed, even though there may be temporal variations in the populations of different life stages.

### 7.3.3 Formulation and Computational Steps of the LCM

In this section, the formulation and computational steps of the LCM are discussed. A computer program was constructed to apply the model more efficiently. The computational steps are given in Figure 7.2.

#### a. Initial Year-Class Structure

The first step in the application of the LCM is the definition of the initial year-class structure of the population. With this intention, the initial number of species in each year-class (age) and their survival rates must be input for the first year of the simulation period. Then, at any subsequent year, the year-class structure of a population can be estimated using the following general approach (Hess et. al., 1975):

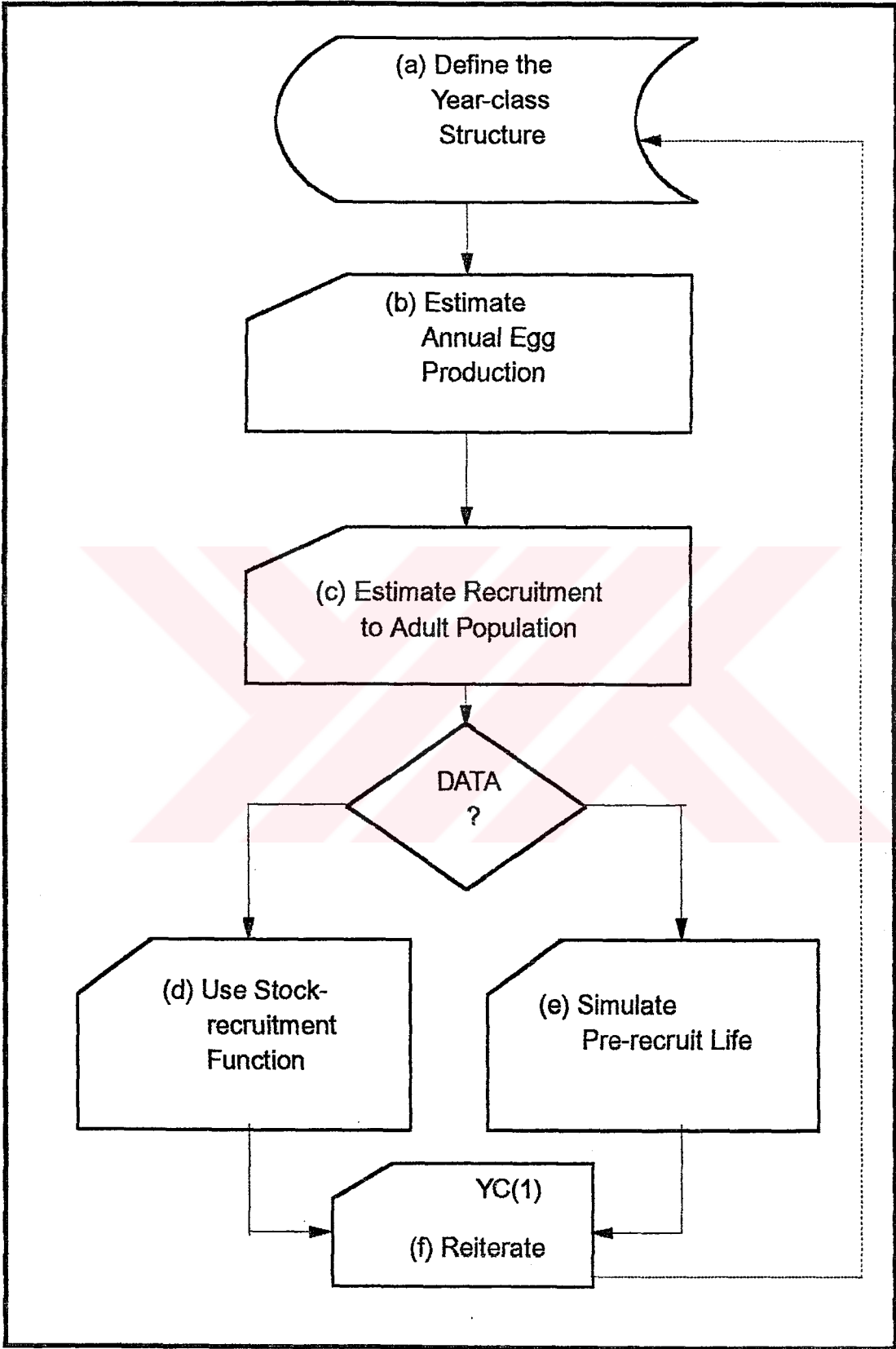


Figure 7.2.Computational Steps of the LCM



$$YC(2) = s_1 \cdot YC(1) \quad (7.1)$$

$$YC(3) = s_2 \cdot YC(2) = s_2 \cdot s_1 \cdot YC(1) \quad (7.2)$$

$$YC(4) = s_2 \cdot YC(3) = s_2^2 \cdot s_1 \cdot YC(1) \quad (7.3)$$

$$YC(j) = s_2^{j-2} \cdot s_1 \cdot YC(1) \quad (7.4)$$

where;       $YC(j)$ : the number of individuals in  
    any given year-class  $j$   
 $j$ :      year-class counter (age of fish)  
 $s_1$ :      annual survival rate of yearlings  
 $s_2$ :      annual survival rate for fish of age 2 and older

In general, the survival rate is defined as the ratio of the fish population remained at time  $t$  to initial population (at  $t=0$ ). The  $s_1$  parameter can be estimated using the following equation (Hess et al., 1975):

$$s_1 = T / YC(1) \cdot \sum_{j=0}^{n-2} s_2^j \quad (7.5)$$

where;       $T$ :      total number of fish age 2 and older  
 $s_2$ :      survival rate  
 $n$ :      life-time of fish species

The value of  $s_2$ , on the other hand, is calculated using the following general equation for survival rate (Ricker, 1975):

$$s_2 = e^{-Z} \quad (7.6)$$

where;        Z:        instantaneous total mortality rate

The instantaneous total mortality rate, Z, is defined as the ratio of the number of deaths per unit time to the population abundance during that time, if all deceased fish were to be immediately replaced so that population does not change. For using the LCM, Z must be given as an input. This parameter can be obtained from either field studies or literature (for details, see Ricker, 1975).

A number of different mortality rate coefficients are used in the LCM. The interrelationship between these mortality rates can be expressed by means of the following equations (Ricker 1975):

$$A = 1 - s_2 = u + v \quad (7.7)$$

$$Z = F + M \quad (7.8)$$

$$\frac{Z}{A} = \frac{F}{u} = \frac{M}{v} \quad (7.9)$$

where;

A:	annual total mortality rate (defined as the number of fish which die during a year or season, divided by the initial number)
$s_2$ :	annual survival rate
u:	annual fishing mortality rate
v:	annual natural mortality rate
Z:	instantaneous total mortality rate
F:	instantaneous fishing mortality rate
M:	instantaneous natural mortality rate

## b. Egg Production

The second step of the LCM is the estimation of the number of eggs produced in a year by all the sexually mature individuals, belonging to different year-classes. In the LCM, the total number of eggs produced in a year is calculated using the following equation:

$$P_i = S_r \cdot T_{m,i} \cdot MF \quad (7.10)$$

where;      i:      year  
               $P_i$ :      total number of eggs produced in any given year i  
               $S_r$ :      fraction of females in the population (sex ratio)  
               $T_{m,i}$ :      total number of sexually mature fish in year i  
              MF:      mean fecundity (average egg production) of a  
                          mature fish

The sex ratio,  $S_r$ , for a given fish species can be found in the pertinent literature. The total number of sexually mature fish in any given year ( $T_{m,i}$ ) can simply be calculated by summing up the number of fish at the age of maturity and older. For the prediction of the mean fecundity (or productivity), one can use the typical ranges given in literature (Benli and Uçal, 1990; Muhtaroğlu, 1988; Toğulga, 1977). For the same purpose, it is also possible to employ various empirical relationships correlating MF with such variables as age, weight, length and environmental conditions (Cihangir 1991; Dremière, 1979; Torcu, 1987).

## c. Recruitment to the Adult Population

The third step is the prediction of the number of pre-recruit species which will be recruited to the adult population. Based on availability of data, the

number of recruited species can be predicted by one of the following approaches:

- by using the so-called Ricker stock-recruitment function
- by simulating the pre-recruit life of the species

d. Stock-Recruitment Function

In lack of sufficient data on the pre-recruit life of fish, the recruitment to year-class 1 can be estimated by using the stock (of eggs) and recruitment (to first year-class) concept, originally developed by Ricker (1954). Modifying the density dependent relationship between egg production and recruitment given by Ricker (1958), the following function was utilized in the LCM in order to predict the number of pre-recruit species which will be recruited to the adult population:

$$YC_i(1) = (1-MPL) \cdot P_{i-1} \cdot e^{a-b \cdot P_{i-1}} \quad (7.11)$$

where;  $YC_i(1)$ : number of individuals in year-class 1 in any given year i  
 $MPL$ : plant-caused mortality  
 $a$ : empirical coefficient representing overall density-independent mortality  
 $b$ : empirical coefficient representing overall density-dependent mortality

The plant-caused mortality (MPL) describes the effect of cooling water operations on recruitment. If sufficient data on the mortality rates of pre-recruit species is not available, the instantaneous entrainment ratio can be used as the entrainment effect on recruitment (MPL) in the above way. As stated in Chapter 6, the instantaneous entrainment ratio represents the ratio between

a pre-recruit population with and without entrainment effect of plant, at any time. So, the instantaneous entrainment ratio at the end of a year represents the decrease in recruitment to fish population.

The determination of the parameters a and b requires detailed and long-term field data. On the other hand, Hess et al. (1975) developed an alternative approach for the determination of a and b, which can be used when such data is unavailable. The following equations, developed by Hess et al. (1975), are used in the LCM:

$$a = \ln \frac{YC_o(1)}{S_r \cdot MF \cdot (T_m)_1} + b \cdot S_r \cdot MF \cdot (T_m)_1 \quad (7.12)$$

$$b = \frac{\ln \frac{v}{S \cdot S_r \cdot MF} - \ln \frac{YC_o(1)}{(T_m)_1 \cdot S_r \cdot MF}}{MF \cdot S_r \cdot ((T_m)_1 - T_{max})} \quad (7.13)$$

where;  $(T_m)_1$ : total number of sexually mature fish in the first year of simulation  
 $YC_o(1)$ : the expected net number of yearlings produced in the first year from  $(T_m)_1$  mature fish  
 $v$ : annual natural mortality rate  
 $s$ :  $s_1, s_2$   
 $T_{max}$ : the maximum level of fish population

The Ricker stock-recruitment function is based on the assumption that, in the absence of artificial adverse conditions such as fishing, any given fish population will reach an equilibrium state between natural mortality and recruitment. At this equilibrium condition, the total number of mature fish will

reach a maximum level,  $T_{max}$ . An estimate for  $T_{max}$  can be obtained from those statistics on fish stocks corresponding to periods of minimum fishing. More conveniently,  $T_{max}$  can also be estimated by running the LCM with zero fishing mortality.

Once the number of individuals recruited to the adult population of a given year (i) is predicted, one should reiterate all the calculations for the subsequent years.

#### e. Pre-recruit Life Simulation

The number of species recruited to the adult population can also be predicted by simulating the pre-recruit life by using empirical mortality rates. In this approach, the natural mortality rates of the pre-recruit individuals (egg, larvae and juvenile) are estimated by using experimental data representing the change of number of pre-recruit individuals with time.

A mass-balance relationship was developed to simulate the pre-recruit phase of the selected fish population. Based on this relationship, the time rate of change of a pre-recruit population,  $P$ , is given as follows:

$$\frac{dP}{dt} = - (k_{pe} + k_{pi}) P - (k_i + k_d P) P \quad (7.14)$$

where;

$P$ :	number of pre-recruit species
$k_{pe}$ :	coefficient of entrainment mortality (time <sup>-1</sup> )
$k_{pi}$ :	coefficient of impingement mortality (time <sup>-1</sup> )
$k_i$ :	coefficient of density-independent natural mortality (time <sup>-1</sup> )
$k_d$ :	coefficient of density-dependent natural mortality (time <sup>-1</sup> )

The first right-hand term in Equation 7.11 represents the decrease in the pre-recruit population due to the operation of the cooling water system. Here, the plant-caused mortality is expressed by two terms,  $k_{pe}$  and  $k_{pl}$ . The second term represents the loss of pre-recruit species due to natural mortality. As can be seen, natural mortality has one density-independent and one density-dependent component.

For ichtioplankton (egg and larvae), there is no impingement effect; hence,  $k_{pl}=0$ . On the other hand, entrainment is not effective on juveniles, and hence  $k_{pe}=0$ . Similarly, it is generally accepted that there is no density-dependent natural mortality for the juveniles ( $k_d=0$ ). In the application of the LCM to the case of the ATPP,  $k_{pe}$  for ichtioplankton was predicted with the three-dimensional, numerical hydrodynamics and transport model, GLLVHT. Since, the ATPP is non-existing (operative),  $k_{pl}$  for juveniles was assumed to be zero. However, in the case of existing facilities,  $k_{pl}$  can be estimated by monitoring the number of species lost due to impingement and comparing this loss to the total number of juveniles predicted proper stock assessment techniques.

The pre-recruit life simulation is based on the life-stage scenario given in Figure 7.1 of Section 7.3.1 and Equation 7.14. If this approach is applied to a given number of eggs produced in a single day, a certain fraction of these eggs will be lost due to both natural and plant-caused mortality. After certain days, the surviving eggs will start the larval stage. Being subjected to similar conditions with that of eggs, the surviving larvae will start the juvenile life-stage. Then as a result of density-independent natural mortality, a certain fraction of the surviving juveniles will be recruited to the adult population.

In this simplified case, by using proper values for  $k_{pe}$  (at the ichtioplankton stage),  $k_{pi}$  and  $k_d$  (for the juvenile stage), one would obtain the hypothetical curve given in Figure 7.3 which represents the change in the number of pre-recruit individuals with time. However, the actual field conditions are quite different due to the fact that the spawning of fish is distributed over a certain period (which is different for different fish species). In this regard, a single fish does not release all the eggs in one day but at certain times during the spawning period.

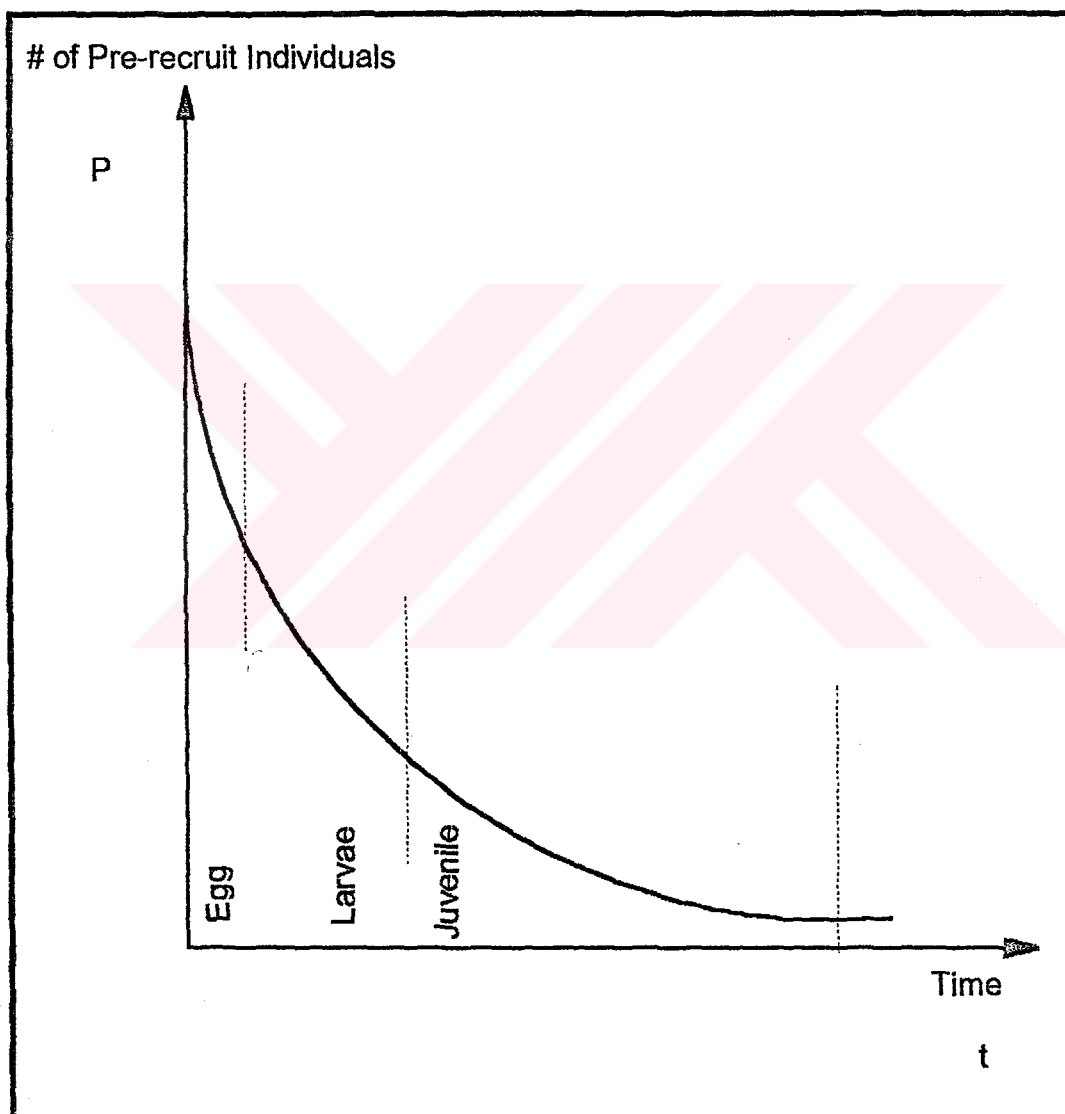


Figure 7.3. Change in the Number and Composition of a Pre-recruit Community



As illustrated in Figure 7.4, the year-long development of the pre-recruit population can be observed in the columns of a hypothetical matrix. The number of columns in this matrix is governed by the length of the spawning period. In this formation, one can follow the evolution of the eggs spawned in a given day in the corresponding column. Similarly, the instantaneous distribution of the pre-recruit species can be perceived by scrutinizing the rows of the matrix.

For instance, at day  $m$ , there are juveniles which descended from the eggs spawned at the first day of the spawning period. On the other hand, the eggs spawned in the next  $(n-1)$  days of the spawning period are still in the ichtioplankton stage.

It should be noted that, due to the density-dependency of natural mortality, Equation 7.14 cannot be directly applied to each cell of the matrix. In this regard, if a single larval cell ( $L$ ) is considered alone ignoring density-dependency, the number of mortalities will be less than that of the actual case in which this cell is just a part of a total larvae population of that day.

For the above reason, it is necessary to estimate the share of an individual cell in the total number of deaths. The developed set of equations describing this phenomenon are given below. The first equation is used to compute the daily total number of individuals belonging to each of the three life-stages:

$$PTOT_m = \sum_{i=first}^{last} P_{m,i} \quad (7.15)$$

where;  $PTOT_m$ : total number of individuals in any given day  $m$  ( $P \equiv E, L$  or  $J$ )

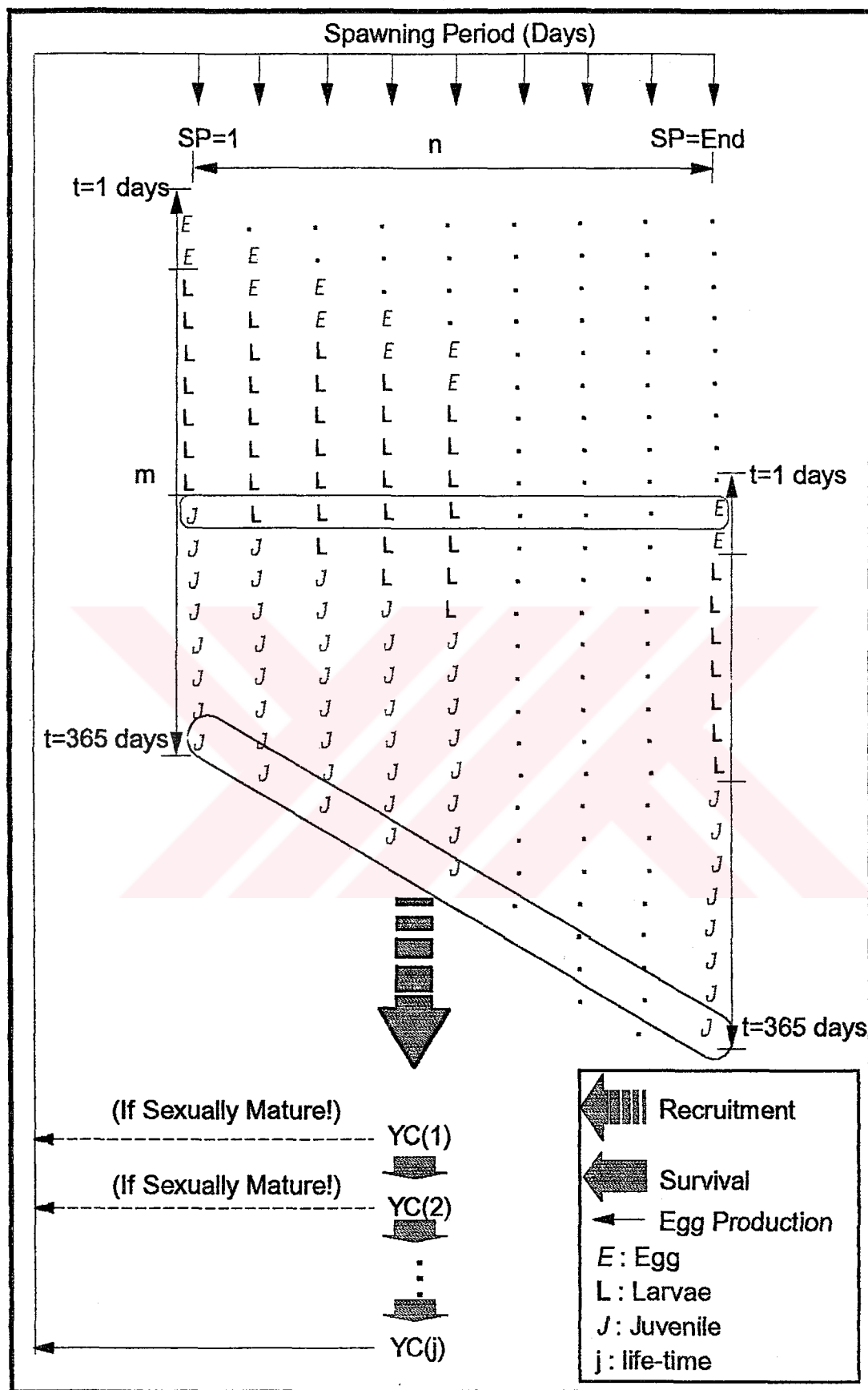


Figure 7.4. Computational Logic of the Pre-recruit Life Simulation

first: the first cell (of the type E, L or J) on row m  
last: the last cell (of the type E, L or J) on row m  
 $P_{m,i}$ : the number of individuals (egg, larvae or juvenile) in any cell of row m

Secondly, the daily total number of deaths of P (E,L or J) is compiled by the following equation:

$$PMORT_m = (k_{pi} + k_{pe}) PTOT_m + (k_i + k_d PTOT_m) PTOT_m \quad (7.16)$$

where;  $PMORT_m$ : total number of deaths of P ( $P \equiv E, L$  or  $J$ ) in any given day m  
 $k_{pe}$ : coefficient of entrainment mortality ( $\text{time}^{-1}$ )  
 $k_{pi}$ : coefficient of impingement mortality ( $\text{time}^{-1}$ )  
 $k_i$ : coefficient density-independent natural mortality ( $\text{time}^{-1}$ )  
 $k_d$ : coefficient density-dependent natural mortality ( $\text{time}^{-1}$ )

Then, the share of an individual compartment cell in the total number of deaths can be found by the following equation:

$$PDELTA_{m,n} = PMORT_m \times \frac{P_{m,n}}{PTOT_M} \quad (7.17)$$

where;  $PDELTA_{m,n}$ : the number of deaths from the  $n^{\text{th}}$  column in any given day m

As discussed earlier, the column number,  $n$ , represents the day of the spawning period in which the first eggs of that column are produced. In the same column, the number of individuals in the  $(m+1)^{th}$  cell of the next day is given by the following equation:

$$P_{m+1,n} = P_{m,n} - PDELTA_{m,n} \quad (7.18)$$

These calculations are repeated until the last cell of the last column (descended from the eggs produced at the last day of the spawning period) is recruited to the adult population.

In the computer program based on this approach, the type of each cell (E,L or J) and the corresponding mortality rate coefficient are determined by means of a counter,  $MC_n$ . This counter distinguishes the pre-recruit life stages in the following manner:

Life-stages:      if  $MC_n < LAR_{st}$  ;  $P \equiv E$  (Egg)  
                          if  $JUV_{st} > MC_n \geq LAR_{st}$  ;  $P \equiv L$  (Larvae)  
                          if  $MC_n < LAR_{st}$  ;  $P \equiv J$  (Juvenile)

Rate constants:    if  $MC_n < JUV_{st}$  ;  $k_{pl} = 0$   
                          if  $MC_n \geq JUV_{st}$  ;  $k_{pe} = 0$  and  $k_d = 0$

where;       $LAR_{st}$ :      the day at which the larval stage begins for  
    the fish species of interest

$JUV_{st}$ : the day at which the juvenile stage begins for the  
    fish species of interest

In terms of application, the developed computer program checks the counter of any individual cell( $P_{m,n}$ ) and by defining the pertinent life-stage applies the relevant mortality rate coefficients.

#### **f. Subsequent Iterations**

After determining the number of individuals recruited to the adult population (year-class 1 of the next year) the year-class structure of a population can be estimated by using Equations 7.1 to 7.4. All the steps are repeated for the subsequent years.

#### **7.3.4 Data Requirement of the LCM**

For a given fish species, the input parameters required to apply the LCM to a specific case are:

- initial year-class structure of the population;
- annual or instantaneous total, fishing and natural mortality rates;
- life-time of the species;
- sex ratio, mean fecundity, spawning period, and the age for sexual maturity;
- instantaneous entrainment ratio;
- entrainment and impingement rates of pre-recruit species (from field data for operating plants);
- data representing the change in the number of pre-recruit species with time (P vs. t) or egg, larvae and juvenile mortality rates of the fish species; and,
- duration of life stages (hatching, incubation, pre-larval, post-larval, etc.).

#### **7.3.5 Estimation of Mortality Coefficients**

Beverton and Holt give the following expression for the natural mortality of pre-recruit individuals at egg and larvae stages (Weatherley, 1972):

$$\frac{dP}{dt} = -(k_1 + k_d P) P \quad (7.19)$$

In the application of LCM, the estimation of natural mortality coefficients for ichtioplankton is based on the analytical solution of Equation 7.19:

$$P_t = \frac{k_1}{k_d \left( \left( 1 + \frac{k_1}{k_d P_o} \right) e^{-tk_1} - 1 \right)} \quad (7.20)$$

where;  $P_t$ : the population of pre-recruit species at time  $t$   
 $P_o$ : the initial population of pre-recruit species at  $t=0$

If sufficient experimental data ( $P_t$  versus  $t$ ) is available, coefficients  $k_1$  and  $k_d$  can be estimated by subjecting Equation 7.20 to least-squares method in an iterative manner.

In the case of the juvenile stage, the density-dependent term ( $k_d$ ) is neglected. Therefore, the juvenile mortality can be given by the following equation:

$$\frac{dP}{dt} = -k_1 P \quad (7.21)$$

Then,  $k_1$  for juvenile individuals can be found from the integrated form of Equation 7.21:

$$\ln \frac{P_t}{P_o} = -k_1 t \quad (7.22)$$

In turn, the initial number of juvenile species,  $P_o$ , can be determined from either experimental data or model estimations for larval species surviving to

the juvenile stage. Similarly, the final number of juvenile species,  $P_t$  can be determined from either experimental data or model estimations of recruitment by using Ricker's stock-recruitment function (to estimate the number of juvenile species just before being recruited).

The relative impact of the plant-caused mortality on the populations are estimated by inserting entrainment (and impingement, in the case of an existing facility) effect into the life cycles of fish populations. The difference between the populations with and without plant effect, at any instant during the simulation period (in the case of ATPP, 100 years), was accepted as the relative plant impact.

For the selection of entrainment mortality coefficient,  $k_{pe}$ , the estimated instantaneous entrainment ratio corresponding to a given year is equally distributed over the period in which the pre-recruit species are most susceptible to entrainment. In this way, the instantaneous entrainment mortality ratio was used as an entrainment rate coefficient in Equations 7.14 and 7.16.

## **7.4 Application of the LCM on *Mullus barbatus***

### **7.4.1 Application Approach**

The developed LCM was first applied to *Mullus barbatus* which is one the commercially important fish species of the Gencelli Harbor. In this application, the stock-recruitment approach (see Sub-section f of Section 7.3.3) was preferred due to lack of detailed field data on pre-recruit life of *Mullus barbatus*.

In the case of the proposed ATPP, the proposed operation period is 26 years. Therefore, in the simulations, the entrainment effect of the plant was eliminated after 26 years. In this context, the overall effect of the plant operations on the *Mullus barbatus* population was determined by executing the LCM with and without entrainment. After determining the effect at the end of 26 years, the LCM simulations were carried for a sufficiently long period of 100 years in order to observe the subsequent recovery.

#### 7.4.2 Model Inputs and Setup

The necessary initial year-class structure of *Mullus barbatus* was adapted from the available field data reported in the literature (Çoral, 1988; Samsun, 1990; Toğulga, 1992). The *Mullus barbatus* population distributions and mortality rates observed in different coastal waters are summarized in Tables 7.1 and 7.2.

A base case was defined for the sensitivity runs and the simulations, based on the data available in the literature. The observed and the selected values of the base case input parameters are given in Table 7.3.

#### 7.4.3 Sensitivity Tests

Since, selection of certain parameter values were based on literature and assumptions, sensitivity runs were felt necessary to determine the sensitivity of the model results to the changes in such parameters as mean fecundity (MF), total number of mature fish in a virgin stock ( $T_{max}$ ) and instantaneous fishing mortality rate (F).



Table 7.1. Year-Class Structures of Different Sites on Turkish Coasts

Number of Individuals in Different Year-Classes										
Period	0	I	II	III	IV	V	VI	Site	Ref.*	
August	11	77	47	28	11	8	5	Aegean Sea	1	
March	2	12	26	9	1	-	-	Gülbahçe Bay, İzmir	2	
September	2	27	16	5	2	0	2	"	2	
December	9	20	15	4	3	1	-	"	2	
January	3	14	21	8	4	1	-	"	2	
Total	16	73	78	26	10	2	2	"	2	
"	70.0	26.0	6.6	0.5	-	0.18	-	Samsun	3	
"	17.2	71.4	37.4	22.3	4.3	1.4	-	Sinop	3	
"	65.1	12.2	17.6	2.7	0.2	0.2	-	Sinop	3	
Total	50.4	21.3	19.1	7.5	1.1	0.4	-		3	

\* [1] Çoral, 1988  
[2] Toğulga, 1992  
[3] Samsun, 1990

Table 7.2. Reported Values of Mortality Rates for *Mullus Barbatius*

Z	A	S	M	V	F	U	Site	Ref.
0.820	0.560	0.440	0.300	0.200	0.520	0.355	Gökçeada	1
0.820	0.560	0.440	0.330	0.225	0.490	0.335	Bozcaada	1
1.580	0.790	0.210	0.350	0.175	1.230	0.615	Edremit Bay	1
1.360	0.740	0.260	0.329	0.175	1.031	0.565	Gülbahçe Bay	1
2.190	0.890	0.110	0.332	0.135	1.858	0.755	Doğanbey	1
1.020	0.640	0.360	0.334	0.210	0.686	0.430	Sığacık Bay	1
0.320	0.270	0.730	0.280	0.236	0.040	0.034	B. Menderes	1
0.670	0.490	0.510	0.290	0.212	0.380	0.378	Bodrum	1
0.950	0.610	0.390	0.390	0.250	0.560	0.360	Samsun, Sinop	2
1.015	0.640	0.360	-	-	-	-	Saronikos Gulf, Greece	3,4
0.940	0.610	0.390	-	-	-	-	"	5
0.852	0.570	0.430	-	-	-	-	"	6
0.936	0.610	0.390	-	-	-	-	"	6

- \* [1] Çoral, 1988  
[2] Samsun, 1990  
[3] Wetherall et al., 1987  
[4] Pauly and Munro, 1984  
[5] Pauly, 1983  
[6] Benerton and Holt, 1956

Table 7.3. Base Case Parameters and Values

Input Parameter	Observed Range	Ref. *	Selected Value
YC(1)		[1]	9,000
YC(2)		[1]	7,000
YC(3)		[1]	4,900
YC(4)		[1]	340
YC(5)		[1]	30
YC(6)		[1]	2
$T_{max}$		[2]	225,840
Z	0.32-2.19	[3]	2.65
F	0.04-1.86	[3]	2.32
M	0.29-0.35	[3]	0.33
$s_z$ (related to Z)	0.11-0.73	[3]	0.07
A (related to Z)	0.27-0.89	[3]	0.93
u (related to M,F)	0.034-0.755	[3]	0.81
v (related to M,F)	0.135-0.250	[3]	0.12
Life Time (years)	6	[4],[5]	6
Sex Ratio	0.50	[6],[7]	0.50
Mean Fecundity ( $10^3$ )	15-100	[8]	70,000
Spawning Duration (months)	April-July	[8],[9],[10],[11]	3
Maturity Age	end of 1	[4],[5]	2
Instantaneous Entrainment Ratio	2%	[12]	2%

[1] see Table 7.1

[2] see Section 7.3.3(d)

[3] see Table 7.2

[4] Toğulga, 1977

[5] Çoral, 1988

[6] Samsun, 1990

[7] Toğulga, 1992

[8] Toğulga, 1976

[9] Kınıkarslan, 1972

[10] Slastenenko, 1956

[11] Arım, 1957

[12] see Section 6.3.1 (d)

The results of the sensitivity tests are presented in Table 7.4. As can be seen, a relatively wide range of MF causes no significant reduction in the overall population at the 26 years. However, one should be more cautious in the selection of the mortality rates and  $T_{max}$ .

Table 7.4. The Results of the Sensitivity Tests

Parameter	Values	Entrainment Effect (%)
MF	50,000	8.5
	70,000	8.3
	90,000	8.2
$T_{max}$	150,560 (2. $T_m$ )	6.1
	225,840 (3. $T_m$ )	8.3
	301,120 (4. $T_m$ )	10.3
F	2.00	11.0
	2.65	8.3
	3.00	6.0

#### 7.4.4 LCM Simulations for *Mullus barbatus*

In order to provide information for impact minimization studies, the LCM was executed for *Mullus barbatus* with different entrainment ratios. The results are given in Table 7.5 and Figure 7.5.

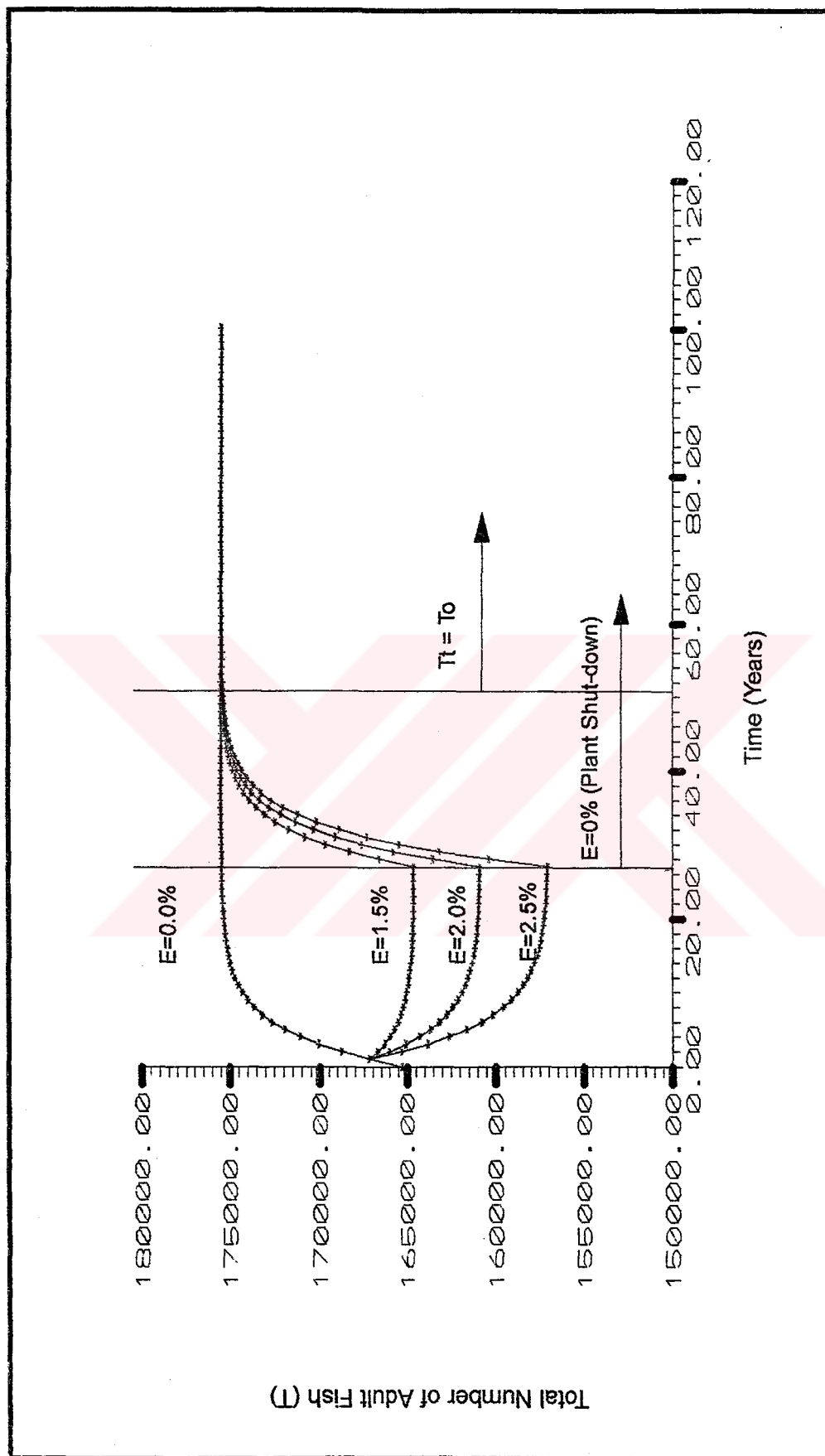


Figure 7.5 Effects of Various Entrainment Levels on *Mullus Barbus* Population of the Gencelli Harbor

Table 7.5. Effects of Entrainment on *Mullus Barbatus* Fish Population of the Gencelli Harbor

Instantaneous Entrainment Ratio (%)	Overall Decrease in the Population in 26 Years (%)
1.5	6.2
2.0	8.3
2.5	10.5

The LCM simulations for *Mullus barbatus* revealed that the entrainment ratio has a considerable effect on the population. However, after 26 years, the recovery rates for all tested entrainment were quite close. The implications of the LCM simulation are discussed in Section 7.6 in more detail.

## 7.5 Application of the LCM on *Sparus aurata*

### 7.5.1 Model Inputs and Setup

In the case of *Sparus aurata* experimental data on the pre-recruit life stages and mortalities was available (Saka, 1988). Therefore, the long-term effect of entrainment was investigated by simulating the pre-recruit life stage of *Sparus aurata*. For this purpose, the computational steps given in Sub-section e of Section 7.3.3, were used. Similar to the case of *Mullus barbatus*, the recruitment with and without entrainment was estimated to predict the overall effect of entrainment on the recruitment to year-class 1 and hence overall population.

Life-time of *Sparus aurata* is reported to be 5 years (FAO, 1979). The species reach to sexual maturity at year-class 2 (Benli and Uçal, 1990). The species show characteristics of a male until the end of year-class 2 and of a female at year-class 3 and older (Benli and Uçal, 1990). During the transition stage the species show the characteristics of a hermaphrodite (Benli and Uçal, 1990). The incubation period for eggs is reported to be about 2-4 days (Muhtaroğlu, 1988; Uçal, 1983). The pre-larval and post-larval stages last 3 and 60 days, respectively (Muhtaroğlu, 1988). Various reported mortality rates for *Sparus aurata* are summarized in Table 7.6.

Table 7.6. Reported Values of Mortality Rates for *Sparus aurata* (Lasserre, 1976)

Z	F	M	Site
1.45	0.28	1.17	Sète, France
1.43	0.26	1.17	Sète, France
2.24	1.07	1.17	Sète, France
1.92	0.75	1.17	Sète, France
2.34	1.17	1.17	Sète, France

Relatively more detailed data is available on the fecundity of *Sparus aurata*. The spawning season covers the months October, November and December. In literature, the reported average fecundity values vary between 50,000 and 150,000/kg weight of fish (Benli and Uçal, 1990; Muhtaroğlu, 1988). In the LCM applications, the average fecundity for each year-class was estimated by using the following relationships:

$$L_t = L_{\infty} (1 - e^{-K(t-t_0)}) \quad (7.23)$$

where;  $L_t$ : length of fish at time  $t$  (cm)  
 $L_{\infty}$ : asymptotic length at infinite age (cm)  
 $K$ : rate at which length reaches  $L_{\infty}$   
 $t$ : time  
 $t_0$ : a conceptual value for age

$$W = aL^b \quad (7.24)$$

where;  $W$ : weight of fish (gr)  
 $a, b$ : coefficients  
 $L$ : length of fish (cm)

For *Sparus aurata*, the reported data for the above parameters are summarized in Tables 7.7 and 7.8. The corresponding values for length and weight at different year-classes during which spawning occurs, are also given in the same tables.

Table 7.7. Length Data for *Sparus aurata* (cm) (Lasserre, 1976)

$L_{\infty}$	$K$	$t_0$	$L_{III}$	$L_{IV}$	$L_V$
45.52	0.372	-0.427	32.7	36.7	39.5
53.89	0.256	-0.735	33.2	37.8	41.5
Average Length (Rounded)			33.0	37.0	40.0



Table 7.8. Weight Data for *Sparus aurata* (gr) (Lasserre,1976)

a	b	W <sub>III</sub>	W <sub>IV</sub>	W <sub>V</sub>
13.9x10 <sup>-3</sup>	3.05	595	843	1,070
11.2x10 <sup>-3</sup>	3.08	532	757	963
44.8x10 <sup>-3</sup>	2.65	473	641	788
Average Wt. (Rounded)		550	750	950
Estimated Fecundity (for MF of 1x10 <sup>5</sup> eggs/kg)		55,000	75,000	95,000

For the ichtioplankton of *Sparus aurata*, the experimental data used in the estimation of density-dependent and density-independent mortality coefficients are given in Table 7.9. Density-dependent mortality coefficient,  $k_d$  and density-independent mortality coefficient,  $k_i$ , estimations for pre-recruit species were based on the experimental data given in Table 7.9.

Table 7.9. Mortality Data on the Pre-recruit Stage of *Sparus aurata* (Saka, 1988)

Age (days)	Mortality Ratio (%) (Experimental)	Mortality Ratio (%) (Assumed)
Incubation	20-30	25
0-3	10	10
4-12	60-90	75
12-15	2-3	2
15-25	5-15	10
25-30	10-20	15
30-50	3-10	5

Due to insufficient data, the mortality coefficients for egg and larvae stages were assumed to be equal. In the case of juvenile species, the initial value for the juvenile population was taken from the final population data of larval species. The final level of juvenile species was estimated from the Ricker's stock-recruitment function. The species recruited to the adult populations represents the final level of the juvenile population. Since the mortality of juvenile species are density-independent, the mortality coefficient was simply estimated using Equation 7.22.

Similar to the case of *Mullus barbatus*, a base case was defined, based on the available data summarized above. The base case parameters are given in Table 7.10.

#### 7.5.2 Sensitivity Tests

In the case of *Sparus aurata*, the sensitivity tests were also felt necessary for the mean fecundity (MF), total number of mature fish in a virgin stock ( $T_{max}$ ) and instantaneous fishing mortality rate (F). In the sensitivity tests performed for *Sparus aurata*, the change of some base case parameters, such as mean fecundity and fishing mortality, required adjustment of related parameters. Since the pre-recruit life stage was also simulated, for instance, the change in the mean fecundity would result in the change of pre-recruit mortality coefficients. The related parameters were adjusted for each case and test, where necessary. The results of the sensitivity tests are given in Table 7.11.

Unlike *Mullus barbatus*, the results of the sensitivity tests showed that the model results for *Sparus aurata* were not highly sensitive to the tested parameters.

Table 7.10. Base Case Parameters and Values for *Sparus aurata*

Input Parameter	Value
YC(1)	5000
YC(2)	2500
YC(3)	375
YC(4)	56
YC(5)	9
$T_{max}$	1320 (3. $T_m$ )
Z	1.87
F	0.70
M	1.17
$s_2$	0.15
A	0.85
u	0.53
v	0.31
Life Time	5 years
Sex Ratio	1.0(for year-class 3 to 5)
Mean Fecundity	100,000/kg fish
Spawning Duration	3 months
Maturity Age	2
$k_d$ (density-dep. mort. c.)	$-1.05 \times 10^{-8}$
$k_i$ (density-indep. mrt. c)	$-1.0 \times 10^{-5}$
$k_i$ for juvenile species	-0.0193
$k_p$ for juvenile species	0
Inst. Entrainment Ratio	2 %

Table 7.11. The Results of the Sensitivity Tests

Parameter	Values	Entrainment Effect (%)
MF (per kg)	50,000	2.23
	100,000	2.02
	150,000	1.91
$T_{\max}$	616 ( $2.T_m$ )	1.83
	924 ( $3.T_m$ )	2.02
	1232 ( $4.T_m$ )	2.22
F	0.75	3.40
	1.07	2.02
	1.17	2.20

### 7.5.3 LCM Simulations for *Sparus aurata*

As in the case of *Mullus barbatus*, the effects various entrainment ratios were investigated for *Sparus aurata*. The results are summarized in Table 7.12 and Figure 7.6.

As described in Section 7.3.5, the instantaneous entrainment ratio was distributed over the egg and larvae period. The effect of this entrainment ratio on the recruitment of juvenile species to the adult population is given in the second column of Table 7.12. In the third column of the table, the long-term impact of a decrease in the recruitment each year is presented as a percent reduction in the population.

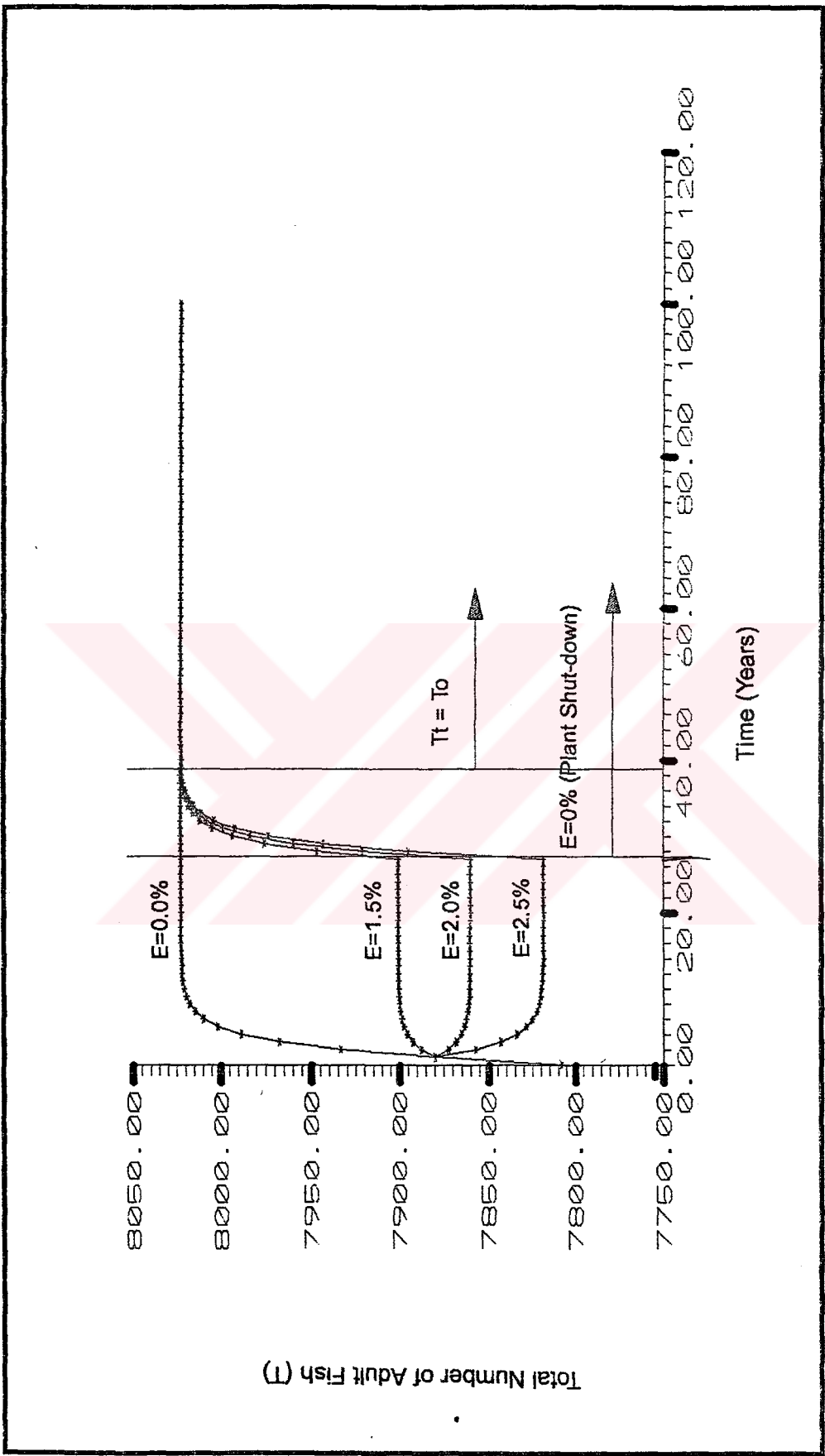


Figure 7.6. Effects of Various Entrainment Levels on Sparus aurata Population of the Gencelli Harbor

It should be noted that the similarity in the first and third columns is coincidental. When the model was run for different entrainment ratios, the results deviated from each other.

The results presented in Table 7.12 and Figure 7.4 indicate that *Sparus aurata* is more tolerant to entrainment than *Mullus barbatus*. However, one should also be reminded that the data used for *Sparus aurata* was compiled from many different sources and hence inherited incompatibility to a certain extent. However, the main purpose of this study is to demonstrate the computational procedure rather than the absolute results.

Table 7.12. Effects of Entrainment on *Sparus aurata* Fish Population of the Gencelli Harbor

Instantaneous Entrainment Ratio (%)	Effect on Recruitment (%)	Overall Decrease in the Population in 26 Years (%)
1.5	0.92	1.52
2.0	1.22	2.03
2.5	1.52	2.54

## 7.6 Summary and Recommendations

In this chapter, the long-term impacts of the proposed ATPP on the valued ecosystem components of the Gencelli Harbor were investigated. Two commercially important fish species, *Mullus barbatus* and *Sparus aurata*, were studied as VEC's of the Gencelli Harbor. Complete data sets for model applications could not be obtained for other commercial species.

Since no specific data set for the fish of the Gencelli Harbor was available, data were collected from various sources. In this regard, parameter values were not detailed enough to make precise predictions. However, as stated earlier, the major objective of the LCM simulation was to demonstrate the applicability and flexibility of the developed procedure.

The uncertainty in the results can be minimized as more detailed and exclusive data becomes available. In this regard, it is possible to accurately predict the long-term impacts of a proposed or existing facility if site specific data are available for the fish species of interest (see Section 7.3.4). Further, since it is not possible to make reliable predictions for the impingement effects of a proposed facility, the LCM applications regarding ATPP were limited to entrainment only. However, it should be noted that the inclusion of impingement will definitely lead to higher impacts. Therefore, for the proposed ATPP and any other proposed or existing facility, the LCM studies should be supported with detailed field studies and stock assessment techniques. In the presence of such data, the developed LCM makes it possible to evaluate the effects of time-variant entrainment and impingement, as well as, time-variant natural mortality or fecundity at different life stages of fish.

Entrainment and impingement are among the most dominant effects of thermal power plants. The investigation of the long-term effects of ichtioplankton entrainment on the *Mullus Barbatus* and *Sparus aurata* populations revealed that the effect is rather considerable. Nevertheless, significant decreases in the long-term impacts of the cooling water operations could be achieved by decreasing entrainment (See Tables 7.5 and 7.12). It should, however, also be noted that decreased entrainment ratios will result in increased excess-temperatures. In this regard, it is experienced that the total damage of a high excess temperature with a low flow rate is less than that of a low excess temperature with a high flow rate on entrained larvae

(Hadderingh, 1979). Therefore, it is strongly recommended to find an optimum combination of the minimum entrainment and minimum excess-temperatures.

Limitation to such approaches given above, is the current environmental legislation. In the case of the proposed ATPP, for instance, slight changes in the proposed design parameters will result in increased excess-temperatures which will violate the Turkish Environmental Regulations. However, short-term impact assessment studies revealed that the ecosystem in the Gencelli Harbor could tolerate worse conditions than those urged by the pertinent legislation. This conclusion is supported with the following points:

- The organisms at the discharge area can withstand higher excess temperatures up to about 10 °C and ambient temperatures up to 35 °C (see Chapter 6).
- In the case of the proposed ATPP, the criteria of 30 °C ambient water temperature is expected to be exceeded at times where sum of the ambient temperature and the initial excess temperature exceeds 30 °C. This condition is expected to be observed rarely.
- The limited exceedance of the criterion will be observed at points a few meters away from the diffusers. Most of the organisms are able to by-pass these areas.

This implies that the heat-exchangers of the proposed facility could operate on a higher temperature difference than 7 °C, thereby discharging a warmer effluent leading to a higher ambient water temperature. It is obvious that under such design conditions, much less water will be withdrawn from the harbor and thus the entrainment effect will be much less significant than the current design targeted to meet the regulatory criteria of 30 °C effluent and 1 °C surface excess-temperatures.



## **CHAPTER VIII**

### **CONCLUSION AND RECOMMENDATIONS**

#### **8.1 General**

The proposed marine impact assessment procedure consists of the following major steps:

- (i) dilution prediction studies for the liquid waste discharge of the proposed power plant
- (ii) hydrothermal modeling studies for the cooling water discharge of the proposed power plant
- (iii) prediction and assessment of the biological effects

In this study, the first two steps addressed the physical effects of the liquid waste and thermal effluent discharges of the proposed ATPP on the Gencelli Harbor. In the third step, the biological impacts due to the changes in the physical characteristics of the marine environment were investigated and assessed.

## 8.2 Conclusions

### 8.2.1 Dilution Prediction Studies for the Liquid Waste Discharge

For the case study, the liquid waste dilution and dispersion studies revealed that the initial dilution ( $S_1$ ) of the discharge will be about 140. Under conservative assumed worst-case conditions, the predicted values for the dilution due to bacterial decay ( $S_2$ ) and dilution due to dispersion ( $S_3$ ) were 11 and 2, respectively, leading to a total (combined) dilution ( $S_{total}$ ) value of about 3500 on the coastline. At a point 200 m away from the coast, the minimum predicted values for  $S_1$ ,  $S_2$ ,  $S_3$  and  $S_{total}$  were about 159, 4, 2 and 1550. Considering the conservative nature of the model applications, it was concluded that the degree of treatment needed a further assessment following the plant start-up. Based on field measurements and statistical analysis of effluent characteristics, necessary precautions should be taken in the case of a violation of water quality standards.

### 8.2.2 Hydrothermal Modeling Studies for the Cooling Water Discharge

Hydrothermal modeling studies were conducted in the following stages:

- near-field analyses
- intermediate and far-field analyses

Based on semi-empirical near-field hydrothermal modeling studies, it is expected that the thermal effluent will rapidly be diluted by the time it reaches to the water surface. The predicted excess temperature values on the surface were predominantly below 1 °C. Such a change in the temperature of the receiving environment is not expected to result in any adverse effects on the quality of sea water.

Based on the intermediate and far-field hydrothermal modeling studies with GLLVHT, it was concluded that:

- sufficient water exchange is available at the open boundary to provide the necessary dilution;
- no shoreline-effects, due to the operations of the proposed ATPP, were expected; and,
- recirculation of warm water and a subsequent heat accumulation were insignificant.

As the thermal plume is dispersed, its excess temperature will decrease. The estimated excess temperature values at the open boundary of the Gencelli Harbor were below 0.15 °C. Surface discharge alternative for the thermal effluent was also investigated. This alternative will result in undesirable surface excess temperature values ranging from 7°C around the discharge point to 1°C at the open boundary.

It is also expected that the cooling water operations of the proposed ATPP will be significantly effective on the circulation patterns of the Gencelli Harbor.

### 8.2.3 Prediction and Assessment Studies of the Biological Effects

The marine biological effects of the proposed ATPP were assessed in the short-term and long-term time-scales. Other than some insignificant local changes in the species distribution and community structure, no significant short-term adverse effects on the marine environment are expected due to the discharge of thermal plume or liquid wastes. An overall temperature increase of less than 1°C was expected to result in increases in growth, respiration and

reaction rates which generally have positive impacts on the organisms. During the construction phase some local and reversible temporary changes in the community were expected.

It was concluded that the entrainment effects of such thermal power plants like the proposed ATPP, dominate over other effects. The entrainment of ichtioplankton is expected to result in a notable long-term decrease in the fish population within the modeled portion of the Gencelli Harbor. It was estimated that the effect of entrainment on the fish population will decrease as the cooling water flow rate decreased. However in this case, higher excess temperatures are expected in the marine environment which may violate the currently effective legislation even though the potential impact will be lesser.

### **8.3 Recommendations**

#### **8.3.1 Recommendations for monitoring studies**

The conclusions of the environmental impact assessment studies are largely based on predictions made by using mathematical models. However, the results of such models are only descriptive estimations which may vary notably due to the input parameters. The precision of the model results can be improved with detailed and comprehensive field data.

For this reason, in the case of the ATPP or any other similar project, all the relevant physical, chemical and biological components of the marine environment should be monitored regularly, before and after the construction of the plant. The design, construction and operation should be flexible such that in the case of the unexpected impacts, the necessary precautions can be taken promptly.

During the field studies conducted by Ege University Biology Department, species like *Mullus surmuletus*, *Pagellus erythrinus*, *Pagellus acarne*, *Chromis chromis*, *Labrus bergylta*, *Coris julis*, *Clinus argentatus*, and *Tripterygion tripteronotus* were observed in the area. These species prefer to live in very clean waters. This proves that the Gencelli Harbor is not polluted, yet. After the start up of ATPP, continuous monitoring of the marine species in Gencelli Harbor together with these sensitive species, are strongly recommended in order to observe and assess the long-term effects of the plant and to take timely measures, if necessary.

It is also strongly recommended that the population dynamics of the commercially important fish species listed in Chapter 7 should be investigated before and after the start-up of the plant. In this regard, a follow-up modeling study, which will be supported with actual field data, can be carried out to update the long-term impact predictions for entrainment and impingement.

### 8.3.2 Recommendations for Project Modifications

It is recommended that the impingement potential should be reduced by a proper selection of barriers which are used to protect the plant from debris and organisms. Various mechanical and behavioral barriers have been used in power plants with considerable success. Studies show that, it is possible to increase impingement survival rates up to 100%, with proper selection and design of barriers (Hadderingh, 1979).

An optimum combination of cooling water flow rate and temperature rise ( $\Delta T$ ) in the condenser should be found. This is essential in order to keep the entrainment mortality of larvae and impingement mortality of young fish to a minimum. In this sense, design flow rates should be kept as low as possible.

### **8.3.3 Recommendations Legislative Modifications**

In the case of the proposed ATPP, it was found out that the restriction of entrainment will conserve more fish than applying temperature criteria to the cooling water discharge. For this reason, it is worthwhile to consider a modification in the pertinent legislation which will allow some flexibility in such scientifically supported cases.



## REFERENCES

- Adams, E. E., and Stolzenbach, K.D.,1977. "Comparison of Alternative Diffuser Designs for the Discharge of Heated Water in Shallow Receiving Water", Proceedings of the First Conference on Waste Heat Management and Utilization, eds., S.S. Lee and S. Sengupa, Coral Gables, Fla., May, pp. II-C-171-189.
- Adams, E.E., 1982. "Dilution Analysis for Unidirectional Difusers", Journal of Hydraulics Division, ASCE, Vol. 108, No. HY3, pp. 327-342.
- Adams, E. E., Douglas J. C., and Karl R. H., 1990. "Evaporation From Heated Water Bodies: Predicting Combined Force Plus Free Convection", Water Resources Research, Vol. 26, pp. 425-435.
- Akşiray, F., 1954. Türkiye Deniz Balıkları Tayin Anahtarı, İstanbul Üniversitesi Fen Fakültesi Hidrobiyoloji Araştırma Enstitüsü, Sayı 1, İstanbul, Türkiye.
- Akyarlı, A., and Y. Arısoy, 1988. "Surveying Works on the Aliğa Thermal Power Station Project", Volume II: Marine Phenomena Observations, Institute of Marine Sciences and Technology, Document No. DBTE-066, Dokuz Eylül University, İzmir, Türkiye.
- Akyarlı, A., 1988. "Surveying Works on the Aliğa Thermal Power Station Project", Institute of Marine Sciences and Technology, Document No. DBTE-066, Dokuz Eylül University, İzmir, Türkiye.

Akyarlı, A., 1990-1991. "Sea Water Quality and Temperature Measurement Works on the Aliğa Thermal Power Station Project", Institute of Marine Sciences and Technology, Document No. DBTE-073, Dokuz Eylül University, İzmir, Türkiye.

Alden III, R. W., 1979. "Effects of a thermal discharge on the mortality of copepods in a subtropical estuary", Environ. Pollut., 20(1), 3-19.

Almquist, C. W., and Stolzenbach, K.D., 1980. "Staged Multiport Diffusers", Journal of Hydraulics Division, ASCE, Vol. 106, No. HY2, pp. 285-302.

Altman, L. P. and Dittmer, S. D. (eds.), 1966. Environmental Biology. Federation of American Societies for Experimental Biology, USA.

Arım, N., 1957. "Marmara ve Karadeniz'deki bazı Kemikli Balıkların (Teleostların) Yumurta ve Larvaların Morfolojileri ile Ekolojileri", İ.Ü. Fen Fak. Hid. Araş. Seri A, 4(1-2), İstanbul, Türkiye.

\_\_\_\_\_, 1990. "ATPP EIA Phase-1 Report", Middle East Technical University, Environmental Engineering Department, Environmental Research Center, Ankara, Türkiye.

\_\_\_\_\_, 1992. "ATPP EIA Phase-2 Report", Middle East Technical University, Environmental Engineering Department, Project Code No. 91-03-11-01-03, Environmental Research Center, Ankara, Türkiye.

Barnabe, G., 1976. "Raport technique sur la ponde induite et l'elevage des larves du Loup Dicentrarchus labrax (L.) et de la Dorade Sparus aurata (L.)", Stud. Rev. Gen. Fish. Coun. Mediter.



Benli, H. A., and O. Uçal, 1990. Deniz Canlı Kaynakları Yetiştirme Teknikleri, T.C. Tarım Orman ve Köy İşleri Bakanlığı, Su Ürünleri Araştırma Enstitüsü Müdürlüğü, Seri A, No.3.

Benon von Unruh, P., and Gaudy, 1979. " R. Toxicité du chlore et des métaux lourds en liaison avec la température sur quelques espèces de copépodes pélagiques, I-III.", Influence des Rejets Thermiques sur le Milieu Vivant en Mer et en Estuaire. 2<sup>es</sup> Journées de la Thermo-ecologie Institut Scientifique et Technique des Pêches Maritimes, 14-15 Novembre, pp. 414-476.

Beverton, R. J. H., and S. J. Holt, 1956. "A review of Methods for Estimating Mortality Rates in Fish Populations, with Special Reference to Sources of Bias in Catch Sampling", Rapp. P. V. Reun. CIEM, 140: 67-83.

Beverton, R. J. H., and S. J. Holt, 1957. "On the Dynamics of the Exploited Fish Populations", U.K. Min. Agric. Fish., Fish. Invest. (Ser.2)19:533 p.

Bodoy, A., and H. Masse, 1978. "Etude expérimentale de influence de la température sur la survie de mollusques bivalves marins endogés", Halictis, 7, 131-132.

Buchak, E. M., and J. E. Edinger. 1984. "Generalized, Longitudinal-Vertical Hydrodynamics and Transport: Development, Programming and Applications", Prepared for U.S. Army Corps of Engineers Waterways Experiment Station, Vicksburg, Miss. Contract No. DACW39-84-M-1636. Prepared by J. E. Edinger Associates Wayne, PA. Document No. 84-18-R, USA.

Buchak E. M., J.E. Edinger, C. Çakıroğlu, and C. Yurteri, 1992. "Hydrothermal Modeling Studies of Aliğa Thermal Power Plant", Environmental Engineering Department, Document No. TR. 92-03-4, Middle East Technical University, Ankara, Türkiye.

Cederwall, K., 1968. "Hydraulics of Marine Wastewater Disposal", Report No.42. Hydraulic Division Chalmers Institute of Technology, Göteborg, Sweden.

Chervinsky, M., 1978. "Preliminary experiments on the adaptability of juvenile European sea bass *Dicentrarchus labrax* (L.) and Gilthead sea bream *Sparus aurata* (L.) to brackish water", Bamidge, 26(4), 110-113.

Cihangir, B., 1991. Ege Denizi'nde Sardalya (*Sardina pilchardus* Walbaum, 1792)nın Üreme Biyolojisi ve Büyümesi, Doktora Tezi, Deniz Bilimleri ve Teknoloji Enstitüsü, Dokuz Eylül Üniversitesi, İzmir, Türkiye.

Crisp, D. S., 1957. "Effect of low temperature on breeding of marine mammals", Nature, 179, 1138-1139.

Çoral, S., 1988. Ege Deniz'ndeki Barbunya Balığının (*Mullus barbatus*, L.) Biyolojisi ve Populasyon Dinamiği Üzerinde bir Ön Çalışma, Yüksek Lisans Tezi, Deniz Bilimleri ve Teknoloji Enstitüsü, Dokuz Eylül Üniversitesi, İzmir, Türkiye.

de Sylva, D. P., 1969. "Theoretical considerations of the effects of heated effluents on marine fishes", Biological Aspects of Thermal Pollution, eds. P. A. Krenkel and F. L. Parker, Vanderbilt University Press, USA.

Defant, A. 1958. Ebb and Flow, the Tides of the Earth, Air, and Water. Ann Arbor Science Paperbacks. The university of Michigan Press, Ann Arbor, Michigan, USA.

Dremière, P. Y., 1979. "Paramètres Biologiques et dynamique Disponibles sur les Principaux Stocks Halieutiques du Golfe du Lion: Sous-zone 37.2 du CGPM", Stock Assessment in the Baltic and Gulf of Lions, Statistical Divisions, FAO, GFCM, Palma de Mallorca, Spain.

Edinger, J.E., D.K. Brady and J.C. Geyer. 1974. Heat Exchange and Transport in the Environment. Cooling Water Studies for the Electric Power Research Institute, Research Project RP-49, Report 14. Palo Alto, California. EPRI Publication Number 74-049-00-3, USA.

Edinger, J. E., and E. M. Buchak. 1980. "Numerical Hydrodynamics of Estuaries", Estuarine and Wetland Processes with Emphasis on Modeling, eds., P. Hamilton and K. B. Macdonald, Plenum Press, New York, New York, pp. 115-146.

Edinger, J. E., and E. M. Buchak. 1985. "Numerical Waterbody Dynamics and Small Computers", Proceedings of ASCE 1985 Hydraulic Division Specialty Conference on Hydraulics and Hydrology in the Small Computer Age, Aug. 13-16, American Society of Civil Engineers, Lake Buena Vista, FL.

Edinger, J. E., E. M. Buchak, Nuh-Chao L. Huang. 1988. "Chalk Point Steam Electric Station Patuxent Estuary Hydrodynamic and Transport Model Verification and Real Time Intake Entrainment Rates for 1985 Larval Sampling", Prepared for Potomac Electric Power Company. Document No. 88-77-R. June.

- \_\_\_\_\_, 1979. Stock Assessment in the Baltic and Gulf of Lions Statistical Divisions, GFCM, Palma de Mallorca, Spain.
- Fonds, M., 1976. "The influence of temperature and salinity on growth of young Sole (*Solea Solea* Linn.)", 10<sup>th</sup> European Symposium on Marine Biology, Oslend, Belgium. Sep. 17-23, Vol.1, pp. 109-125.
- Fraizier, A., 1974. "A study of the accumulation of soluble and insoluble forms of Fe-59 by Marine Mollusks and fish (*M. edulis* and *Blennius pholis*)", I. Effects of temperature and light on species pollutant interactions. CEA-R-4630 Commissariat a L'Energie Atomique Cherbourg, France.
- \_\_\_\_\_, 1984. "Thermal Discharges in the Marine Environment", Food and Agriculture Organization of the United Nations, Reports and Studies No.24, Rome, Italy.
- Ginn, T. C., and J. M. O'Connor, 1978. "Response of estuarine amphipod *Gammarus daiberi* to chlorinated power plant effluent", Estuarine and Coastal Marine Science, 6, 459-469.
- Grace, R. A., 1978. Marine Outfall Systems. Prentice-Hall, Inc. New Jersey, USA.
- Hadderingh, R.H., 1979. "Fish intake mortality at power stations: The problem and its remedy", Hydrobiology Bulletin, 13(2-3), 83-93.
- Hayashi, T., and M. Ito, 1974. "Initial dilution of effluent discharging into stagnant sea water", Discharge of Sewage from Sea Outfalls, eds. A. L. H. Gameson. Pergamon Press Ltd., Great Britain.

Hrs-Brenko, M., 1974. "Temperature and salinity requirements for embrionic development *Mytilus galloprovincialis*", Thalassia Jugoslavica, 10(1-2), 131-138.

Hess, K. W. *et al*, 1975. "Simulating the Impact of the Entrainment of the Winter Flounder Larvae", Fisheries and Energy Production: A Symposium, D.C Heath and Company, Canada.

Jirka, G. H., M. Watanabe, K. H. Octavio, C. F. Cerco, and D. R. F. Harleman. 1978. "Mathematical Predictive Models for Cooling Ponds and Lakes, Part A: Model Development and Design Considerations", Prepared by Ralph M. Parsons Laboratory. Prepared for Water Resources and Dynamics, Department of Civil Engineering, Massachusetts Institute of Technology, Cambridge, Massachusetts. Report No. 238. December.

Jones, M.B., 1975. "Synergistic effects of salinity, temperature and heavy metals on mortality and osmoregulation in marine and estuarine Isopodes (Crustacea)", Marine Biology, 30, 13.

Kınıkarslan, N., 1972. Edremit Körfezi Barbunya (*Mullus Barbatius*, L.)'lerinin Büyüme İndeksi ve Yıllık Büyümeleri Üzerine Araştırmalar, İ.Ü. Fen Fak. Hid. Araş. Ens. Yay. 8, 10 p.

Klöckner, K., 1978. "Zur ökologie von *Pomatoceros triqueter* (Serpulidae -Polychaeta)", Helgolander wiss. Meeresunters, 31, 257-284.

Koutitas, C. G. 1988. Mathematical Models in Coastal Engineering, Pentech Press. London, U.K.

- Lasserre, G., 1976. Dynamique des Populations Ichtiologique Lagunaires.  
Application à *Sparus aurata* L., Thèse Doctorat d'Etat Univ. Sci. et Tech.  
du Languedoc, Montpellier.
- Leendertse, J.J., and A.B. Nelson, 1978. "A Water-Quality Simulation Model  
for Well Mixed Estuaries and Coastal Seas: Volume IX, the Computer  
Program", R-2298-RC. RAND, April, Santa Monica, CA 90406, USA.
- Marcy, B.C. JR., 1973. "Vulnerability and survival of young Connecticut River  
fish entrained at a nuclear power plant", J. Fish. Res. Bd. Canada  
30(8), 1195-1203.
- Muhtaroglu, C. G., 1988. Çipura Balığı (*Sparus aurata*, L.) Yumurta ve  
Larvalarında Gelişim ve Larval Safhada Canlı Besin Alımı. Yüksek  
Lisans Tezi, Deniz Bilimleri ve Teknoloji Enstitüsü, Dokuz Eylül  
Üniversitesi, İzmir, Türkiye.
- Lamadrid-Rose, Y., and Boehlert, G. W., 1988. "Effects of cold shock on egg,  
larval and juvenile stages of tropical fishes: Potential impacts of ocean  
thermal energy conversion", Marine Environ. Res.
- Langford, T. E., 1983. Electricity Generation and the Ecology of Natural  
Waters, Liverpool University Press.
- Moazzam, M., and S. H. N. Rizvi, 1980. "Fish entrapment in the seawater  
intake of power plant at Karachi coast", Env. Biol. Fish. 5(1), 49-57.
- Ogawa, H., and W. J. Mitsch, 1979. "Modeling of Power Plant Impacts on Fish  
Populations", Environmetal Management, Vol. 3, No. 4, pp. 321-330.

Okubo, A., 1971. "Oceanic diffusion diagrams", Deep-Sea Res., 18, 789.

Parent, J. F., 1979. "Problemes poses par l'evaluation previsionnelle de l'impact d'ure centrale electrique lors de l'etablissement du dossier d'impact", Influence des rejets thermiques sur le miliev vivant en mer et en estuaire. 2<sup>es</sup> Journees de la thermo-ecologie institut scientifique et technique des peches maritimes, 14-15 Novembre 1979, pp.414-476.

Pauly, D., 1983. "Length Converted Catch Curves: A Powerfull Tool for Fisheries Research in the Tropics (Part I)". Fishbyte, 2(1):17-19.

Pauly, D., and J. L. Munro, 1984. "Once More on Growth Comparison in Fishes and Invertebrates", Fishbyte, 2(1):21p.

Ricker, W.E., 1954. Stock and Recruitment, Journal of the Fisheries Research Board of Canada, 11(5): 559-623.

Ricker, W.E., 1958. Handbook of Computation for Biological Statistics of Fish Populations, Journal of the Fisheries Research Board of Canada, 119: 1-300.

Ricker, W.E., 1975. Computation and Interpretation of Biological Statistics of Fish Populations, Bulletin of the Fisheries Research Board of Canada, Department of the Environment Fisheries and Marine Service, Ottawa, Canada.

Ryan, Patrick J., Donald R. F. Harleman and Keith D. Stolzenbach. 1974. "Surface Heat Loss From Cooling Ponds". Water Resources Research, Vol. 10, No. 5, pp. 930 - 938.

- Saka, Ş., 1988. Çipura Yumurtlama ve Larva Yetiştiriciliği, Diploma Tezi, Su Ürünleri Yüksek Okulu, Ege Üniversitesi, İzmir, Türkiye.
- Samsun, O., 1990. Orta Karadeniz'de Trollerle Avlanan Barbunya Balığı (*Mullus barbatus ponticus* Ess. 1927) Balığının Balıkçılık Biyolojisi Bakımından Çeşitli Özelliklerinin Araştırılması, Doktora Tezi, Fen Bilimleri Enstitüsü, Ondokuz Mayıs Üniversitesi, Samsun, Türkiye.
- Schubel, J.R., 1975. "Some Comments on the Thermal Effects of Power Plants on Fish Eggs and Larvae", Fisheries and Energy Production: A Symposium, D.C Heath and Company, Canada.
- Slastenenko, E., 1955-56. Karadeniz Havzası Balıkları, Çev: H. Karataş, EBK. Um. Mdl. Yay. 711 XLIX p.
- Sorensen, J.C. and S. T. McCreary, 1990. "Institutional Arrangements for Managing Coastal Resources and Environments", National Park Service U.S. Department of the Interior and U.S. Agency for International Development, U.S.A.
- Stolzenbach et al., 1976. "Analytical and Experimental Studies of Discharge Designs for the Cayuga Station at the Somerset Alternate Site", R. M. Parsons Laboratory for Water Resources and Hydrodynamics, Department of Civil Engineering, Technical Reoprt No.2111, Massachusetts Institute of Technology, Cambridge, Mass., USA.
- Tchobanoglous, G., 1979. Wastewater Engineering: Treatment Disposal and Reuse, TATA McGraw-Hill Publishing Company Ltd., New Delhi, India.



Thomson, J. M., 1963. "Synopsis of Biological Data on the Grey Mullet (*mugil* *Cephalus* L., 1758)", CSIRO Fisheries and Oceanography Fisheries, Synopsis No:1.

Toğulga, M., 1976. İzmir Körfezinde Barbunya Balığının (*Mullus barbatus* *Linné*) Biyolojisi ve Populasyon Dinamiği Üzerinde Araştırmalar, Yüksek Lisans Tezi, Genel Zooloji Kürsüsü, Ege Üniversitesi Fen Fakültesi İzmir, Türkiye.

Toğulga, M., 1977. İzmir Körfezinde Barbunya Balığının (*Mullus barbatus* *Linné*) Biyolojisi ve Populasyon Dinamiği Üzerinde Araştırmalar", E.Ü. Fen Fakültesi Dergisi, Seri B, C.1, S.2, pp. 175-194.

Toğulga, M., 1992. Unpublished Field Data on *Mullus Barbatius* Population of the Güzelbahçe Bay, İzmir, Türkiye.

Torcu, H., 1987. İzmir Körfezi'nde, Sardalya (*Sardina pilchardus* *Walbaum*,1792), Yüksek Lisans Tezi, Deniz Bilimleri ve Teknoloji Enstitüsü, Dokuz Eylül Üniversitesi, İzmir, Türkiye.

Turnpenny, A. W. H., T. E. Langford and R. J. Aston, 1984. Power Stations and Fish. CEEB Research.

Uçal, O., 1983. "*Sparus aurata* (Çipura) Balığı Yumurtalarında Embriyonik Gelişim", Ege Üniversitesi Fen Fakültesi Dergisi, Sei B, Cilt I, pp. 87-98.

U. S. Army Engineer Waterways Experiment Station, Environmental Laboratory, Hydraulics Laboratory. 1986. "CE-QUAL-W2: A Numerical Two-Dimensional, Laterally Averaged Model of Hydrodynamics and Water Quality; User's Manual", Prepared for Department of the Army,

U.S. Army Corps of Engineers, Final Report. August, Washington, DC.,USA.

Verlaque, M., 1977. "Impact du recjet termique de martigues", Ponteau sur le Macrophytobenthos Tethys, 8(1), 19-46.

Weatherley, A. H., 1972. Growth and Ecology of Fish Populations, Academic Press, New York, USA.

Wetherall, J.A., J. J. Polovina and S. Ralston, 1987. "Estimating Growth and Mortality in Steady State Fish Stocks from Length-frequency Data", Length Based Methods in Fisheries Research, eds. D. Pauly and G. R. Morgan, ICLARM Conf. Proc. 13, Manila, Philippines.





## **APPENDIX A**

### **LIST OF MARINE SPECIES OBSERVED IN THE GENCELLI HARBOR**

Table A.1. List of Fish Species Captured in Gencelli Harbor

SPECIES	COMMON NAME
<i>Arnoglossus laterna</i>	Scaldfish
<i>Atherina boyeri</i>	Sand smelt
<i>Belennius pavo</i>	Tompot blenny
<i>Belone belone</i>	Garpike
<i>Blennius gattorougine</i>	Tompot
<i>Blennius sanguinolentus</i>	Red speckled blenny
<i>Blennius tentacularis</i>	Horned blenny
<i>Blennius pavo</i>	Tompot blenny
<i>Bobius cobitis</i>	Giant goby
<i>Boops boops</i>	Bogue
<i>Buglossidium luteum</i>	Yellow sole
<i>Chromis chromis</i>	Damselfish
<i>Citharus linguatula</i>	Spotted flounder
<i>Clinus argentatus</i>	-
<i>Conger conger</i>	-
<i>Coris julis</i>	Rainbow wrasse
<i>Dasyatis pastinaca</i>	Common stingray
<i>Dentex dentex</i>	Dentex
<i>Dicentrarchus labrax</i>	Bass
<i>Diplodus annularis</i>	Annular gilthead
<i>Diplodus sargus</i>	-
<i>Diplodus vulgaris</i>	Annular gilthead
<i>Engraulis encrasicolus</i>	Anchovy
<i>Gobius bucchichi</i>	Bucchich' s goby
<i>Gobius cobitis</i>	Giant goby
<i>Gobius cruentatus</i>	Red-mouthed goby
<i>Gobius niger</i>	Black goby
<i>Gobius paganellus</i>	Rock goby
<i>Labrus bergylta</i>	Ballan wrasse
<i>Labrus merula</i>	Brown wrasse
<i>Lepadogaster candollei</i>	Cornish sucker
<i>Lepadogaster cavillone</i>	Cornish sucker
<i>Lepidotrigla cavillone</i>	Large scale gumard
<i>Lithognathus mormyrus</i>	-
<i>Liza aurata</i>	Golden gray mullet
<i>Liza ramada</i>	Thin-lipped grey mullet
<i>Liza saliens</i>	Mullet
<i>Microchirus variegatus</i>	Thick back sole
<i>Mugil cephalus</i>	Mullet
<i>Mullus barbatus</i>	Stripped mullet
<i>Mullus surmuletus</i>	Red mullet
<i>Muraena helena</i>	Moray eel
<i>Mustelus mustelus</i>	Smooth hound (shark)

Table A.1. (Cont'd)

Species	Common Name
<i>Myliobatis aquila</i>	Eagle ray
<i>Oblada melanura</i>	Saddled bream
<i>Pagellus acarne</i>	Spanish bream
<i>Pagellus erythrinus</i>	Pandora
<i>Puntazzo puntazzo</i>	-
<i>Raja miraletus</i>	Brown ray
<i>Raja radula</i>	Rough ray
<i>Sardina pilchardus</i>	Sardine (pilchard)
<i>Sarpa salpa</i>	Saupe
<i>Sciaera umbra</i>	-
<i>Scorpaena notata</i>	Small red scorpion fish
<i>Scorpaena porcus</i>	Brown scorpion fish
<i>Scorpaena scrofa</i>	Red scorpion fish
<i>Scyllorhinus canicula</i>	Small-spotted dogfish
<i>Serranus cabrilla</i>	Comber
<i>Serranus hepatus</i>	Brown comber
<i>Serranus scriba</i>	Painted comber
<i>Solea vulgaris</i>	Common sole
<i>Sparus aurata</i>	Gilthead
<i>Spicara maena</i>	-
<i>Symphodus cinereus</i>	-
<i>Symphodus doderleini</i>	-
<i>Symphodus mediterraneus</i>	-
<i>Symphodus ocellatus</i>	-
<i>Symphodus rostratus</i>	-
<i>Symphodus tinca</i>	Peacock wrasse
<i>Syngnathus acus</i>	Greater pipefish
<i>Thalassoma pavo</i>	Turkish wrasse
<i>Torpedo marmorata</i>	Electric ray
<i>Trachurus trachurus</i>	Horse mackerel
<i>Trigla lucerna</i>	-
<i>Trigla lyra</i>	Piper
<i>Tripterygion tripteronotus</i>	Black/faced blenny
<i>Trisopterus minutus capellanus</i>	-

Table A.2. Fish Larvae of Gencelli Harbor

Species	
<i>Ammodytes sp.</i>	<i>Labrus bergylta</i>
<i>Amoglossus laterna</i>	<i>Mugil sp.</i>
<i>Blennius sp.</i>	<i>Mullus barbatus</i>
<i>Buglossidium luteum</i>	<i>Serranus cabrilla</i>
<i>Callionymus lyra</i>	<i>Serranus hepatus</i>
<i>Callionymus maculatus</i>	<i>Serranus scriba</i>
<i>Coris julis</i>	<i>Solea sp.</i>
<i>Diplodus annularis</i>	<i>Sparidae</i>
<i>Diplodus sargus</i>	<i>Spicara smaris</i>
<i>Engraulis encrasicolus</i>	<i>Symphodus melops</i>
<i>Gobius niger</i>	<i>Symphodus sp.</i>
<i>Gobius paganellus</i>	<i>Trachurus sp.</i>
<i>Gobius sp. 1</i>	<i>Trigla sp.</i>
<i>Gobius sp. 2</i>	

Table A.3. Fish Eggs of Gencelli Harbor

Species	
<i>Amoglossus laterna</i>	<i>Engraulis encrasicolus</i>
<i>Boops boops</i>	<i>Mugil sp.</i>
<i>Buglossidium luteum</i>	<i>Scorpaena scrofa</i>
<i>Callionymus lyra</i>	<i>Serranus cabrilla</i>
<i>Callionymus sp.</i>	<i>Serranus hepatus</i>
<i>Carapus dentatus</i>	<i>Serranus scriba</i>
<i>Coris julis</i>	<i>Solea variegata</i>
<i>Diplodus annularis</i>	<i>Trachurus sp.</i>
<i>Diplodus sargus</i>	

Table A.4. List of Algal Species in Gencelli Harbor

Species	
<b>ANGROSPERMAE</b>	<i>Dilophus fasciola</i>
<i>Cymodocea nodosa</i>	<i>Ectocapus siliculosus</i>
<i>Halophila stipulacea</i>	<i>Halopteris filicina</i>
<i>Posidonia oceanica</i>	<i>Hydroclathrus clathratus</i>
<i>Z. noltii</i>	<i>Mesogloia vermiculata</i>
<i>Zostera marina</i>	<i>Padina pavonica</i>
	<i>S. horschuchii</i>
<b>CHLOROPHYTA</b>	<i>S. vulgare</i>
<i>Acetabulasia acetabulum</i>	<i>Sargassum acinarum</i>
<i>Anadyomene stellata</i>	<i>Scytosiphon lomentasia</i>
<i>C. pellucida</i>	<i>Spacelaria cirrosa</i>
<i>C. polifera</i>	
<i>Cladophora coelethrix</i>	<b>RHODOPHYTA</b>
<i>Codium bursa</i>	<i>Amphiroa rigida</i>
<i>Dasycladus vermicularis</i>	<i>Boergeseniella fruticulose</i>
<i>E. lima</i>	<i>Bonnemaisonia asparagoides</i>
<i>Enteromorpha compressa</i>	<i>C. muirei</i>
<i>Halimada tuna</i>	<i>Ceramium ciliatum</i>
<i>U. rigida</i>	<i>Ceramium diaphanum</i>
<i>Udotea petiolata</i>	<i>Ceramium rubrum</i>
<i>Ulva fasciata</i>	<i>Chondria dosyphylla</i>
<i>Valonia utricularis</i>	<i>Dermatolithon cystoseirae</i>
<b>CYANOPHYTA</b>	<i>Falkenbergia rufolanosa</i>
<i>Symploca hydroides</i>	<i>Grateloupia filicine</i>
	<i>H. secunda</i>
<b>PHAEOPHYTA</b>	<i>Herposiphonia secunda</i>
<i>Castagnea zosterae</i>	<i>Jania rubens</i>
<i>Cladostephus spongiosus</i>	<i>Laurencia obtusa</i>
<i>Colpomenia sinuosa</i>	<i>Liagora viscida</i>
<i>Cutleria multifide</i>	<i>Lophosiphonia obscura</i>
<i>Cystoseira compressa</i>	<i>Meloberia meunbranaceae</i>
<i>D. dichotome var. implexa</i>	<i>Nitophyllum punctatum</i>
<i>D. mediterraneus var. crassus</i>	<i>Peysonnelia squamaria</i>
<i>D. mediterraneus var. mediterraneus</i>	<i>Polysiphonia opara</i>
<i>Dictyopteris membranacea</i>	<i>Spyridida filamentosa</i>
<i>Dictyota dichotoma var. dichotoma</i>	<i>Botryocladia botryaides</i>
	<i>D. pustulatum</i>

Table A.5. Phytoplanktons and Protozooplanktons of Gencelli Harbor

Species	
<b>BACILLARIOPHYCEAE</b>	
<i>Bacteriastrum delicatulum</i>	<i>Ceratium contortum</i> var. <i>karstenii</i>
<i>Bacteriastrum hyalinum</i>	<i>Ceratium contrarium</i>
<i>Biddulphia pulchella</i>	<i>Ceratium declinatum</i>
<i>Cerataulina pelagica</i>	<i>Ceratium euarquatum</i>
<i>Chaetoceros affine</i>	<i>Ceratium falcatum</i>
<i>Chaetoceros anastomosans</i>	<i>Ceratium furca</i> var. <i>furca</i>
<i>Chaetoceros curvisetum</i>	<i>Ceratium fusus</i> var. <i>fusus</i>
<i>Chaetoceros decipiens</i>	<i>Ceratium fusus</i> var. <i>seta</i>
<i>Chaetoceros rostratum</i>	<i>Ceratium hexacanthum</i> var. <i>hexacanthum</i>
<i>Chaetoceros teres</i>	<i>Ceratium kofoidii</i>
<i>Chaetoceros tortissimum</i>	<i>Ceratium longirostrum</i>
<i>Guinardia flaccida</i>	<i>Ceratium macroceros</i> var. <i>gallicum</i>
<i>Hemiaulus hauckii</i>	<i>Ceratium massiliense</i> var. <i>massiliense</i>
<i>Leptocylindrus danicus</i>	<i>Ceratium trichoceros</i>
<i>Leptocylindrus minimus</i>	<i>Ceratium tripos</i> var. <i>atlanticum</i>
<i>Navicula</i> sp.	<i>Ceratium tripos</i> var. <i>pulchellum</i> f. <i>pulchellum</i>
<i>Rhizosolenia alata</i> f. <i>gracillima</i>	<i>Ceratium tripos</i> var. <i>pulchellum</i> f. <i>semipulchellum</i>
<i>Rhizosolenia alata</i> f. <i>indica</i>	<i>Ceratocorys armata</i>
<i>Rhizosolenia calcar-avis</i>	<i>Dinophysis caudata</i>
<i>Rhizosolenia fragilissima</i>	<i>Gonyaulax polygramma</i>
<i>Rhizosolenia imbricata</i> var. <i>shrupsolei</i>	<i>Gonyaulax</i> sp. Cysts
<i>Rhizosolenia robusta</i>	<i>Heteraulacus polyedricus</i>
<i>Rhizosolenia stolterfothii</i>	<i>Noctiluca scintillans</i>
<b>CILIATA</b>	<i>Oxytoxum constrictum</i>
<i>Eutimninus elongatus</i>	<i>Oxytoxum scolopax</i>
<i>Favella ehrenbergii</i>	<i>Podolampas bipes</i>
<i>Rhabdonella spiralis</i>	<i>Protoperdinium claudicans</i>
<i>Steenstrupiella steenstrupii</i>	<i>Protoperdinium conicum</i>
<i>Tintinnopsis campanula</i>	<i>Protoperdinium divergens</i>
<b>DINOPHYCEAE</b>	<i>Protoperdinium pyriforme</i>
<i>Ceratium biceps</i>	<i>Pyrophacus horologium</i>
<i>Ceratium candelabrum</i> var. <i>candelabrum</i>	
<i>Ceratium candelabrum</i> var. <i>depressum</i>	<b>RADIOLARIA</b>
<i>Ceratium carriense</i> var. <i>volans</i>	<i>Collosphaera huxleyi</i>
<i>Ceratium contortum</i> var. <i>contortum</i>	<i>Sphaezoum punctatum</i>



Table A.6. Zooplankton Species of the Gencelli Harbor

Species	
<b>CNIDARIA:</b> Hydrozoa: Hydromedusae: Gen. Sp. Gen. Sp. <i>Obelia sp.</i> Siphonophora: Gen. Sp. Gen. Sp. Gen. Sp. Gen. Sp. Gen. Sp. Gen. Sp. Gen. Sp. Gen. Sp.	<i>Evadne spinifera</i> <i>Evadne tergestina</i> <i>Penilia avirotris</i> <i>Podon intermedius</i> <i>Podon polyphemoides</i> Copepoda: <i>Acartia clausi</i> <i>Acartia latisetosa</i> <i>Calanus minor</i> <i>Calanus sp.</i> <i>Calanus sp.</i> <i>Calocalanus contractus</i> <i>Calocalanus pavo</i> <i>Calocalanus plumulosus</i> <i>Calocalanus styliremis</i> <i>Centropages typicus</i> <i>Centropages kroyeri</i> <i>Centropages violaceus</i> <i>Clausocalanus arcuicornis</i> <i>Clausocalanus furcatus</i> <i>Clytemnestra rostrata</i> <i>Clytemnestra scutellata</i> <i>Copilia quadrata</i> <i>Copilia sp.</i> <i>Corycaeus sp.</i>
<b>CHAETOGNATHA:</b> <i>Sagitta sp.</i> <i>Sagitta sp.</i> <i>Sagitta sp.</i>	
<b>TUNICATA:</b> Appendicularia (larvacea): <i>Fritillaria borealis</i> <i>Fritillaria sp.</i> <i>Oikopleura dioica</i> <i>Oikopleura fusiformis</i> <i>Oikopleura longicauda</i> Thaliacea: <i>Doliolum sp.</i> <i>Salpa sp.</i>	
<b>CRUSTACEA:</b> Cladocera: <i>Evadne nordmanni</i>	<b>MOLLUSCA:</b> Pteropoda: Gen. Sp. Gastropoda larva: Gen. Sp. Gen. Sp. Gen. Sp. Lammellibranchiata larva: Gen. Sp. Gen. Sp.

Table A.6. (Cont'd)

Species	
<i>Corycella rostrata</i>	Decapoda larva:
<i>Ctenocalanus vanus</i>	<i>Athanas</i> sp.
<i>Cymbasoma</i> sp.	<i>Callianassa</i> sp.
<i>Eucalanus</i> sp.	<i>Galathea</i> sp.
<i>Euterpina acutifrons</i>	Gen. Sp. ( <i>Branchyura</i> )
<i>Isias clavipes</i>	Gen. Sp. ( <i>Branchyura</i> )
<i>Labidocera wollastoni</i>	<i>Jaxea nocturna</i>
<i>Mecynocera clausi</i>	<i>Pagurus</i> sp.
<i>Oithona helgolandica</i>	<i>Palaemo</i> sp.
<i>Oithona nana</i>	<i>Pisidia</i> sp.
<i>Oithona plumifera</i>	<i>Processa</i> sp.
<i>Oncaea</i> sp.	<i>Squilla</i> mantis
<i>Paracalanus parvus</i>	<i>Upogebia pusilla</i>
<i>Paracalanus navus</i>	
<i>Sapphirina</i> sp.	POLYCHAETA Larva:
<i>Temora stylifera</i>	Gen. Sp.
Euphausiacea:	Gen. Sp.
<i>Euphausia</i> sp.	Gen. Sp.
Mysicadea:	
Gen. Sp.	ECHINODERMATA Larva:
Gen. Sp.	Gen. Sp. <i>Auricularia</i>
Gen. Sp.	Gen. Sp. <i>Bipinnaria</i>
Girripedia larva:	Gen. Sp. <i>Echinopluteus</i>
Gen. Sp.	Gen. Sp. <i>Echinopluteus</i>
Gen. Sp.	Gen. Sp. <i>Ophiopluteus</i>

Table A.7. Zoobenthose Species in the Gencelli Harbor

Species	
<b>PORIFERA</b>	<i>Eunice vittata</i>
<i>Chondrosis sp.</i>	<i>Glycera convoluta</i>
<i>Euspongia officinalis</i>	<i>Glycera sp.</i>
<i>Porifera (sp.)</i>	<i>Harmothoe areolata</i>
<i>Porifera (sp3)</i>	<i>Harmothoe impar</i>
<i>Suberites domuncula</i>	<i>Harmothoe sp.</i>
<i>Sycon raphanus</i>	<i>Hermione hystrix</i>
<i>Tethya aurantium</i>	<i>Hermodice carunculata</i>
	<i>Hyalinoecia brement</i>
<b>CNIDARIA</b>	<i>Hyalinoecia sp.</i>
<i>Actinaria (sp.)</i>	<i>Hydroides pseudouncinata</i>
<i>Actinia equina</i>	<i>Hydroides uncinata</i>
<i>Adamsia palliata</i>	<i>Jaunapagenstecheri</i>
<i>Anemonia sulcata</i>	<i>Janua sp.</i>
<i>Balanophylla sp.</i>	<i>Josephella marenzelleri</i>
<i>Cladocora cespitosa</i>	<i>Kefersteinia cirrata</i>
<i>Parazoanthus sp.</i>	<i>Lanice conchilcega</i>
<i>Sagartia sp.</i>	<i>Laonica cirrata</i>
	<i>Lepidonotus clava</i>
<b>POLYCHAETA</b>	<i>Lubriconereis fragilis</i>
<i>Amphicteis gunneri</i>	<i>Lumbriconereis coccinea</i>
<i>Amphiglena mediterranea</i>	<i>Lumbriconereis latreilli</i>
<i>Amphitrite edwardsi</i>	<i>Lumbriconereis sp.</i>
<i>Amphitrite sp.</i>	<i>Lysidice ninetta</i>
<i>Ancystrosyllis parva</i>	<i>Lysidice sp.</i>
<i>Arabella iricolor</i>	<i>Maldane sp.</i>
<i>Asychis biceps</i>	<i>Melinna palmata</i>
<i>Autolytus prolifer</i>	<i>Mermodice carunculata</i>
<i>Brada villosa</i>	<i>Nematonereis unicornis</i>
<i>Chone collaris</i>	<i>Nephtys caeca</i>
<i>Chone filicaudata</i>	<i>Nephtys hombergi</i>
<i>Chrysopetalum debile</i>	<i>Nephtys sp.</i>
<i>Cirratulus sp.</i>	<i>Nereis pelagica</i>
<i>Clymena lumbricoides</i>	<i>Nereis sp.</i>
<i>Clymena oerstedii</i>	<i>Nicoles venustula</i>
<i>Dasybranchus gajolea</i>	<i>Notomastus fauveli</i>
<i>Dasychone lucullana</i>	<i>Notomastus latericeus</i>
<i>Eunice sp.</i>	<i>Notomastus sp.</i>
<i>Eunice torquata</i>	<i>Owenia fusiformis</i>
	<i>Pantogenia chrysocoma</i>
	<i>Paralacydonia sp.</i>
	<i>Pectinaria koreni</i>

Table A.7. (Cont'd)

Species	
<i>Perinereis</i> sp. <i>Petaloproctus terricola</i> <i>Pherusa</i> sp. <i>Phyllodoce paretii</i> <i>Phyllodoce</i> sp. <i>Pileolaria militaris</i> <i>Pista cristata</i> <i>Platynereis dumerilii</i> <i>Polycirrus haematodes</i> <i>Polycirrus haematodes</i> <i>Polydora</i> sp. <i>Polydontes maxillosus</i> <i>Polyopthalmus cretacea</i> <i>Polyopthalmus pictus</i> <i>Pomatoceros triqueter</i> <i>Pontogenia chrysocoma</i> <i>Potamilla reniformis</i> <i>Prionospia cirrifera</i> <i>Prionospia malmgreni</i> <i>Protula</i> sp. <i>Psammolyce</i> sp. <i>Pterosyllis formose</i> <i>Sabella</i> sp. <i>Sabellaria spinulosa</i> <i>Salmacina dysleri</i> <i>Scalisetosus</i> sp. <i>Selmacina disteri</i> <i>Serpula vermicularis</i> <i>Sphaerosyllis erinaceus</i> <i>Spirobranchus polytrema</i> <i>Spirogrophis spallanzanii</i> <i>Staurocephalus rudolphii</i> <i>Sthenelais boa</i> <i>Syllis prolifera</i> <i>Syllis variegata</i> <i>Syllis</i> sp. <i>Telephus</i> sp. <i>Terebella</i> sp. <i>Terebellides stroemi</i> <i>Trypanosyllis zebra</i> <i>Vermiliopsis infundibulum</i> <i>Vermiliopsis</i> sp.	SIPUNCULIDA <i>Aspidosiphon mulleri</i> <i>Phascolion</i> sp. <i>Phascolosoma</i> sp. <i>Spinculus nudus</i>  CRUSTACEA  <i>Acanthonyx lunulatus</i> <i>Acidostoma laticorne</i> <i>Acanthonyx lunulatus</i> <i>Alpheus glaber</i> <i>Ampelisca</i> sp. <i>Ampherusa</i> sp. <i>Amphilochus</i> sp. <i>Amphithoe ramondi</i> <i>Amphithoe</i> sp. <i>Apherusa bispinosa</i> <i>Apherusa</i> sp. <i>Apseudes latreillei</i> <i>Apseudes</i> sp. <i>Athanas nitescens</i> <i>Balanus perforatus</i> <i>Balanus</i> sp. <i>Bodotria</i> sp. <i>Caprella danilewskyi</i> <i>Caprella</i> sp. <i>Chthamalus stellatus</i> <i>Cirratulus</i> sp. <i>Clibanarius erythropus</i> <i>Cumella limicola</i> <i>Dexamine spiniventris</i> <i>Dexamine spinosa</i> <i>Dynamene</i> sp. <i>Dynamene torelliae</i> <i>Ebalia granulosa</i> <i>Elasmopus pocillimanus</i> <i>Elasmopus</i> sp. <i>Erichthonius difformis</i> <i>Erichthonius</i> sp. <i>Ethusa mascarone</i> <i>Eurinome aspera</i>

Table A.7. (Cont'd)

Species	
<i>Eurydice</i> sp.	<i>Peudoprotella phasma</i>
<i>Eurystheus maculatus</i>	<i>Philocheras</i> sp.
<i>Galathea squamifera</i>	<i>Phitisicea marina</i>
<i>Gammarus</i> sp.	<i>Pilimnus spinifer</i>
<i>Gnathia</i> sp.	<i>Pilimnus turtellus</i>
<i>Hablostylus</i> sp.	<i>Pilumnus hirtellus</i>
<i>Harpinia</i> sp.	<i>Pisa armata</i>
<i>Hippolyte</i> sp.	<i>Pisa nodipes</i>
<i>Hyale schmidtii</i>	<i>Pisa</i> sp.
<i>Hyale</i> sp.	<i>Pisa tetraodon</i>
<i>Idotea</i> sp.	<i>Pseudopratella phasma</i>
<i>Inachus communissimus</i>	<i>Pisidia longimana</i>
<i>Iphinoe</i> sp.	<i>Pisidia</i> sp.
<i>Jaeropsis</i> sp.	<i>Podocerus variegatus</i>
<i>Janaia cavolini</i>	<i>Ponopoea minuta</i>
<i>Janira</i> sp.	<i>Pontocaris cataphracta</i>
<i>Leptachelia sawignyi</i>	<i>Porcellana plathycheles</i>
<i>Leptochelia</i> sp.	<i>Primula denticulata</i>
<i>Leucothoe</i> sp.	<i>Processa edulis</i>
<i>Leucothoe spinicarpa</i>	<i>Pseudocuma</i> sp.
<i>Limnoria</i> sp.	<i>Pseudoprotella phasma</i>
<i>Lysianassa costata</i>	<i>Scopelecheurus</i> sp.
<i>Lysianassa</i> sp.	<i>Siriella</i> sp.
<i>Macropipus</i> sp.	<i>Sirpus zaruquieii</i>
<i>Macropipus corrugatus</i>	<i>Sphaeroma serratum</i>
<i>Macropodia longirostris</i>	<i>Stenothoe monoculoides</i>
<i>Maia</i> sp.	<i>Synisoma capito</i>
<i>Maera inaequipes</i>	<i>Tanaia cavolini</i>
<i>Megaluropus</i> sp.	<i>Thoralus cranchii</i>
<i>Melita palmata</i>	
<i>Metaphoxus fultoni</i>	<b>MOLLUSCA</b>
<i>Monculoides</i> sp.	<i>Acanthocardia</i> sp.
<i>Monoculades</i> sp.	<i>Alvania</i> sp.
<i>Orchestia</i> sp.	<i>Anomia epiphium</i>
<i>Pachygrapsus marmoratus</i>	<i>Anomia</i> sp.
<i>Pagurister</i> sp.	<i>Aporrhais pespelecani</i>
<i>Paguristes ocellatus</i>	<i>Arca lactea</i>
<i>Pagurus arrosor</i>	<i>Arca</i> sp.
<i>Pagurus</i> sp.	<i>Arca tetragona</i>
<i>Panopaea minuta</i>	<i>Bittium reticulatum</i>
<i>Papuristes oculatus</i>	<i>Brachydontes minimus</i>
<i>Paranthura constans</i>	<i>Cardita colyculate</i>
<i>Parthenope</i> sp.	<i>Cardita trapezia</i>
<i>Pereionotus testudo</i>	<i>Cardium oblongum</i>

Table A.7. (Cont'd)

Species	
<i>Cardium</i> sp. <i>Cerithium vulgatum</i> <i>Chama gryphoides</i> <i>Chiton olivaceus</i> <i>Chiton</i> sp. <i>Clathrus clathrus</i> <i>Columbella rustica</i> <i>Conus mediterraneus</i> <i>Corbula gibba</i> <i>Cuspidari cuspidata</i> <i>Dentalium</i> sp. <i>Diadora</i> sp. <i>Echinochama lazarus</i> <i>Eulima</i> sp. <i>Fasciolaria lignaria</i> <i>Gibbula</i> sp. <i>Haliotis lamellosa</i> <i>Haliotis tuberculata</i> <i>Hiatella arctica</i> <i>Hiatella</i> sp. <i>Hiatella striata</i> <i>Littorina neritoides</i> <i>Middendorffia caprearum</i> <i>Modiolus barbatus</i> <i>Monodonta</i> sp. <i>Monodonta turbinata</i> <i>Murex brandaris</i> <i>Murex trunculus</i> <i>Musculus costulatus</i> <i>Mytilus galloprovincialis</i> <i>Nassa</i> sp. <i>Natica</i> sp. <i>Nucula nucleus</i> <i>Nuculana fragilis</i> <i>Ocenebra edwardsi</i> <i>Octopus vulgaris</i> <i>Ostrea edulis</i> <i>Patella coerulea</i> <i>Patella lucitanica</i> <i>Patella</i> sp. <i>Rissoa</i> sp. <i>Rocellaria dubia</i>	<i>Sepia officinalis</i> <i>Tellina distorta</i> <i>Tellina</i> sp. <i>Venerupis</i> sp. <i>Venus verrucosa</i> <i>Vermetus</i> sp. <i>Vermetus triqueter</i>  <b>BRYOZOA</b>  <i>Cellepora</i> cf. <i>Pumicosa</i> <i>Cryptosula</i> sp. <i>Membranipora</i> sp. <i>Porella</i> sp. <i>Sertella</i> sp. <i>Tubucellaria opuntioides</i>  <b>ECHINODERMATA</b>  <i>Amphipholis squamata</i> <i>Arbacia lixula</i> <i>Asterina gibbosa</i> <i>Astropecten irregularis</i> <i>Astropecten</i> sp. <i>Echinaster sepositus</i> <i>Echinaster</i> sp. <i>Holothuria forskali</i> <i>Holothuria tubulosa</i> <i>Marthasterias glacialis</i> <i>Ophiothrix fragilis</i> <i>Ophiura albida</i> <i>Ophiura texturata</i> <i>Paracentrotus lividus</i> <i>Psammechinus microtuberculatus</i> <i>Psammechinus</i> sp.  <b>TUNICATA</b>  <i>Alocynthia papillosa</i> <i>Ascidia</i> sp. <i>Botryllus schilosseri</i> <i>Didemnum maculosum</i>

## APPENDIX B

### SENSITIVITY TESTS FOR THE LIQUID WASTE DISCHARGE

#### B.1 General

In the case of lack of detailed field data, which are essential for the calculation or selection of certain parameters, sensitivity tests are necessary. In this chapter, sensitivity tests are used to provide information for further similar studies. This information can be used to observe the effects of the changes in the design parameters, if needed.

Several sensitivity runs were performed in order to test the sensitivity of the target parameters,  $S_1$ ,  $S_2$  and  $S_3$ , to changes in input parameters. For this purpose, a base case was defined by using both fixed design parameters and estimated or assumed values. In these tests, all the parameters were kept constant except the one which is being tested. The base-case parameters and their assigned values are given in Table B.1. The following parameters were used for the purpose of testing the sensitivity of the target parameters:

- discharge depth
- discharge velocity
- degree of stratification
- $T_{90}$  parameter
- Discharge length
- wastewater density
- ambient current velocity



Table B.1. Base-case Parameters and Abbreviations of Tests

Parameter	Abbr.	Value
Depth	H	20 m
Discharge velocity	v	1.3 m s <sup>-1</sup>
Initial wastewater density	WW. D.	1000 kg m <sup>-3</sup>
Ambient water density gradient	Delta	0.0 kg m <sup>-3</sup> /m
Ambient water density	AW. D.	1028 kg m <sup>-3</sup>
T <sub>90</sub>	T90	3 hr
Surface current velocity	u	0.1 m s <sup>-1</sup>
Discharge to coastline distance	d	500 m

B.2 Tests for the Discharge Depth

Deep sea discharges are preferred in order to use the dilution capacity of sea from the discharge point until it reaches to the surface. Various possible dilution ratios which can be achieved by the wastewater discharge structure of the proposed ATPP at different discharge depths are given in Figure B.1.

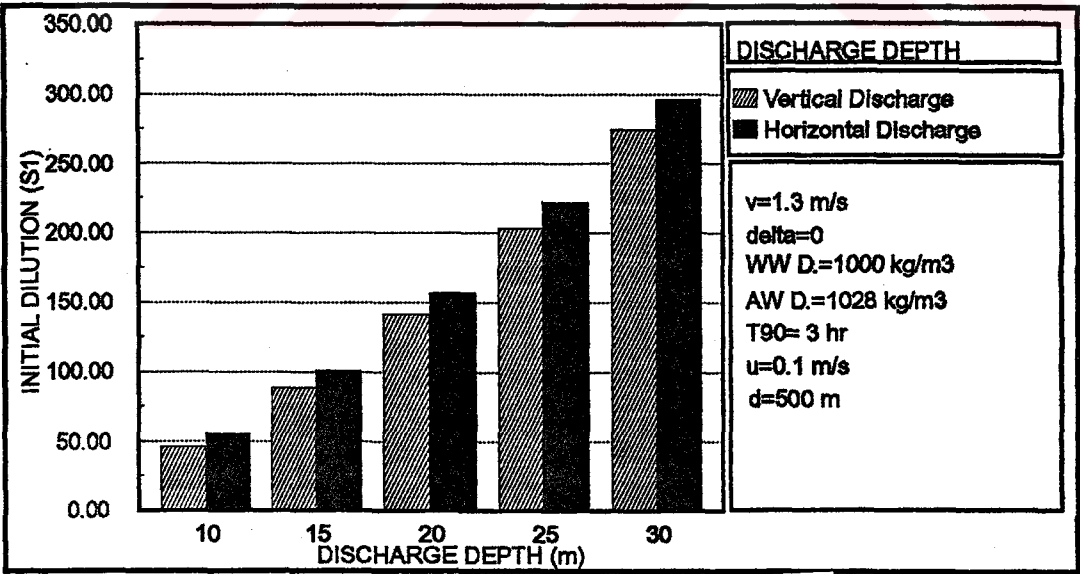


Figure B.1. Tests for Discharge Depth



### B.3 Tests for the Discharge Velocity

In the jet theory, the discharge velocity is an important factor in wastewater dilution. As the jet velocity increases the free turbulence (therefore dilution) increases. Various centerline dilution ( $S_1$ ) values were obtained for different discharge velocities. The results are given in Figure B.2.

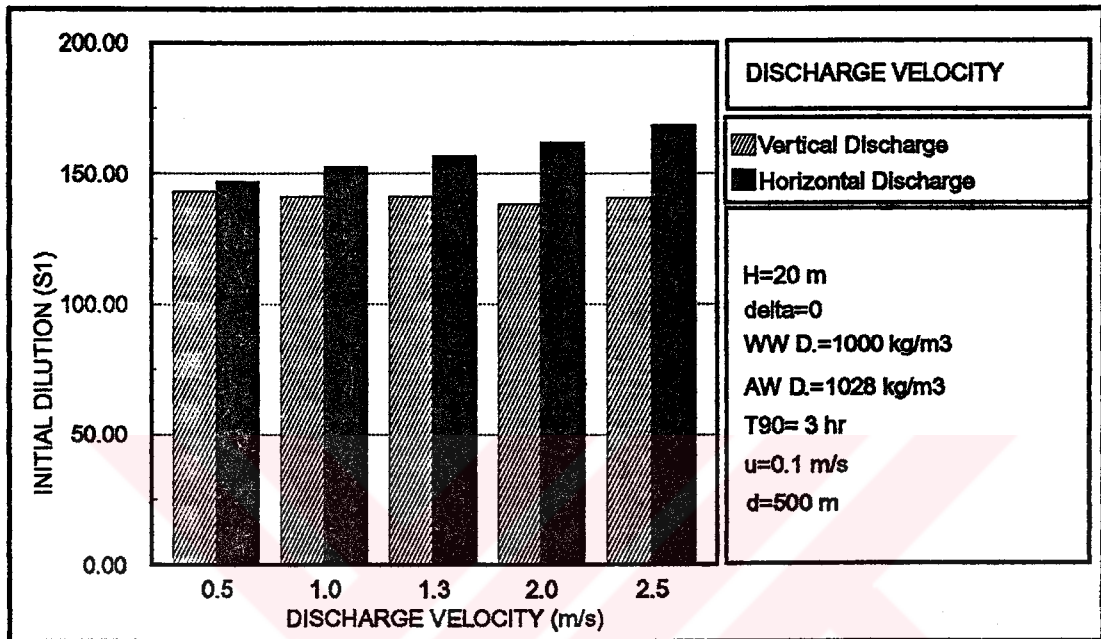


Figure B.2. Tests for Discharge Velocity

The results of the tests for discharge velocity revealed that the centerline dilution increases as the discharge velocity increases, for horizontal discharges. However, no significant trend for the centerline dilution was indicated in the tests. This was due to the nature of the model. It is reported (Hayashi and Ito, 1974) that the model overestimates the dilution ratio at low Froude numbers of about 2.5. The range of Froude number corresponding to velocities tested in this section varies between 2 to 15. In this regard, it can be stated that this fact might result in a limited overestimation of the the initial dilution values corresponding to the lower velocities.

B.4 Tests for the Degree of Stratification

A positive density gradient term represents the vertical increase in sea water density with the increase in depth. The higher degree of stratification is represented by a greater density gradient.

A decrease in the buoyancy effect may be expected due an increase in the degree of stratification. Various possible dilution levels which can be achieved by the wastewater discharge structure of the proposed ATPP, in different conditions of stratification, are given in Figure B.3.

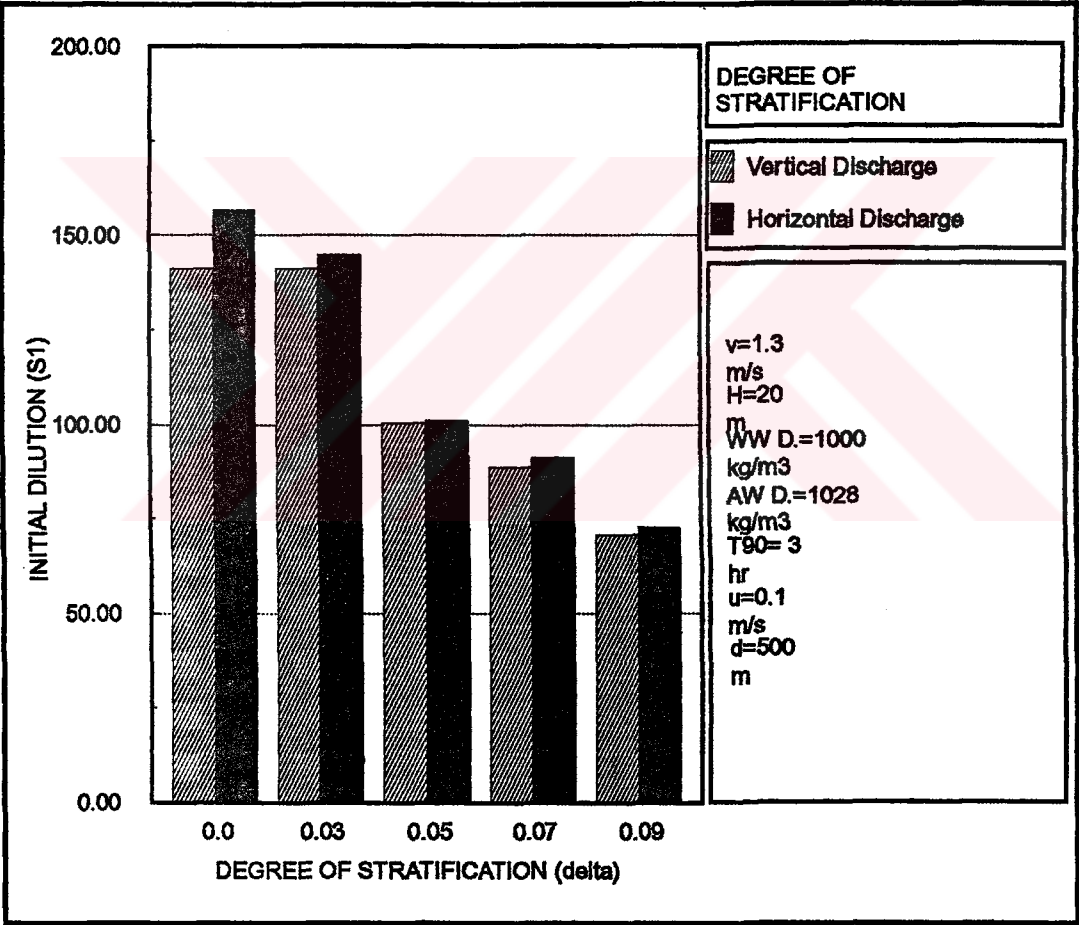


Figure B.3. Tests for the Degree of Stratification

B.5 Tests for the  $T_{90}$  Value

The  $T_{90}$  parameter is the major parameter controlling the dilution due to bacterial decay,  $S_3$ . Various possible dilution levels that may be achieved by the wastewater discharge structure of the proposed ATPP for different  $T_{90}$  values are given in Figure B.4.

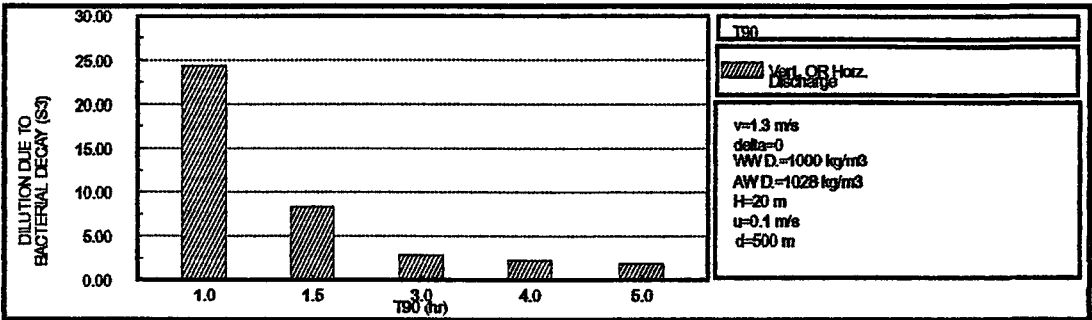


Figure B.4. Tests for the  $T_{90}$  Value

B.6 Tests for the Discharge Length

As the length increases larger dilution values are expected due to the availability of sufficient time for bacterial decay and for the dispersion of the wastewater field. This condition will result in lower levels of pollution in the coastal waters. Various possible dilution levels that may be achieved by the wastewater discharge structure of the proposed ATPP for different  $T_{90}$  values are given in Figure B.5.

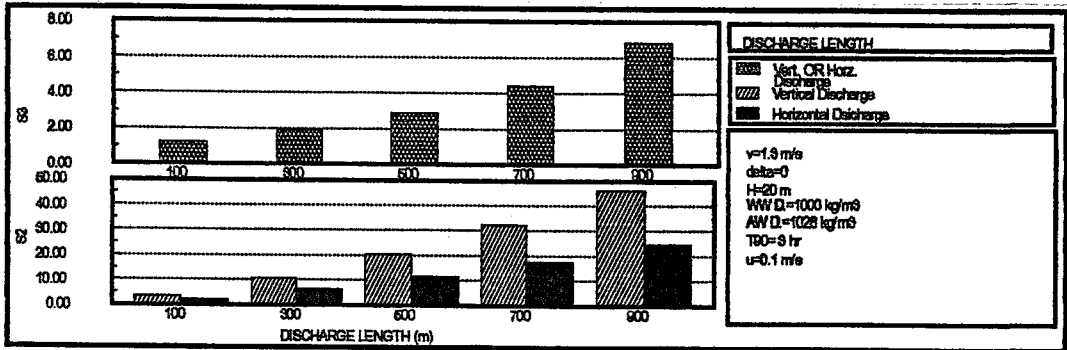


Figure B.5. Tests for the Discharge to Coastline Distance

B.7 Tests for the Wastewater Density

Wastewater and ambient water densities are together an important factor affecting the dilution and motion of a wastewater field. The greater the difference between the values of these two parameters, the greater the buoyancy effect on a jet and, therefore, the greater the dilution.

It is possible to estimate the approximate density of ambient water. However, the possible variations in the density of the wastewater, which will be discharged from the proposed ATPP, is not completely known. With this intention, various possible dilution levels which may be achieved by the wastewater discharge structure of the proposed ATPP are given in Figure B.6. for different wastewater densities.

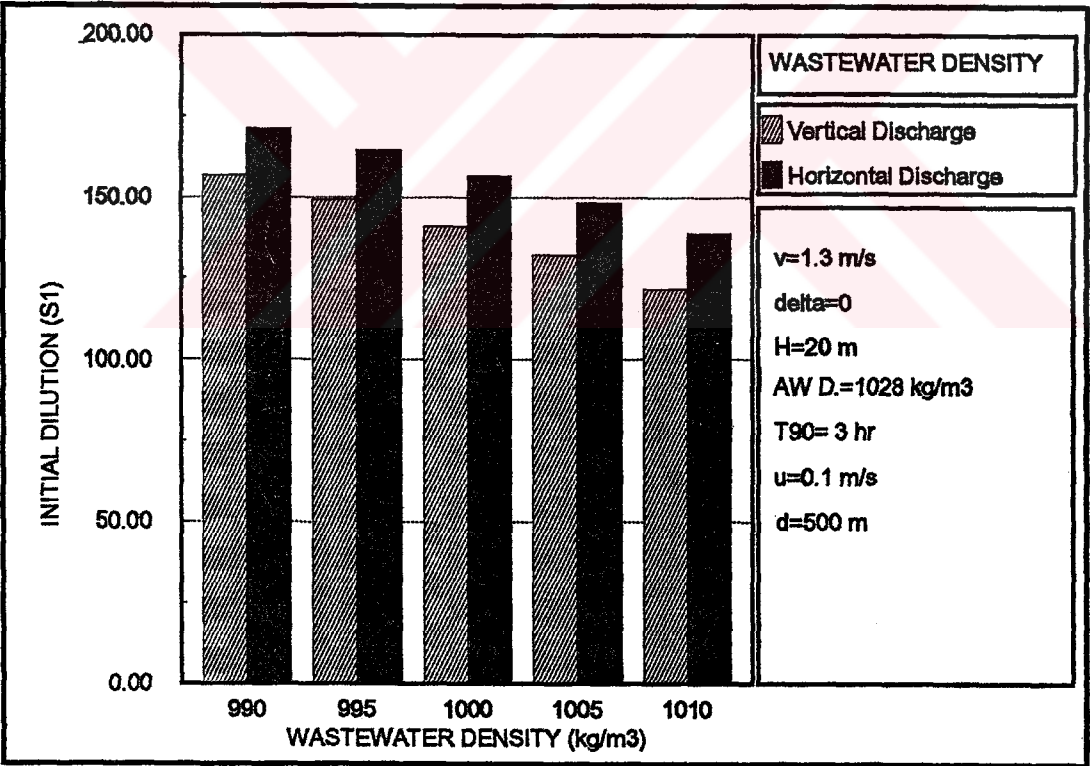


Figure B.6. Tests for the Wastewater Density

B.8 Tests for the Ambient Current Velocity

Sea current is an advective mechanism in pollutant transport. As the velocity increases, the dilution due to dispersion achieved until the wastewater field reaches the coastal waters decreases. This is due to insufficient time for dispersion in the case of strong landward currents. The strong landward current quickly advects the plume to coast without being sufficiently diluted. Various possible dilution levels that may be achieved by the wastewater discharge structure of the proposed ATPP for different landward current velocities are given in Figure B.7.

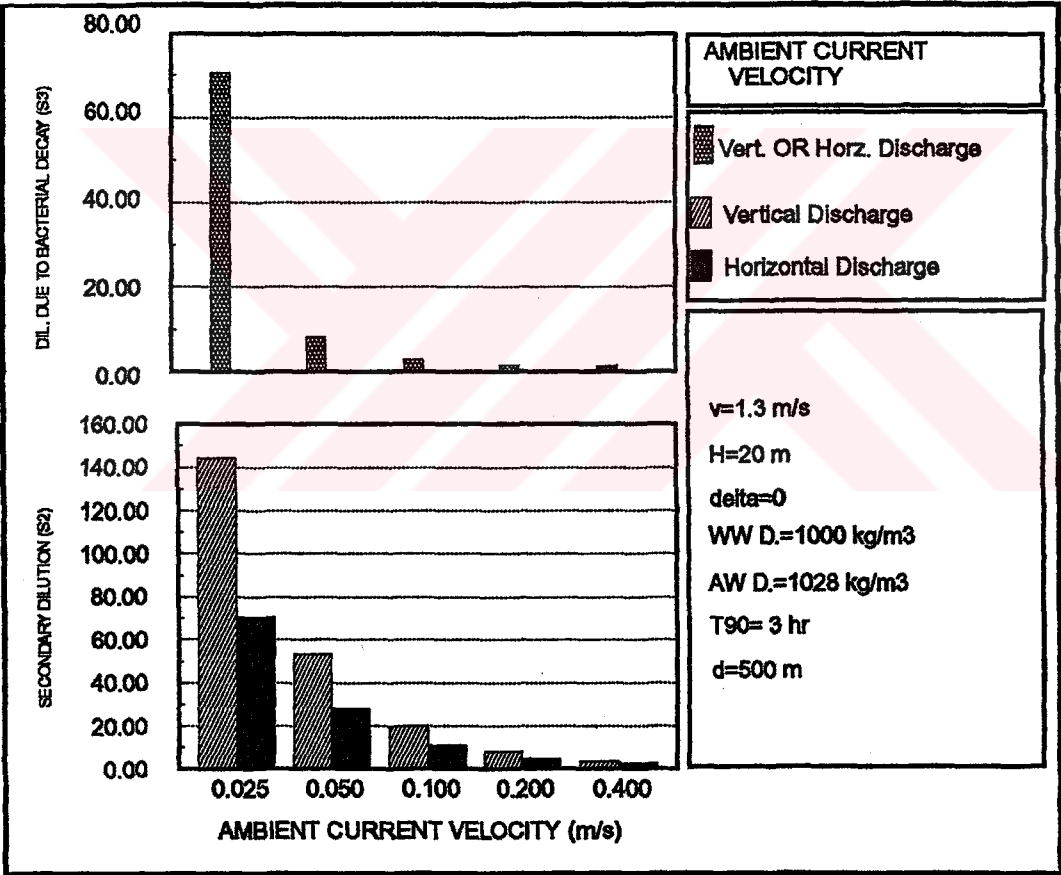


Figure B.7. Tests for the Ambient Current Velocity

## APPENDIX C

### THEORETICAL BASIS OF GLLVHT

The time-varying solution technique of the model is based on an implicit scheme that results from the simultaneous solution of the longitudinal and lateral momentum equations and the free-water surface equation of vertically integrated continuity. This technique results in the surface long wave equation that is solved on each time step to give the water surface profiles, from which the vertical pressure distribution can be determined. The longitudinal and lateral momentum balances are then computed. The computations are followed by internal continuity and constituent transport computations. Upwind differencing is used for the advective processes in the momentum and constituent transport balances. Vertical turbulent transfer of momentum and constituents is determined from the vertical shear of horizontal velocity and a density gradient dependent Richardson number function.

The model has a layer/cell add/subtract module. When the water surface elevation decreases to the point where an unacceptably thin surface layer develops, the computational properties of each cell in the thin layer are transferred to the cells of the layer below. If this layer subtraction results in fewer surface cells, the module eliminates these nearly-dry cells, renumbers the grid and proceeds with the computation. The process for a rising water surface is similar. A surface layer whose thickness exceeds the desired vertical resolution is divided into two. If this division results in additional surface cells, these cells are activated, the grid is renumbered and the

computation continues. Layers and cells may be added or subtracted many times during a simulation. On each occasion, correct water and constituent balances are maintained.

The hydrodynamic and transport relationships used in GLLVHT can be developed from the basic horizontal momentum balance, continuity relationship, constituent transport and the equation of state. The horizontal momentum balances for the horizontal velocity components, U and V in the x- and y-coordinate horizontal directions, with z taken positive downward, are:

$$\begin{aligned} \partial U / \partial t = & g \partial z' / \partial x - g / \rho \int_{z'}^z (\partial p / \partial x) \partial z + f V - \partial U U / \partial x - \partial V U / \partial y - \partial W U / \partial z \\ & + \partial A_x (\partial U / \partial x) / \partial x + \partial A_y (\partial U / \partial y) / \partial y + \partial A_z (\partial U / \partial z) / \partial z + S M_x \end{aligned} \quad (C.1)$$

$$\begin{aligned} \partial V / \partial t = & g \partial z' / \partial y - g / \rho \int_{z'}^z (\partial p / \partial y) \partial z - f U - \partial U V / \partial x - \partial V V / \partial y - \partial W V / \partial z \\ & + \partial A_x (\partial V / \partial x) / \partial x + \partial A_y (\partial V / \partial y) / \partial y + \partial A_z (\partial V / \partial z) / \partial z + S M_y \end{aligned} \quad (C.2)$$

Local continuity for the vertical velocity component W, is given as:

$$\partial W / \partial z = - \partial U / \partial x - \partial V / \partial y \quad (C.3)$$

Vertically integrated continuity for the surface elevation, z', is given as:

$$\partial z' / \partial t = - \int_z^h \partial U / \partial x - \int_z^h \partial V / \partial y \quad (C.4)$$

The constituent transport relationships for n number of constituents (for example, salinity and heat) is given by:

$$\begin{aligned} \partial C_n / \partial t = & - \partial U C_n / \partial x - \partial V C_n / \partial y - \partial W C_n / \partial z + \partial (D_x \partial C_n / \partial x) / \partial x \\ & + \partial (D_y \partial C_n / \partial y) / \partial y + \partial (D_z \partial C_n / \partial z) / \partial z + H_n \end{aligned} \quad (C.5)$$



An equation of state relating density,  $\rho$ , to constituents is used as:

$$\rho = g(C_1, C_2, \dots, C_n) \quad (C.6)$$

These relationships have six unknowns ( $U$ ,  $V$ ,  $W$ ,  $z'$ ,  $\rho$ ,  $C_n$ ) in six equations, assuming that the momentum and constituent dispersion coefficients ( $A_x$ ,  $A_y$ ,  $A_z$ ,  $D_x$ ,  $D_y$ ,  $D_z$ ) can be evaluated from velocities and the density structure.

In the  $x$  and  $y$  momentum balances, the right-hand terms are successively the barotropic or water surface slope, the baroclinic or density gravity slope, the Coriolis acceleration, the advection of momentum in each of the three coordinate directions, and the dispersion of momentum in each of the coordinate directions. The baroclinic and barotropic slopes are arrived at from the hydrostatic approximation to vertical momentum and horizontal differentiation of the density-pressure integral by Leibnitz' rule. The baroclinic slope is seen to be the vertical integral of the horizontal density gradient and becomes the major driving force for density-induced flows that vary with depth. In particular, even a vertically mixed waterbody, as indicated by salinity and temperature, that has horizontal density gradients can and does have significant density-induced flows.

The hydrodynamic relationships are integrated numerically, implicitly forward in time, by evaluating the horizontal momentum balances as:

$$\partial U / \partial t = g \partial z' / \partial x + F_x \quad (C.7)$$

$$\partial V / \partial t = g \partial z' / \partial y + F_y \quad (C.8)$$

where  $U$ ,  $V$  and  $z'$  are taken simultaneously forward in time and all the other terms are incorporated in  $F_x$  and  $F_y$  and are lagged in time. Equations



C.7 and C.8 are substituted (either by cross-differentiation or algebraically from the finite difference forms) into vertically integrated continuity to give the surface wave equation of:

$$\frac{\partial z'}{\partial t^2} + g \frac{\partial}{\partial z'} \left[ \left( \frac{\partial z'}{\partial x} \right) \frac{\partial z}{\partial x} + g \frac{\partial}{\partial z'} \left[ \left( \frac{\partial z'}{\partial y} \right) \frac{\partial z}{\partial y} = \int_{z'}^h F_x \partial z + \int_{z'}^h F_y \partial z \right] \quad (C.9)$$

The computational steps in GLLVHT on each time step of integration are:

- (1) to evaluate  $F_x$  and  $F_y$  from  $U$ ,  $V$ ,  $W$ ,  $p$  known from the previous time step;
- (2) to solve the surface wave equation for new  $z'$  for the spatial grid using a modified form of Gaussian elimination by back substitution;
- (3) to solve for new  $U$  and  $V$  using Equations C.7 and C.8;
- (4) to solve for  $W$  using Equation C.3;
- (5) to re-evaluate  $z'$  from Equation C.4 for precision; and,
- (6) to solve the constituent relationships in Equation C.5.

The semi-implicit integration procedure has the advantage that computational stability is not limited by the Courant condition that  $\partial x / \partial t$ ,  $\partial y / \partial t < (ghm)^{1/2}$  where  $hm$  is the maximum water depth that can lead to inefficiently small time steps of integration. Since the solutions are semi-implicit (for example, explicit in the constituent transport and the time lagged momentum terms) the stability is controlled by the Torrence condition ( $U \partial t / \partial x$ ,  $V \partial t / \partial y < 1$ ). Hence, the integration time step can be chosen to realistically represent the details of the boundary data which is about 15 minutes for tides and up to one hour for meteorological data.

There are a number of auxiliary relationships which enter the computations and bring the boundary data to bear on the evaluation. First, the

vertical momentum dispersion coefficient and vertical shear is presently (but not limited to) evaluated from a Von Karman relationship modified by the local Richardson number,  $Ri$ , (the ratio of vertical buoyant acceleration to vertical momentum transfer) as:

$$Az = kL^2/2[(\partial U/\partial z)^2 + (\partial V/\partial z)^2]^{1/2} F(Ri) \quad (C.10)$$

where  $k$  is the Von Karman constant;  $L$  is a mixing length that can be a function of depth and time; and,  $F(Ri)$  is the Richardson number function.

Wind surface stress enters the relationships for each of the coordinate directions as:

$$Az \partial U / \partial z|_z = W(W_x) \quad (C.11)$$

$$Az \partial V / \partial z|_z = W(W_y) \quad (C.12)$$

where  $W(W_x)$  and  $W(W_y)$  are surface shear functions of wind speed.

In addition to surface wind shear, there are two further windwave effects that enter the momentum relationships through the specific momentum terms,  $SM_x$  and  $SM_y$ . These effects are due to the spatial change in windwave height ( $H$ ) and period ( $T$ ) as  $g\partial(H^2/T)/\partial x$  and  $g\partial(H^2/T)/\partial y$  (the windwave gradients). One of the windwave effects is for windwaves that propagate into the waterbody region from offshore (and not found in the  $z'$  boundary elevation record) and for which the spatial distribution of  $H$  and  $T$  can be found from a wave refraction computation for the waterbody region geometry (for example, Koutitas, 1988). The second is due to the change of  $H$  and  $T$  along the wind fetch and is a function of fetch length and duration of given windspeeds (for example, Darbyshire-Draper relationships). The windwave gradients also decay with depth from known windwave properties, but fundamentally they

augment the longwave barotropic slope by the difference in average wave heights along the coordinate direction and enter directly into the momentum balance.

Bottom friction enters the computations through a Chezy friction relationship as:

$$Az\partial U/\partial z|_h=(g/Ch^2)U^2 \quad (C.13)$$

$$Az\partial V/\partial z|_h=(g/Ch^2)V^2 \quad (C.14)$$

where  $Ch$  is the local Chezy friction coefficient and  $h$  is the bottom elevation at which bottom friction is evaluated.

The horizontal momentum and constituent dispersion coefficients, ( $A_x$ ,  $A_y$ ,  $D_x$ ,  $D_y$ ), have not been adequately evaluated within three-dimensional numerical models but are thought to be primarily a function of the scale of the computational grid. In GLLVHT they are presently evaluated from grid size using an Okubo (1971) length scaling. Experience has shown that the velocity computations, and hence advection and dispersion in the constituent relations, become less sensitive to the horizontal momentum and constituent dispersion coefficients the more detailed the integration time step and spatial detail.

The source and sink terms,  $H_n$ , in the constituent balances, Equations C.5, depend on the constituent being examined. For heat, the source and sink terms are for surface heat exchange, radiation attenuation through the water column, and advective sources such as river inflows. Surface heat exchange includes incoming shortwave solar radiation and longwave atmospheric radiation, their reflective loss components, and the water surface temperature dependent processes of back radiation, evaporation and conduction. These

terms are evaluated using the complete term by term heat budget methods of Jirka et al. (1978) in subroutines to the hydrodynamic and transport model. The heat budget includes the following major components:

- shortwave solar radiation,  $H_s$
- long wave atmospheric radiation,  $H_a$
- long wave back radiation,  $H_b$
- heat loss or gain due to evaporation or condensation,  $H_e$
- reflected solar radiation,  $H_{sr}$
- reflected atmospheric,  $H_{ar}$
- loss or gain by conduction,  $H_c$

The processes of surface heat exchange are briefly illustrated in Figure C.1 along with their approximate range in magnitude of daily average values for mid-latitudes.

All the incoming and reflected radiation components are independent of the water temperature. The processes of surface heat loss are back-radiation, evaporation, and conduction. Their magnitudes are all dependent on the temperature of the water surface. Of the above heat budget components, only a few are measurable. Some are too expensive to be measured. The general approach is to compute or estimate the heat budget components based on the measurable meteorological parameters. The measurable meteorological variables of significance are:

- solar radiation
- air temperature
- dew-point temperature
- wind speed

Measurements of the above parameters are needed to evaluate the rates of back-radiation, evaporation and conduction. The measured and computed parameters are given in Table C.1.

Table C.1. Heat Exchange Components and Relevant Measurable Parameters Necessary to Compute the Components

Heat Exchange Component	Measurable Parameters*
Shortwave solar radiation ( $H_s$ )	$H_s$
Reflected solar radiation ( $H_{sr}$ )	$H_s$
Atmospheric radiation ( $H_a$ )	$H_s, T_a$
Reflected atmospheric radiation ( $H_{ar}$ )	$T_d$
Back-radiation ( $H_b$ )	$T_s$
Evaporation ( $H_e$ )	$T_s, T_d, W$
Conduction ( $H_c$ )	$T_s, T_a, W$

- $H_s$ : Shortwave solar radiation
- $T_a$ : Air temperature
- $T_d$ : Dew-point Temperature
- $T_s$ : Surface water temperature
- $W$ : Wind speed

The windspeed function used in the computation of evaporative heat loss is found in Adams et al. (1990) and is based on the experiments conducted at the National Geothermal Test Facility at East Mesa, CA and the Savannah River Plant, SC. This windspeed function is more conservative (results in higher computed water temperatures) than the widely used and generally accepted functions found in Ryan et al. (1974). The windspeed function is used to compute evaporative heat losses consisting of a forced component that increases with increasing windspeed and a free component which is dependent on the difference between surface temperature and the temperature of the air above the water surface.

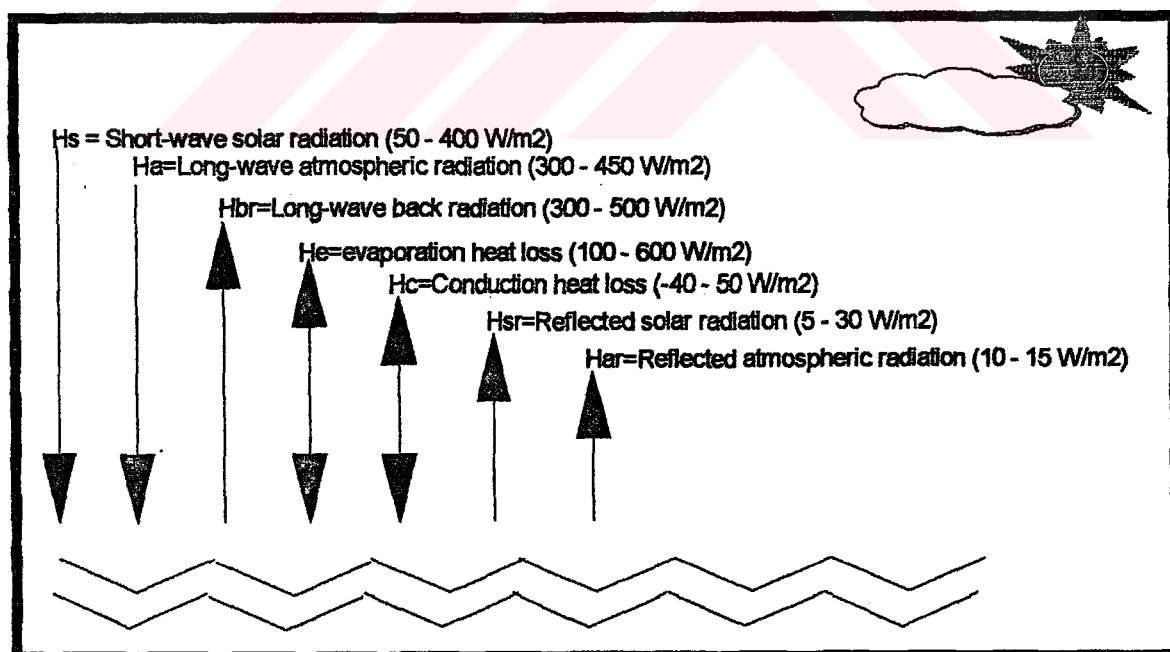


Figure C.1. Process of Heat Exchange At a Natural Surface

## **APPENDIX D**

### **SENSITIVITY TESTS FOR COOLING WATER DISCHARGE**

#### **D.1 General**

In lack of detailed field data, which are essential for the calculation and/or selection of certain parameters, the following would be useful:

- running a range of selected values and evaluating the results based on comparisons with field observations
- model calibration by means of reproducing well known physical characteristics
- testing the sensitivity of the model to changes in parameter values

In the case of the proposed ATPP, comparison to field observations except in a qualitative sense, was beyond the scope of the stationary state simulation approach. Further, reproduction of such general characteristics as circulation, derived from observations and physical models of the Gencelli Harbor was also not used as an alternative. Under these circumstances, the most important tool is testing the sensitivity of the target parameter (in the case of the ATPP, excess temperature) to the changes in other input parameter values.

In the current study, over two hundred sensitivity runs were performed to test the sensitivity of the model to the changes in its important input parameters, in the current study. For testing the aptness of parameter selection, sensitivity runs were used by analysing the effects of input parameter changes on the modeled parameter. The need for sensitivity tests arises from the dependency of input parameter selection on engineering experiences in the absence of sufficient field data. Sensitivity runs will thus abate the uncertainty in parameter selection.

In this study, the sensitivity tests were used to test the model's sensitivity to the changes in the following parameters:

- bathymetry
- chezy coefficient
- horizontal momentum dispersion coefficient
- tidal height
- cloud cover and solar radiation
- rate of return ratio
- wind speed

A base case was defined, based on engineering experiences and previous applications, for the sensitivity runs. In these runs, all the parameters were kept constant except for the tested one. The sensitivity runs were repeated for the four wind directions, N, W, S and E by using one of them as a base case parameter in each set. A wind speed of  $5.5 \text{ m s}^{-1}$  was selected as a base case parameter to cover a wide range of wind speed values recorded at Aliğa.

The base case parameters and their values are listed in Table D.1. The results of the sensitivity runs are given in the following sections.



**Table D.1. Base Case Parameters And Their Abbreviations Used in Sensitivity Tests**

Parameter	Value
Bathymetry number(from Surfer)	4
Chezy coefficient-(CHEZY)	35.0 m <sup>0.5</sup> s <sup>-1</sup>
Rate of return ratio-(RR)	50 %
Tidal Amplitude-(TIDE)	30 cm (60 cm between MLWS and MHWS)
Horizontal momentum dispersion coefficients-(Ax=Ay)	0.1 m <sup>2</sup>
Shortwave solar radiation-(SSR)	120 W m <sup>-2</sup>
Cloud cover-(CC)	0.2
Dry bulb temp. (air)-(D.B.TEMP.)	21 °C
Dew point temp. (air)-(D.P.TEMP)	13 °C
Ambient temperature-(AMB. TEMP.)	20 °C
Cooling water intake depth	10 m
Cooling water discharge depth	10 m
Wind speed-(W.S.)	5.5 m s <sup>-1</sup>

**D.2 Tests for the Bathymetric Data**

Bathymetry is a very important parameter which controls the flow and, as a result, constituent transport. The sensitivity of the model to the bathymetric input was tested and the results are presented in this section.

The first part of the study on sensitivity tests for bathymetric inputs, involved constructing the alternatives for bathymetry and therefore establishing depth contours for each one. The first alternative for the bathymetry of the bay was determined by interpolating average depths for each of the resulting 250

m x 250 m cells from the soundings and contours, using a bathymetric map shown in Figure 5.2 of Chapter 5. This alternative was a relatively crude one and numbered as Bathymetry-1 in the tests.

Another bathymetric information was used to test the sensitivity of excess temperature to bathymetric data, by means of a package program. This second alternative is detailed in Section 5.4.1 of Chapter 5. This alternative was numbered as Bathymetry-4 in the tests.

Two other alternatives were obtained by decreasing and increasing the average depths of the second bathymetry by 2 meters. The four bathymetry alternatives for Gencelli Harbor, are shown in Appendix E. These alternatives were numbered as 2 and 3, respectively.

The second part of the model bathymetry sensitivity test study involved the sensitivity runs for these bathymetry alternatives, using the base case parameters. Bathymetry-4 had critical depths between Bathymetry-3 (relatively deep) and Bathymetry-2 (relatively shallow), in which the dominant factor in the dilution of excess temperature was volume and bottom friction, respectively. Bathymetry-4 gave the maximum excess temperature values for all cases, except for the one in which the wind direction was west. This condition was in agreement with the worst case approach. For the calm case (no wind), the sensitivity results are given in Table D.2..

Table D.2. Bathymetric Data Test Results for the Calm Case

Bathymetry	Max. Surface Excess Temp., °C (Calm Case)
3 (Deep)	0.74
4 (SURFER)	0.79
2 (Shallow)	0.87
1 (Crude)	0.61

Since, it is a relatively refined one, Bathymetry-4 was used as a base case parameter for the other sensitivity runs and simulations. The comparison of Bathymetry-1 and -4 are shown for sixteen wind directions, in Figure D.1. The results for four different wind directions are presented in Figure D.2. As can be seen from the figures cited above, it can be concluded that the variation of surface excess temperature with different alternatives of bathymetry is not significant.

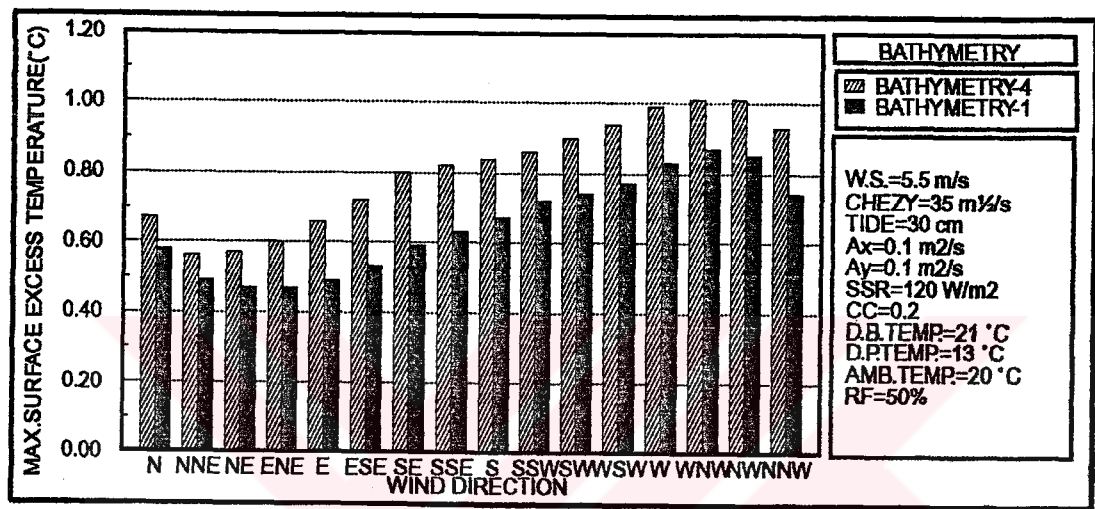


Figure D.1. Comparison of Bathymetry-4 and 1

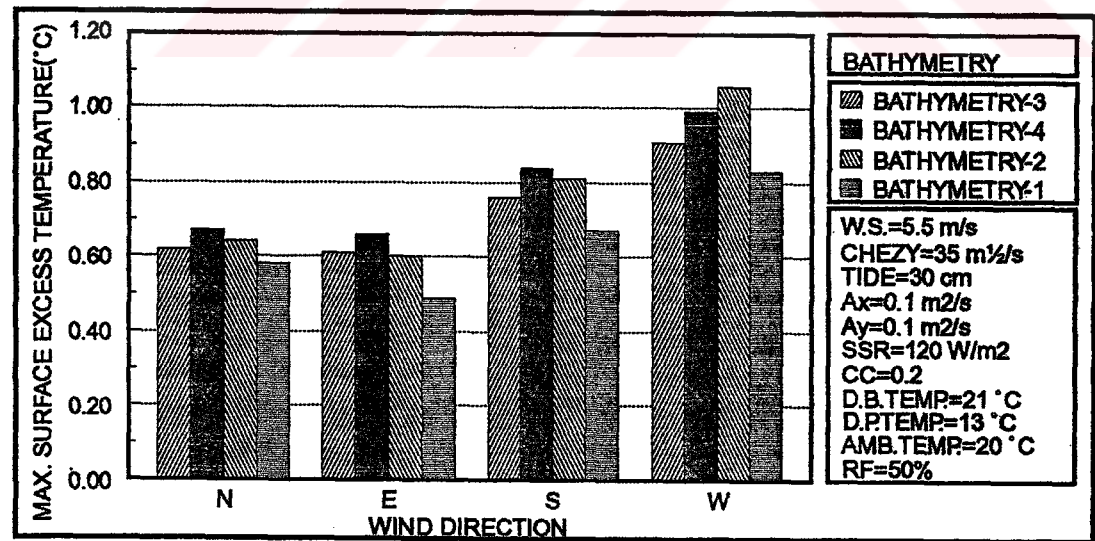


Figure D.2. Sensitivity Tests for Bathymetry

### D.3 Tests for the Chezy Coefficient

In the sensitivity runs, excess temperature was found to be relatively sensitive to the Chezy coefficient. Five different values were selected as test parameters.

In shallow coastal waters small values of Chezy coefficient between 30-40  $\text{m}^{0.5} \text{s}^{-1}$  are used. For instance, a value of 30  $\text{m}^{0.5} \text{s}^{-1}$  once was used in Jamaica Bay (Leendetrse, 1978). Relying upon engineering experiences, a value of 35  $\text{m}^{0.5} \text{s}^{-1}$  was selected. To test the sensitivity, the value was halved and doubled. Since bottom friction is proportional to the square root of the coefficient, halving and doubling the coefficient means decreasing and increasing bottom coefficient by a factor of four. The values 30 and 40 were also tested besides 35. The results for the four different wind directions are presented in Figure D.3. For the calm case, the results are given in Table D.3.

Table D.3. Chezy Coefficient Test Results for the Calm Case

Chezy Coefficient ( $\text{m}^{0.5}\text{s}^{-1}$ )	Max. Surface Excess Temp., °C (Calm Case)
17.5	0.94
30.0	0.82
35.0	0.79
40.0	0.77
70.0	0.72

Although, Chezy coefficient is one of the most effective factor in controlling flow and dilution, the results of the sensitivity runs showed that the selected value was proper and other values would not result in significant changes in the prediction of excess temperature values.

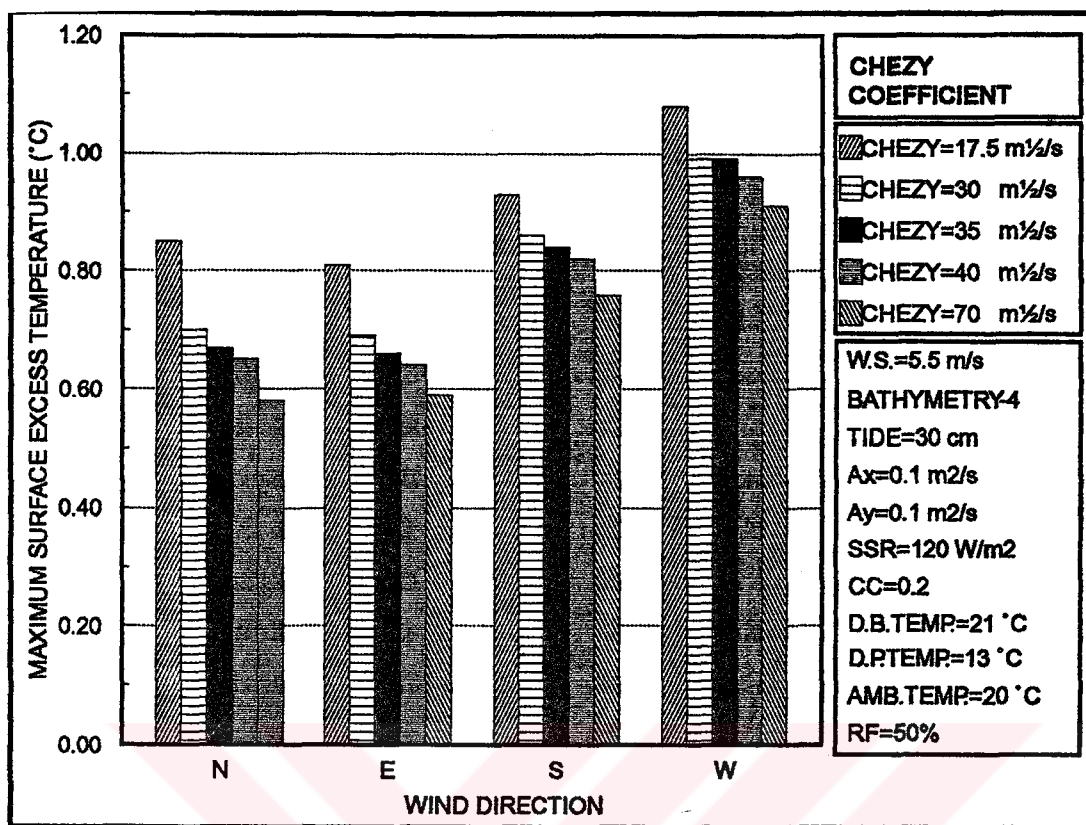


Figure D.3. Sensitivity Tests for Chezy Coefficient

#### D.4 Tests for the Horizontal Momentum Dispersion Coefficient

For the horizontal momentum dispersion coefficients,  $A_x$  and  $A_y$ , a value of  $0.1 \text{ m}^2 \text{ s}^{-1}$  was selected. Since the momentum dispersion coefficient was used as a factor in constituent dispersion coefficient calculations, these sensitivity tests indirectly include the constituent dispersion coefficient sensitivity tests. To test the model's sensitivity to dispersion coefficient, the selected value was increased and decreased by an order of magnitude. The results for four wind directions are presented in Figure D.4. The results for the calm case are listed in Table D.4.

Table D.4. Dispersion Coefficient Test Results for the Calm Case

Horizontal Dispersion Coefficient	Max. Surface Excess Temp., °C (Calm Case)
1.00	0.86
0.10	0.79
0.01	0.80

A change of an order of magnitude in the coefficient did not lead to significant changes in the results. The coefficient selection based on field and engineering experience, was considered proper.

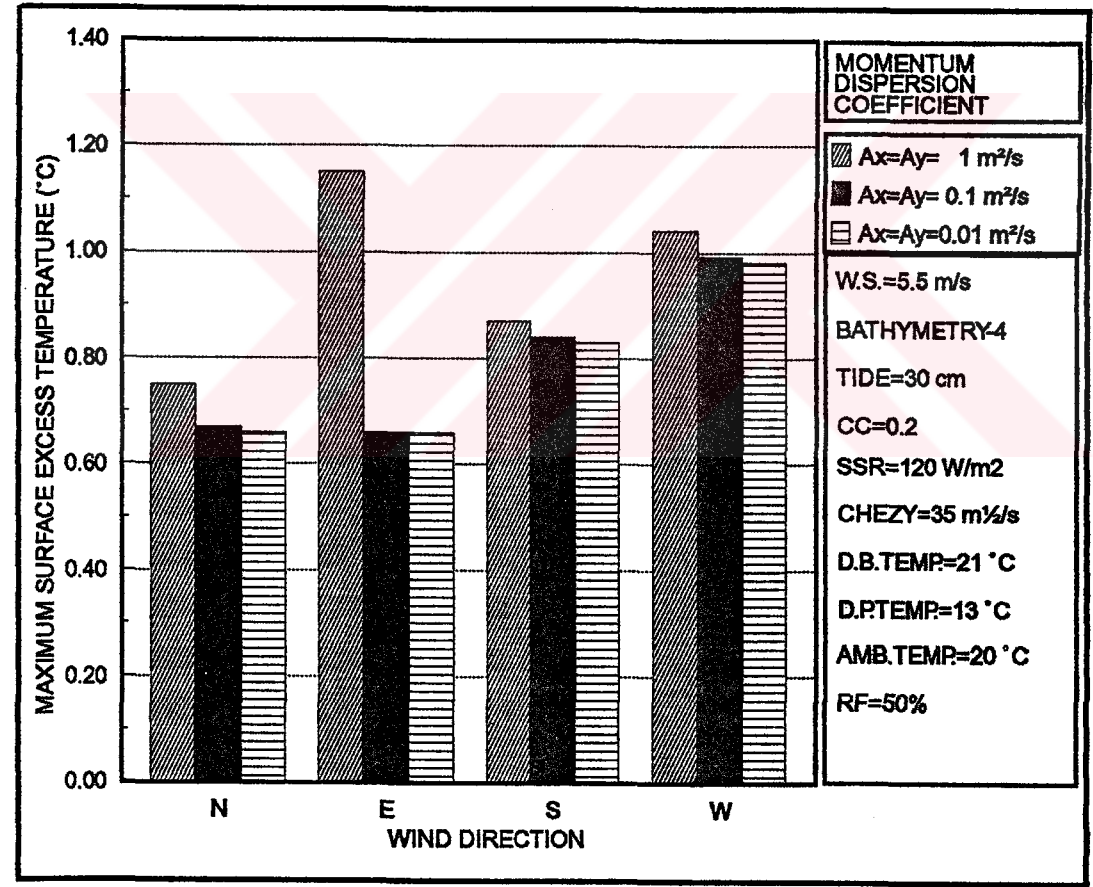


Figure D.4. Sensitivity Tests for Momentum Dispersion Coefficients



D.5 Tidal Height

As stated in the previous sections, tidal amplitudes are low on Turkish coasts. Based on the observations presented by Akyarlı and Arısoy (1988), 30 cm was taken as the tidal amplitude in the model. Three other tidal amplitudes, 10, 20 and 50 cm were tested to examine the tidal effects. The results are given in Figure D.5. The calm case results are given Table D.5.

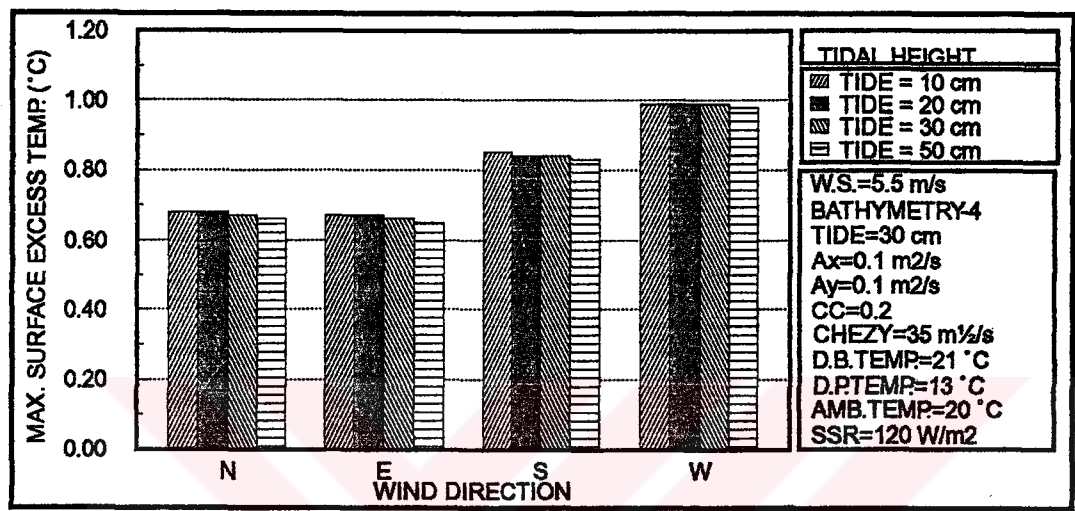


Figure D.5. Sensitivity Tests Tidal Height

In the absence of strong tidal and density forcing functions, surface wind stress and effect of the cooling water system on circulation patterns may become important features of the overall system. The results of tidal height sensitivity runs indicate that this statement is valid for the case of ATPP.

Table D.5. Tidal Amplitude Test Results for the Calm Case

Tidal Amplitude (cm)	Max. Surface Excess Temp., °C (Calm Case)
10	0.80
20	0.80
30	0.79
50	0.79

D.6 Cloud Cover and Shortwave Solar Radiation

The respective values used for the cloud cover (CC) and shortwave solar radiation (SSR) were 0.2 and 120 W m<sup>-2</sup>. To test the aptness of selection, two alternative values were used in sensitivity runs. The values were 0.9 and 5.0 for CC, 20.0 and 720.0 W m<sup>-2</sup> for SSR. In general, for submerged discharges or even in the case of surface discharges, these parameters are not the parameters which primarily control the change in excess temperature. Sensitivity tests showed that these meteorological parameters were ineffective on the surface excess temperature for deep sea discharge, in any case. The results for cloud cover are presented in Figure D.6 and shortwave solar radiation in Figure D.7.

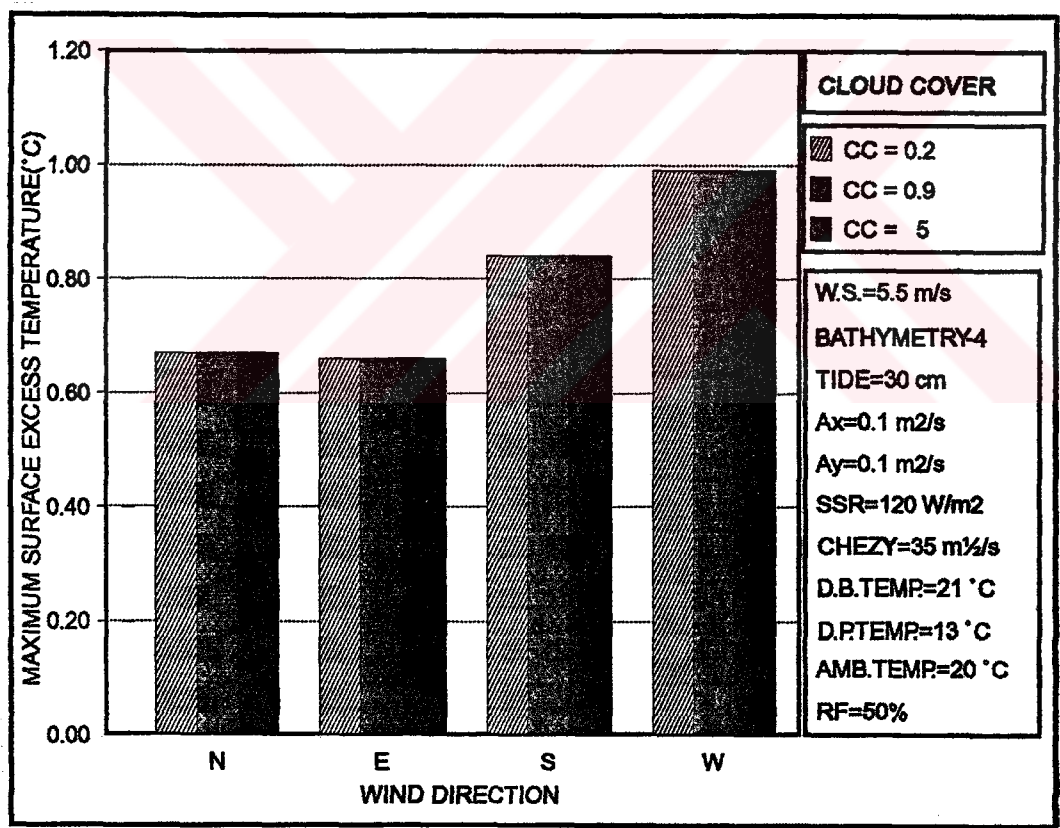


Figure D.6. Sensivity Tests for Cloud Cover



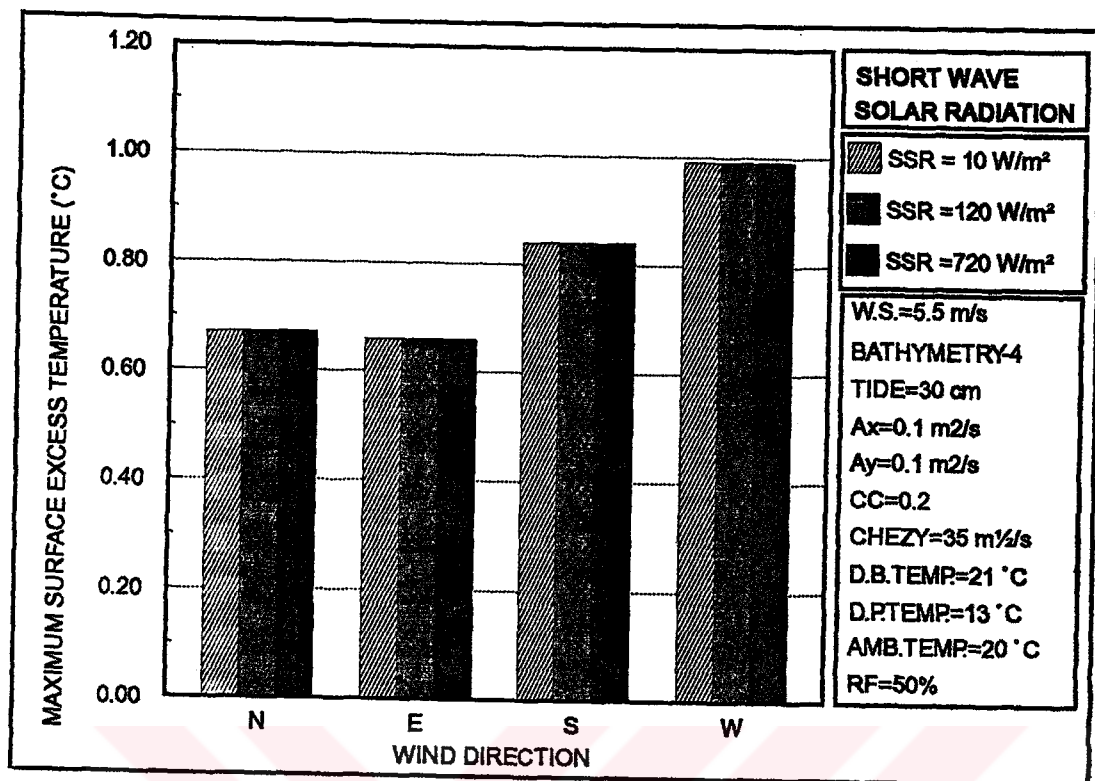


Figure D.7. Sensitivity Tests for Solar Radiation

## D.7 Tests for the Rate of Return Ratio

The model setup included the assumption that some of the excess temperature returns back with the incoming tide. The amount of excess temperature returning on an incoming tide was assumed to be equal to 50 percent of the value inside the model grid. To test the sensitivity of the model to this ratio, the values 10 and 90 percent were also used in sensitivity tests. Since, the tidal effects are nearly insignificant in the case of ATPP, the maximum surface excess temperatures were nearly identical for the three alternatives. The results are shown in Figure D.8. The results of the rate of return ratio sensitivity tests for the calm case are given in Table D.6.

Table D.6. Rate of Return Ratio Test Results for the Calm Case

Rate of Return Ratio (%)	Max. Surface Excess Temp., °C (Calm Case)
10	0.79
50	0.79
90	0.80

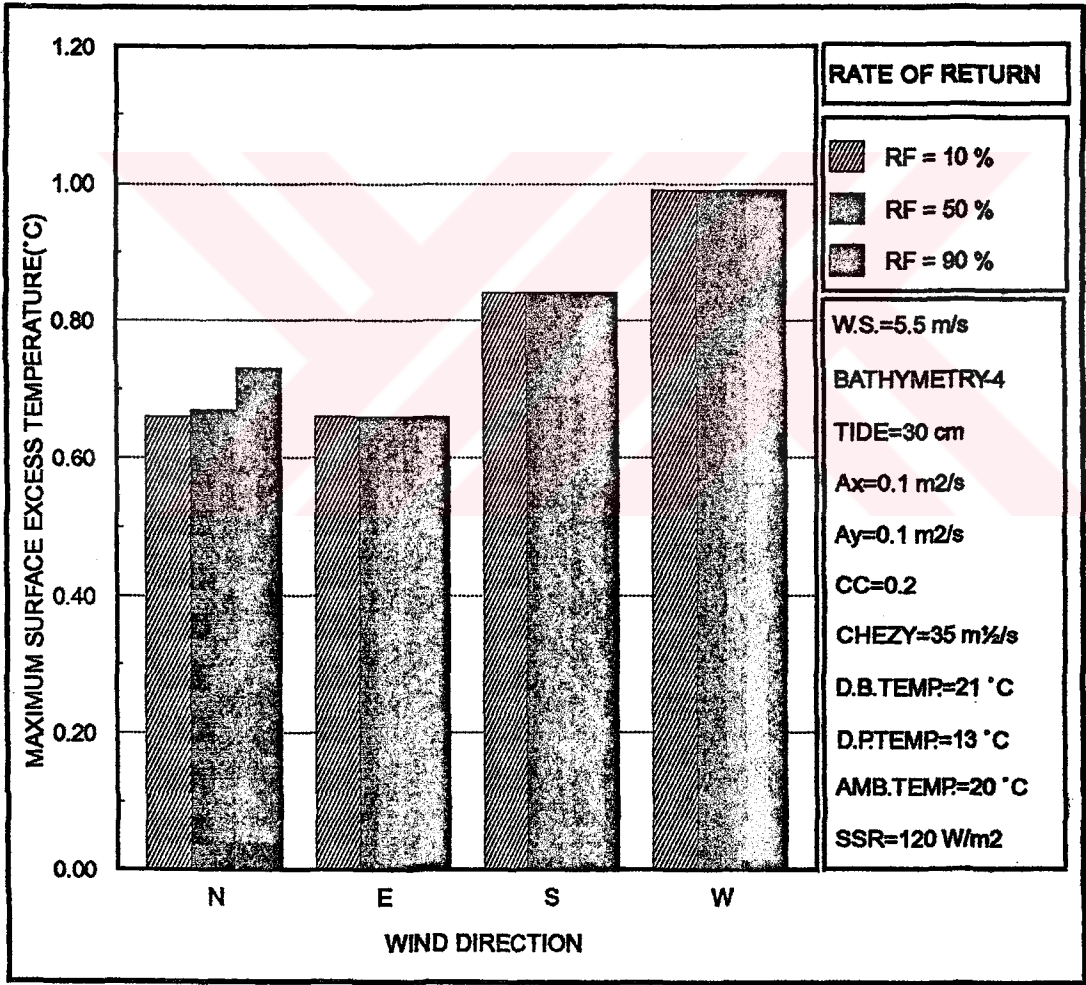


Figure D.8. Sensitivity Tests for Return Rate

## D.8 Wind Speed

The sensitivity of the model to wind speed was tested for four different wind speeds, 1.0, 4.0, 5.5 and 8.5 m s<sup>-1</sup>. The results for the wind speed of 1.0 m s<sup>-1</sup> were nearly identical with the results of the calm case. The results for the other three wind speeds in 16 directions are given in Figure D.9.

It can be seen in Figure D.9 that the effect of high wind speeds reverses rapidly, with a change of wind direction from N (north) to NNW (north northwest). This can be attributed to the mathematical representation of the bathymetry of the modelled area.

Since the horizontal grid sizes used in the hydrothermal studies, were in the order of 250 m, it was not possible to represent the curvatures of the coastline with high precision. This may result in some "mathematical corners" where it is not possible to represent the coastline and bathymetry precisely, as in the grids with codes, I=16, J=5 and I=16, J=8 (see Figure 5.3). The north winds easily disperse the plume which is discharged from more than 250 m away from the shoreline; but, the NNW and NW winds carry the plume to the "mathematical corner" with the code I=16, J=5 and results in the accumulation of excess temperature in the grid. Same condition is valid for the wind directions WSW, SW and the grid I=16, J=8.

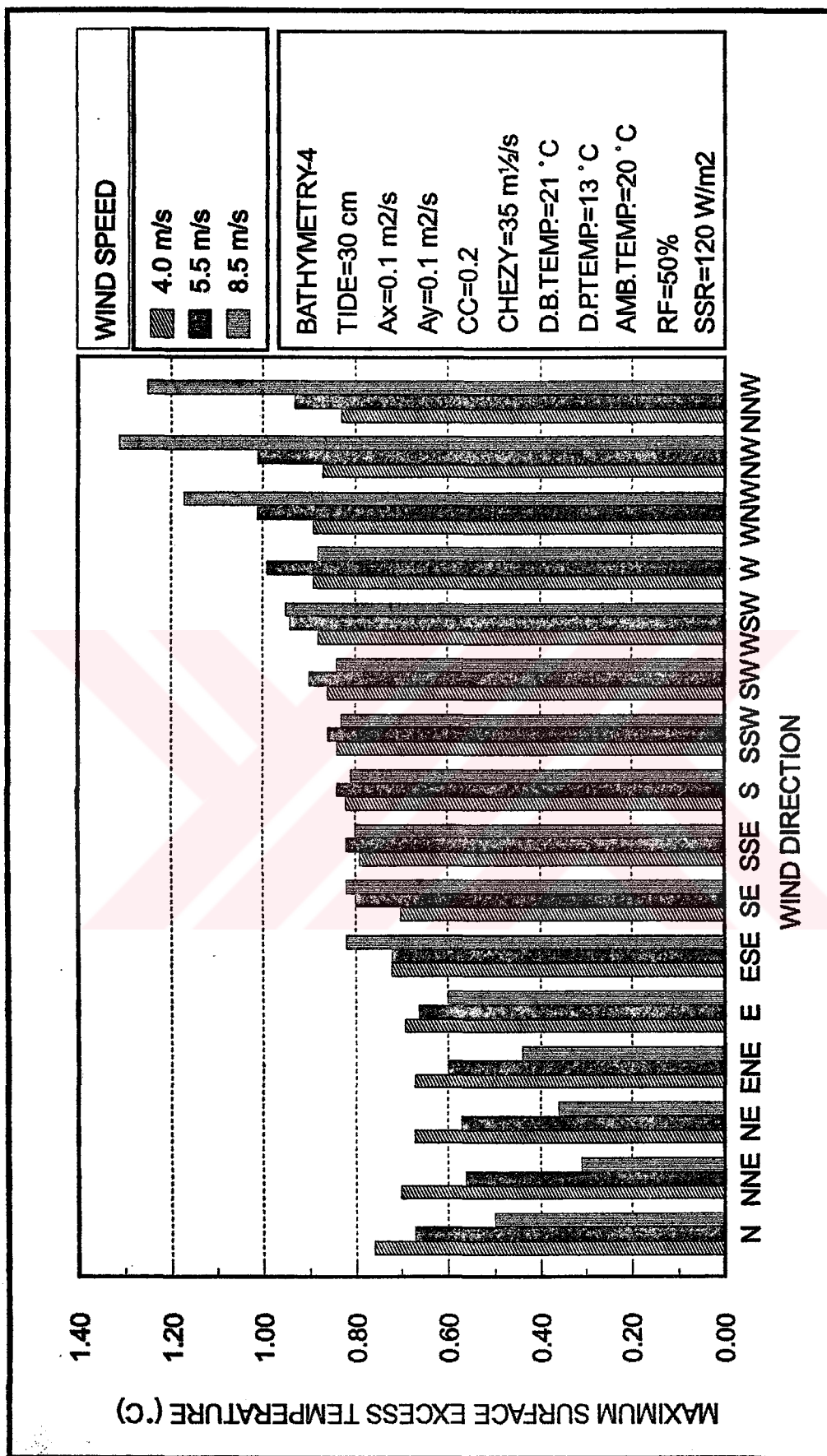
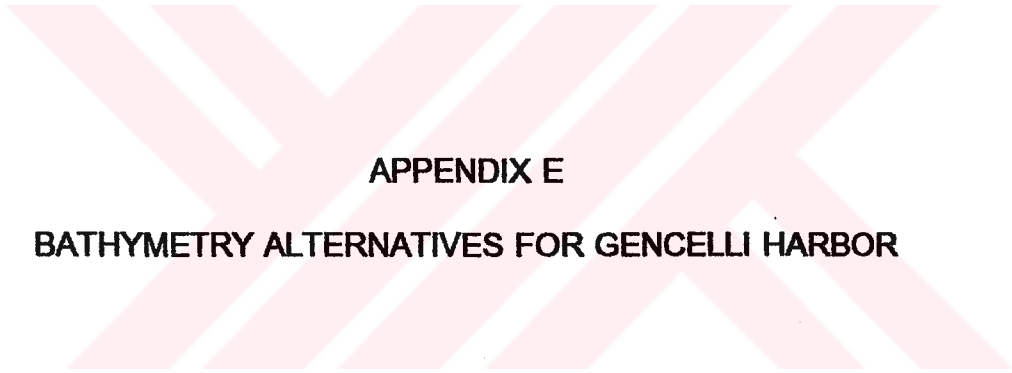


Figure D.9. Sensitivity Tests for Wind Speed



**APPENDIX E**  
**BATHYMETRY ALTERNATIVES FOR GENCELLI HARBOR**

Table E.1. Mean Depth of Each Cell of Bathymetry-1 (m)\*

I	J 1	2	3	4	5	6	7	8	9	10	11
1	0	0	0	0	0	0	0	0	0	0	0
2	0	0	0	0	0	0	0	0	0	0	0
3	0	0	0	0	0	0	0	0	8	18	0
4	0	0	0	0	0	0	6	8	10	26	0
5	0	0	0	0	0	6	8	18	30	40	0
6	0	0	0	0	0	8	10	20	38	48	0
7	0	0	0	8	10	18	26	32	38	50	0
8	0	0	8	10	18	28	32	38	40	50	0
9	0	0	8	16	20	32	34	38	44	46	0
10	0	6	8	20	26	32	34	40	50	50	0
11	0	6	10	20	26	30	36	42	48	46	0
12	0	6	12	20	26	30	34	38	46	44	0
13	0	6	8	18	24	26	32	34	38	36	0
14	0	0	8	12	16	22	24	26	22	28	0
15	0	0	6	6	12	12	18	10	6	10	0
16	0	0	0	0	8	8	8	8	0	0	0
17	0	0	0	0	0	0	0	0	0	0	0

Table E.2. Mean Depth of Each Cell of Bathymetry-2 (m)\*

I	J 1	2	3	4	5	6	7	8	9	10	11
1	0	0	0	0	0	0	0	0	0	0	0
2	0	0	0	0	0	0	0	0	0	0	0
3	0	0	0	0	0	0	0	0	4	16	0
4	0	0	0	0	0	0	4	6	10	24	0
5	0	0	0	0	0	2	6	16	28	34	0
6	0	0	0	0	0	4	14	24	34	44	0
7	0	0	0	2	8	10	22	30	38	44	0
8	0	0	2	10	16	24	28	34	38	44	0
9	0	0	4	14	20	28	34	40	40	44	0
10	0	2	6	14	24	28	34	40	44	46	0
11	0	2	10	16	24	28	34	40	44	44	0
12	0	2	10	16	22	28	32	36	40	40	0
13	0	2	8	14	20	24	28	28	40	32	0
14	0	0	4	10	14	16	22	18	16	24	0
15	0	0	4	8	10	10	12	10	6	8	0
16	0	0	0	0	2	2	2	2	0	0	0
17	0	0	0	0	0	0	0	0	0	0	0

\* Column: J, Row: I

Table E.3. Mean Depth of Each Cell of Bathymetry-3 (m)\*

	J 1	2	3	4	5	6	7	8	9	10	11
1	0	0	0	0	0	0	0	0	0	0	0
2	0	0	0	0	0	0	0	0	0	0	0
3	0	0	0	0	0	0	0	0	8	20	0
4	0	0	0	0	0	0	8	10	14	28	0
5	0	0	0	0	0	6	10	20	32	38	0
6	0	0	0	0	0	8	18	28	38	48	0
7	0	0	0	6	12	14	26	34	42	48	0
8	0	0	6	14	20	28	32	38	42	48	0
9	0	0	8	18	24	32	38	44	44	48	0
10	0	6	10	18	28	32	38	44	48	50	0
11	0	6	14	20	28	32	38	44	48	48	0
12	0	6	14	20	26	32	36	40	44	44	0
13	0	6	12	18	24	28	32	32	44	36	0
14	0	0	8	14	18	20	26	22	20	28	0
15	0	0	8	12	14	14	16	14	10	12	0
16	0	0	0	0	6	6	6	6	0	0	0
17	0	0	0	0	0	0	0	0	0	0	0

Table E.4. Mean Depth of Each Cell of Bathymetry-4 (m)\*

	J 1	2	3	4	5	6	7	8	9	10	11
1	0	0	0	0	0	0	0	0	0	0	0
2	0	0	0	0	0	0	0	0	0	0	0
3	0	0	0	0	0	0	0	0	6	18	0
4	0	0	0	0	0	0	6	8	12	26	0
5	0	0	0	0	0	4	8	18	30	36	0
6	0	0	0	0	0	6	16	26	36	46	0
7	0	0	0	4	10	12	24	32	40	46	0
8	0	0	4	12	18	26	30	36	40	46	0
9	0	0	6	16	22	30	36	42	42	46	0
10	0	4	8	16	26	30	36	42	46	48	0
11	0	4	12	18	26	30	36	42	46	46	0
12	0	4	12	18	24	30	34	38	42	42	0
13	0	4	10	16	22	26	30	30	42	34	0
14	0	0	6	12	16	18	24	20	18	26	0
15	0	0	6	10	12	12	14	12	8	10	0
16	0	0	0	0	4	4	4	4	0	0	0
17	0	0	0	0	0	0	0	0	0	0	0

\* Column: J, Row: I